Oxygen and Asteroids

**Thomas H. Burbine[1], Andrew S. Rivkin[2], Sarah K. Noble[3],
Thais Mothé-Diniz[4], William F. Bottke[5], Timothy J. McCoy[6],
M. Darby Dyar[1], and Cristina A. Thomas[7]**

[1]Dept. of Astronomy, Mount Holyoke College, South Hadley, MA 01075, U.S.A.

[2]Johns Hopkins University Applied Physics Laboratory, Laurel, MD 20723, U.S.A.

[3]NASA Johnson Space Center, Houston, TX 77058, U.S.A.

[4]Observatoire de Paris, 92195 Meudon Cedex, France

[5]Southwest Research Institute, Boulder, CO 80302, U.S.A.

*[6]Department of Mineral Sciences, National Museum of Natural History,
Smithsonian Institution, Washington, D.C. 20560-0119, U.S.A.*

*[7]Department of Earth, Atmospheric and Planetary Sciences,
Massachusetts Institute of Technology, Cambridge, MA 02139, U.S.A.*

contact e-mail: tburbine@mtholyoke.edu

ABSTRACT

Hundreds of thousands of asteroids have been discovered in the asteroid belt and in near-Earth space. Oxygen is an abundant element in meteorites and presumably in most asteroids. Spectral reflectance measurements of asteroids in the visible and near-infrared can identify oxygen-bearing minerals such as those found in the olivine, pyroxene, and serpentine groups due to their distinctive absorption features. Interpretation of the mineralogy of asteroids is complicated by the effects of space weathering, which tends to redden and darken the surfaces of asteroids. Asteroids are primarily classified into a number of taxonomic classes and subclasses according to their spectral properties in the visible wavelength region. However, asteroids with similar spectral properties in the visible may have different spectral properties in the near-infrared and, therefore, different interpreted mineralogies. Definite trends in the abundances of different taxonomic classes versus heliocentric distance are apparent. These trends appear to be a function of both composition differences and degree of heating. However, dynamical processes have significantly affected these trends. Close observation of asteroids by spacecraft, such as NEAR-Shoemaker to 433 Eros and Hayabusa to 25143 Itokawa, are currently the best way to discern the mineralogies of individual asteroids.

INTRODUCTION

Oxygen is the most abundant element in the Earth's crust and mantle, most meteorites (e.g., Hutchison 2004), and presumably in most asteroids. Many studies of oxygen's importance in the formation of different meteorite types investigate the oxygen fugacity experienced during the formation and subsequent metamorphism of minerals in meteorites, the effects of aqueous alteration, and differences in oxygen isotopic compositions.

Asteroids are defined as small bodies that orbit the Sun. Over 300,000 asteroids have been discovered so far. Comets are also small bodies that orbit the Sun, but are thought to be much more volatile-rich than asteroids. An object is identified as a comet and not an asteroid if it has a tail or appears diffuse, which indicates that volatiles are evaporating off the object's surface.

Asteroids appear as single points of light in the sky. Extinct cometary nuclei may look like asteroids because they have lost most of their volatiles (Weissman et al. 1989).

With the exception of lunar and Martian fragments, meteorites are believed to be from asteroids. However, meteorites are found out of geologic context; by linking meteorites with specific asteroids or asteroid types, we can place them into context, with the knowledge gained on large spatial scales complementing the smaller scales studied in the laboratory. Observations of objects in different regions of the asteroid belt provide a cross-section of conditions early in Solar System history. Cometary meteorites may exist (Campins and Swindle 1998), but none have been unequivocally identified.

Different meteorite groups formed in environments ranging from very reducing to very oxidizing (Weisberg et al. 2006). Approximately 300 different minerals have been identified in meteorites (Rubin 1997a,b), and mineral assemblages predicted by theoretical condensation sequences (e.g., Grossman 1972; Ebel 2006) (Table 1) are found within some meteorites.

To interpret the oxygen fugacity and amount of aqueous alteration that a particular asteroid has experienced, telescopic data must be analyzed. Many mineral groups commonly found in meteorites have distinctive absorption features in different wavelength regions. The presence or absence of specific minerals allows constraints to be placed on the oxygen fugacity and/or temperatures during mineral formation and any subsequent alteration due to pressure and/or temperature.

This chapter will discuss how remote sensing can be used in constraining the oxygen fugacity and degree of aqueous alteration experienced by asteroids, in determining meteoritic analogs, and in understanding compositional and oxidation gradients in the solar nebula. The main belt is a dynamic place where asteroids have experienced up to ~4.6 b.y. of collisional evolution and alteration of the optical properties of their surfaces, which complicates our ability to derive any of these constraints. To truly understand how oxygen has affected the mineralogy of asteroids, these dynamical and space weathering-related issues must also be considered.

Table 1. Condensation sequence for different minerals from Grossman (1972) and Lewis (1997). The temperatures in parentheses are the temperatures where the condensate disappears.

| Temperature (K)	Mineral
1758 (1513)	Corundum (oxide), Al_2O_3
1647 (1393)	Perovskite (oxide), $CaTiO_3$
1625 (1450)	Melilite group, $Ca_2Al_2SiO_7$-$Ca_2MgSi_2O_7$
1513 (1362)	Spinel (oxide), $MgAl_2O_4$
1471	FeNi metal
1450	Diopside (pyroxene), $CaMgSi_2O_6$
1444	Forsterite (olivine), Mg_2SiO_4
1362	Anorthite (feldspar), $CaAl_2Si_2O_8$
1349	Enstatite (pyroxene), $Mg_2Si_2O_6$
<1000	Alkali-bearing feldspar, $(Na,K)AlSi_3O_8$-$CaAl_2Si_2O_8$
<1000	Ferrous olivines, $(Mg,Fe)_2SiO_4$; Ferrous pyroxenes, $(Mg,Fe)_2Si_2O_6$
700	Troilite (sulfide), FeS
490	Serpentine (phyllosilicate), $(Fe.Mg)_3Si_2O_5(OH)$
405	Magnetite (oxide), Fe_3O_4
400	Talc (phyllosilicate), $Mg_3Si_4O_{10}(OH)_2$

DYNAMICAL STRUCTURE OF THE ASTEROID BELT

The position of an asteroid in the Solar System is usually given by its semi-major axis (*a*), the sine of its proper inclination (*i*), and its proper eccentricity (*e*). The semi-major axis is the average distance from the Sun in astronomical units (AU); the sine of the proper inclination gives the tilt of an asteroid's orbit to the ecliptic; and the eccentricity is the degree to which an asteroid's orbit deviates from circular. These proper elements remain practically unchanged over astronomically long timescales unless the bodies are in a dynamically unstable region.

The main asteroid belt is defined as the region between Mars (1.4 AU) and Jupiter (5.2 AU). The majority of known asteroids fall between ~2.1 and ~3.2 AU (Fig. 1). Current estimates of the number of asteroids in the main belt, that have diameters greater than 1 km, range from 6.7×10^5 (Ivezić et al. 2001) to 1.9×10^6 (Tedesco et al. 2005). Only ~220 main-belt asteroids have diameters greater than 100 km. Except for the largest objects (e.g., 1 Ceres, 2 Pallas, 4 Vesta), almost all asteroids are thought to be fragments of once-larger bodies.

The main belt is bounded and crossed by a number of resonances (Fig. 1). Mean motion resonances occur when the orbital period of an asteroid is a simple fraction of the orbit of Jupiter. These mean motion resonances tend to result in depletions or concentrations in asteroids. The 3:1, 5:2, and 2:1 resonances (at ~2.5, ~2.83, and ~3.28 AU, respectively) all result in depletions due to embedded secular resonances that are thought to generate chaotic orbits (e.g., Lecar et al. 2001), making them the likely source regions of near-Earth asteroids (NEAs) and meteorites. The arcing gap (ν_6) that bounds the inner main belt is due to a secular resonance with Saturn. Resonances where groupings of asteroids are located include the Hilda asteroids, which are in a 3:2 resonance (~3.9 AU) with Jupiter, and the Trojan asteroids, which are in a 1:1 resonance with Jupiter at ~5.2 AU and are found at the two Lagrangian points 60° ahead of (L4 Trojans) and 60° behind (L5 Trojans) Jupiter.

Asteroid families are groupings identified by finding clusters in proper element space. They are thought to be the direct outcomes of collisional events between asteroids. The collisional origin of asteroid families has been established by a series of theoretical and observational studies (e.g., Bendjoya and Zappalà 2002; Zappalà et al. 2002, Cellino et al. 2002). There are several tens of known asteroid families (e.g., Zappalà et al. 2002). The number of members and the dynamical bounds of a family are dependent on the number of asteroids with proper elements known at any given time as well as the statistical technique that is used to identify
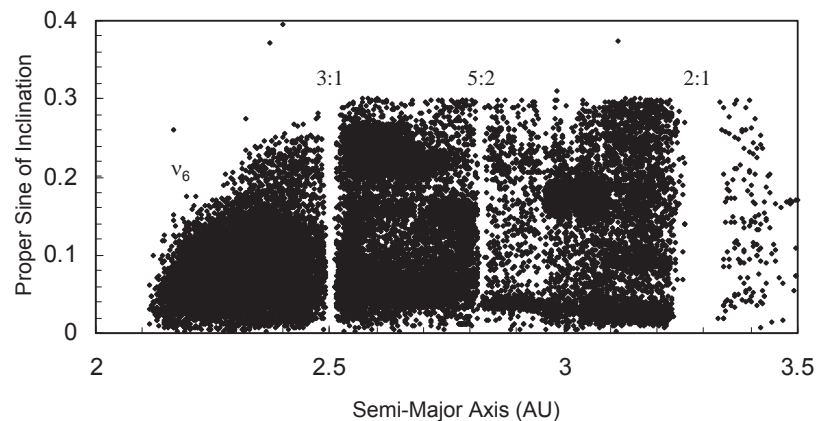
Figure 1. Plot of semi-major axis versus proper sine of inclination for ~62,000 asteroids. A number of resonances are indicated.

these clusters (Zappalà et al. 1995). Families are customarily named after the first member of that family or group that was discovered.

Originally, it was thought that spectroscopic observations of families would allow disrupted differentiated objects to be identified, since these disrupted bodies should have large metallic iron cores and many associated, smaller olivine-dominated objects and basaltic bodies (e.g., Granahan and Bell 1991; Granahan 1993). Spectral observations of asteroid family members (e.g., Bus 1999; Florczak et al. 1999; Cellino et al. 2002; Mothé-Diniz et al. 2005), however, have found that most family members have similar spectral properties. These spectral similarities imply that either the original parent body was not differentiated, or the disruption produced relatively homogeneous fragments. For the latter scenario, Michel et al. (2003, 2004) found that the disruption of pre-shattered parent bodies produces family members that are formed by the gravitational reaccumulation of smaller bodies. This may suggest that differentiated, pre-fragmented bodies could produce family members that may appear homogenous. Objects with proper elements that fall within the bounds of a family, but are not actually fragments of the disrupted parent body, are called interlopers (Migliorini et al. 1995). Interlopers are usually identified by having spectral properties that are thought to be incompatible with most of the other family members (e.g., Chapman et al. 1989).

ASTRONOMICAL TECHNIQUES

Brightness

The apparent brightness of an object as seen from Earth is defined as its apparent magnitude. Because the Earth's atmosphere absorbs radiation and the amount of absorption is a function of the thickness of the atmosphere, apparent magnitudes are normalized to values outside the atmosphere. The scale is logarithmic, with brighter objects having lower values. The star Vega has an apparent magnitude of ~0, with A0-type stars with surface temperatures of 10,600 K defined as zero magnitude at all wavelengths. An object with an apparent magnitude of −1 would be ~2.5 times brighter than Vega, and an object with an apparent magnitude of +1 would be ~2.5 times fainter than Vega. The magnitude for the Sun is −26.7, that of the full Moon is −12.6, and for the faintest stars observable with the naked eye, the magnitude is approximately +6.

The apparent magnitude of an asteroid is a function of its diameter, visual albedo, and its distance from Earth. Almost all asteroids, with the exception of Vesta, tend to be fainter than +6 in the visible wavelengths and cannot usually be observed without a telescope. Visual albedo (p_V) is the amount of light reflected in the visible wavelength region from an asteroid. An albedo of 1.0 indicates a perfect reflector. The distance of an asteroid from Earth can easily be determined, but the diameter and visual albedo are much more difficult. At the same distance from the Sun, a large, dark body and a small, bright one could have the same magnitude. The magnitude independent of distance, or absolute magnitude (H), of an asteroid is defined as the visual magnitude of an asteroid if it were placed one AU away from the Earth, one AU from the Sun, and observed at zero phase angle. (Phase angle is the angle between the Sun, the target, and the detector.) This definition of absolute magnitude is only theoretical since it is impossible to situate an asteroid at those locations and have it also be at zero phase angle. If you know the absolute magnitude and assume an albedo, the diameter (D) of an asteroid in kilometers can be estimated from the formula $D = (1329 \times 10^{-0.2H})/(p_V)^{\frac{1}{2}}$ (Harris and Harris 1997).
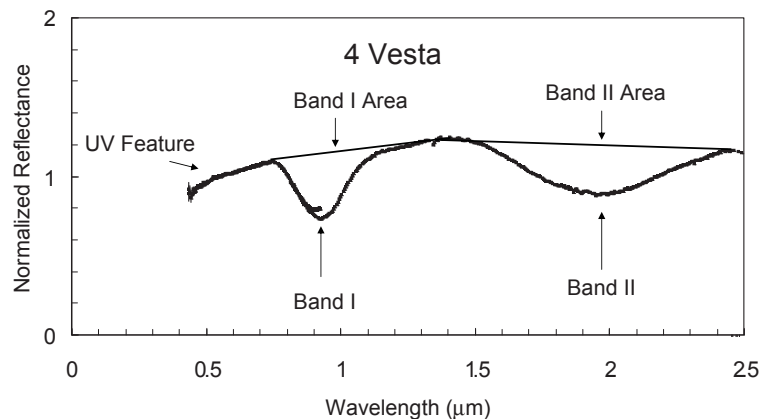
Reflectance spectroscopy

The photons measured from an asteroid by a telescope are those emitted by the Sun that have either been reflected from the asteroid's surface or are the result of the absorption and then emission by electrons associated with different transition elements in a variety of

different minerals as the electrons change energy levels. Different wavelengths of light do not interact equally with the surface. The fraction of light that is reflected and absorbed and then emitted at different wavelengths is a function of a number of properties of the surface such as composition, particle size, and temperature. Absorption features are due to the preferential absorption of light at particular wavelengths.

An asteroid's reflectance spectrum is a plot of the intensity of light detected from its surface as a function of wavelength (e.g., 4 Vesta in **Fig. 2**). Labeled in Figure 2 are a number of important absorptions such as Band I, Band II, and a feature that extends into the UV (ultraviolet). The area between the spectrum and a line tangent to the peaks at ~0.7 and ~1.4 μm is the Band I Area and the area between the spectrum and a line tangent to the peaks at ~1.4 and ~2.5 μm is the Band II Area. The distinctive "symmetric" Band I and II absorptions are characteristic of the mineral pyroxene. Error bars are one-sigma, but are smaller than the points for most of the spectrum. The disconnect in the spectrum at ~0.9 μm is due to the overlap of a visible spectrum and a near-infrared (IR) spectrum, which were taken at two different times and with two different instruments. A spectrum is said to be red-sloped if the reflectance of the object tends to increase with increasing wavelength, blue-sloped if the reflectance tends to decrease with increasing wavelength, and to be spectrally flat if the reflectance is generally monotonic with increasing wavelength.

As in Figure 2, asteroid reflectance spectra are commonly normalized to unity at a particular wavelength because, as mentioned earlier, the flux versus wavelength measured from an asteroid is a function of both the size and albedo of the object plus its distance from Earth. Therefore, it is very difficult to determine how well an asteroid reflects light from simple measurements of its brightness. The normalizing wavelength is usually 0.55 μm, which corresponds to the peak sensitivity to bright light for the human eye and approximately the peak of the emission curve for the Sun. Albedo has a number of slightly different definitions (Hanner et al. 1981), but in this chapter will be defined as the percentage of light reflected at a particular wavelength from an object.

Most asteroid albedos are from measurements by the IRAS (Infrared Astronomical Satellite) (Matson et al. 1986, 1989; Tedesco et al. 2002), which measured the emission from

Figure 2. Reflectance spectrum of 4 Vesta with important features labeled. These important features include the UV (ultraviolet) feature, Band I, and Band II. The Band I Area is the area between the spectrum and a line tangent to the peaks at ~0.7 and ~1.4 μm and the Band II Area is the area between the spectrum and a line tangent to the peaks at ~1.4 and ~2.5 μm. Spectrum is a combination of SMASS II (Bus and Binzel 2002a) and SpeX data. Spectrum is normalized to unity at 0.55 μm. Error bars are one-sigma.

asteroids at four bandpasses centered at approximately 12, 25, 60, and 100 μm. The IRAS observations, in conjunction with a visual magnitude measurement, allow an albedo and diameter for an asteroid to be determined that simultaneously matches the reflected sunlight and thermal emission from the object (Lebofsky and Spencer 1989). The underlying physics is Planck's law of blackbody radiation. Observations of asteroid polarization can also yield albedos, though while this technique was commonly used in the 1970s in particular, there have been relatively few recent albedo determinations made in this fashion.

Spectral data

There are two distinct types of spectral data that are relevant for determining asteroid compositions. Photometric observations record the absolute brightness of an object. Filters are used to control the bandpass of the recorded light and to allow the intercomparison between datasets taken with different detectors that have different sensitivities. Using a set of filters with different central wavelengths and measuring the magnitude of an asteroid with each filter allows a spectrum to be constructed. The color index is the difference in magnitude between two spectral regions and is always defined as the short-wavelength magnitude minus the long-wavelength magnitude. Usually, these spectra are of relatively low resolution, such as those produced in the Eight-Color Asteroid Survey (ECAS) (Zellner et al. 1985b), and the Sloan Digital Sky Survey (SDSS) (Ivezić et al. 2001), but higher resolutions are possible, such as those found in the 24-color (Chapman and Gaffey 1979) or 52-color asteroid surveys (Bell et al. 1988). Such data are termed spectrophotometric and were the most common form of asteroid spectral data until the late 1980s. The SDSS has provided visible data on ~11,000 asteroids with known orbits out of over 58,000 observations (Ivezić et al. 2002).

Spectroscopic data, by contrast, have all wavelengths of interest obtained simultaneously. CCDs (charge-coupled devices) sensitive to extended visible wavelengths (~0.4-1.0 μm) are now commonly available (e.g., Bus et al. 2002), and objects as faint as 19th magnitude (corresponding to a size of ~5 km at 3 AU) can be observed spectroscopically with a 4-m telescope. Visible spectroscopic surveys include SMASS (Small Main-Belt Asteroid Spectroscopic Survey) (Xu et al. 1995), SMASS II (Bus and Binzel 2002a), and S3OS2 (Small Solar System Objects Spectroscopic Survey) (Lazzaro et al. 2004).

The development of IR arrays has revolutionized asteroid science. The near-IR (0.8-2.5 μm) spectral region is crucial for inferring asteroid mineralogies because both olivine (ol) and pyroxene (pyx) have strong absorption bands in this region, as detailed in Gaffey et al. (2002) and Burbine et al. (2002b). The NASA Infrared Telescope Facility (IRTF) SpeX instrument (Rayner et al. 2003), located on Mauna Kea, can observe 17th-18th magnitude objects, allowing high-quality data (e.g., Binzel et al. 2001; Sunshine et al. 2004; Hardersen et al. 2005, 2006) to be obtained for objects of sizes comparable to those available in the visible region. Much fainter objects can be observed using larger telescopes, of course, but such telescopes have not often been brought to bear in asteroidal studies, and the majority of asteroid data are obtained at 3-4 m-class observatories.

Water and OH have strong absorptions in the 3-μm region, which can also be observed using SpeX. While the first wave of HgCdTe IR detectors were only sensitive to 1-2.5 μm, InSb detectors, such as used with SpeX, extend that coverage out to 5.5 μm. This spectral region is considered by some to be part of the near-IR, while others put it in the "thermal IR" or "mid-IR." The absorptions due to OH that make this region of interest in mineralogy, however, also can wreak havoc with ground-based observations. Few sites have instruments capable of observing in this wavelength region, with most published observations coming from the telescopes on Mauna Kea.

Beyond this spectral range is the mid-IR. Spectral datasets at these longer wavelengths include the Cornell MIDAS (Mid-IR Asteroid Spectroscopy) Survey (~8 to 13 μm) (Lim et

al. 2005) and observations using the Spitzer Space Telescope (Cruikshank 2005; Emery et al. 2005). Compositional data have been more difficult to interpret at these wavelengths than at shorter wavelengths, but there are advantages to this wavelength region. In the mid-IR, any minerals that do not contain Fe^{2+} have diagnostic absorption features, and absorption features due to different minerals add linearly. Continuing detector development and the availability of Spitzer data could lead to a revolution in this field. Although compositional work has been less common in this region due to the high number of spectral features (Salisbury et al. 1991), most asteroid albedos determined from earth-based observations are determined using 10- and 20-µm spectrophotometry, effectively very low-resolution spectra.

There is a general tradeoff between the faintness of an object and the spectral resolution that can be profitably obtained. Spectrophotometric analysis can be done on very faint objects, but the data produced usually do not allow detailed interpretations to be made, due to their low resolution compared to spectroscopic data. A comparison between spectrophotometric data (large squares) and spectroscopic data (small squares) for asteroid 11 Parthenope is displayed in Figure 3. Note the absence of spectrophotometric data around ~1.4 and ~1.9 µm, which is due to problems in obtaining enough signal around atmospheric water bands. In addition, because time elapses between the measurement of the flux at each wavelength, care must be taken to account for possible changes in sky conditions as well as for changes in asteroid cross-sectional area, which can skew the results. The main drawback with spectroscopic data is the restriction to relatively bright objects relative to the objects obtainable by spectrophotometric means for the same size aperture.
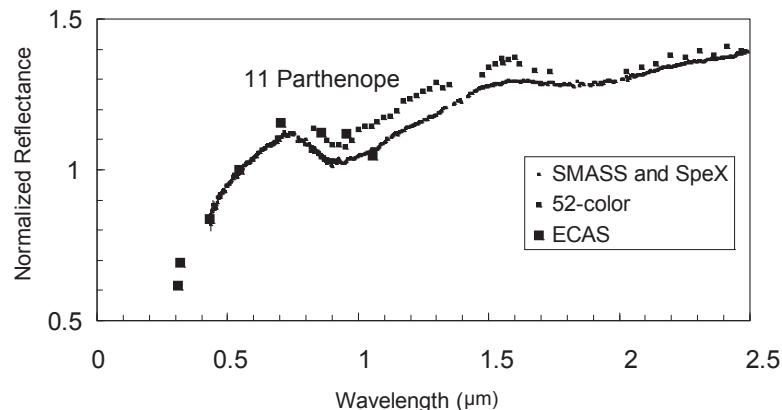
Figure 3. Reflectance spectra for 11 Parthenope. The largest squares are spectrophotometric ECAS data (Zellner et al. 1985b) and the medium-sized squares are spectrophotometric 52-color observations (Bell et al. 1988). The smallest squares are spectroscopic data and are a combination of SMASS II (Bus and Binzel 2002a) and SpeX data. Spectra are normalized to unity at 0.55 µm. Error bars are one-sigma, but are smaller than the data points for most parts of the spectrum.

Corrections

The radiation emitted from the Sun primarily follows a blackbody curve that peaks in the visible; however, the transmission of light through the Earth's atmosphere changes dramatically with wavelength (Fig. 4). When combined with the differences in detector technology and their sensitivities in different wavelength regions, the mineralogical analysis of different types of asteroids has been necessarily uneven. In order to provide accurate results, remote sensing data need to be corrected for the various ways that the spectral distribution changes between
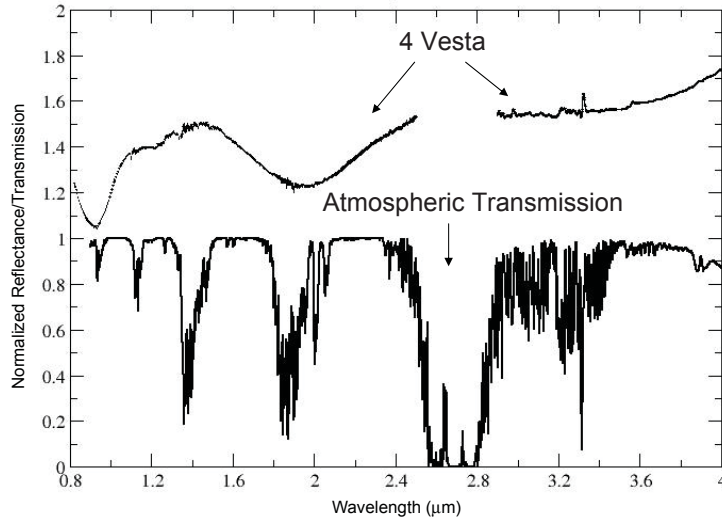
Figure 4. Atmospheric transmission in the 0.8-4 μm region (bottom line) compared to the spectrum of Vesta (top line) (Rivkin et al. 2006a). Regions where the atmosphere is less transmissive (near 1.4 and 1.9 μm) show increased scatter in the asteroid spectrum. The 2.5-2.8 μm region, where transmission goes to zero, results in a region where no good data can be obtained from the ground, and that spectral region is omitted from the asteroid spectrum.

leaving the Sun and arriving on the observer's computer screen. That distribution carries the signature of the Sun, modified by the surface properties of the asteroid, then modified again by the Earth's atmosphere and the properties of the detector. Only the modification by the surface of the asteroid is actually of interest for compositional studies, and the other effects need to be calibrated or corrected for.

Because the Sun cannot be directly observed during asteroid observations, standard stars with colors similar to the Sun, such as those classified as G2 spectral types, are observed. To correct for absorption by the atmosphere, standard stars should be observed at similar airmasses to an asteroid, or standards should be observed over a wide range of airmasses to calculate the atmospheric behavior that evening. These corrections entail dividing the measured flux of the asteroid by the measured flux of a standard star (or series of standard stars) at each measured wavelength. In the wavelength region where most asteroids are observed (0.3 to 2.5 μm), thermal emission from main-belt asteroids is usually not a significant contributor to the flux of an asteroid. The basic formula (Gaffey et al. 2002) for the asteroid reflectance at each wavelength is

$$Reflectance_\lambda \ (asteroid) \ = \ \frac{Flux_\lambda \ (asteroid)}{Flux_\lambda \ (standard \ star)} \ \times \ \frac{Flux_\lambda \ (standard \ star)}{Flux_\lambda \ (Sun)} \qquad (1)$$

where $Flux_\lambda$ of an object is the number of measured photons at a particular wavelength for that object. A discussion of asteroid observing techniques can be found in Gaffey et al. (2002). Corrections also may also have to be made for phase reddening for observations at high phase angle. At higher phase angles, the spectra of asteroids become redder (e.g., Luu and Jewitt 1989, 1990; Michelsen et al. 2006).

At wavelengths near 3 μm (or shorter wavelengths for NEAs), the thermal flux from objects in the asteroid belt can become a significant fraction of the total flux and must be modeled and removed to give a true idea of the reflectance spectrum. The specifics of how much thermal flux is emitted depends critically on variables such as solar distance at the time

of observation, as well as fixed values such as diameter and albedo; however, for most main-belt low-albedo asteroids, the thermal contribution is 1-10% of the total flux at 3.1-3.5 μm. A "Standard Thermal Model" (STM) for asteroids was formulated by Lebofsky et al. (1986) for use with 3-μm observations.

Rivkin et al. (2005) found that NEAs can have a noticeable thermal flux at ~2.5 μm at perihelion. The thermal flux of these objects can then be modeled to constrain their albedos. Thermophysical models (Lebofsky and Spencer 1989; Harris and Lagerros 2002) including values for thermal inertia and rotation rate have been developed, as well as refinements to the STM for NEAs. Because the uncertainty in the thermal contribution is normally much smaller than the observational uncertainties at 2.95 μm, where 3-μm feature band depths are typically calculated, the uncertainties in the thermal flux are normally neglected in band depth measurements. Thermal effects do affect the band shape beyond 3.1 μm, and typically the preferred thermal model is one which gives a continuum slope at the long-wavelength end of the 3-μm band consistent with the continuum slope shortward of 2.5 μm.

Interaction of photons with a surface

As a photon strikes a mineral grain, the photon is either absorbed, reflected from the grain surface, or it passes through the grain (Clark 1999). For a single grain, photons are absorbed according to Beer's law, $I = I_o e^{-kx}$, where I is the observed intensity, I_o is the original light intensity, k is the absorption coefficient, and x is the distance traveled through the grain. The absorption coefficient varies according to wavelength and is different for different minerals. The degree to which photons are absorbed at a particular wavelength by a mineral grain is a function of the size of the grain and its absorption coefficient at that wavelength. A larger grain has a higher probability of absorbing a photon than a smaller grain. A grain with a higher absorption coefficient at a particular wavelength will tend to be more absorbing than a grain with a smaller absorption coefficient, which means that darker grains tend to be more absorbing than grains of lighter colors.

Asteroidal surfaces are composed of different mineral grains. The photons that are scattered (reflected from a grain's surface or refracted through a grain) may either encounter another grain or be scattered away from the surface. The photons scattered away from the surface can be detected and measured by a telescope. Because the grains are at a finite temperature, they will also emit photons, but most of these photons have wavelengths in the mid-IR. The relative abundance of mineral phases does not correlate directly with the spectral abundance for intimate mixtures. As shown by the spectral reflectance model derived by Hapke (1981), the reflectance of a mixture is a function of viewing geometry and properties of the grains, such as the single scattering albedo (efficiency of an average particle to scatter and not absorb light), porosity, diameters, and mass fractions (Mustard and Pieters 1989). The single scattering albedo is the ratio of the scattering coefficient to the sum of the absorption and scattering coefficients. Hapke (1981) modeling (e.g., Clark 1995; Clark et al. 2004a) has been used to try to derive the mineralogies of a number of asteroids. The visible-NIR spectrum of a mixture will generally be dominated by the species that is most absorbing at those wavelengths (e.g., Gaffey 1976). For example, a very small abundance of opaque material will tend to dominate the spectrum and suppress absorption features due to other minerals. Pyroxene tends to be more absorbing than olivine, so it will spectrally dominate any olivine-pyroxene mixture unless the mixture is predominantly olivine.

ABSORPTION BANDS

Electronic absorption features

Visible and near-IR spectra are dominated by electronic absorption features that are primarily due to the absorption of photons by electrons associated with different transition

elements, e.g. Fe, Ni, Co, Cu, Ti, and Cr (e.g., Gaffey et al. 1989; Dyar and Gunter 2007) in a variety of different minerals. Crystal field bands result from the absorption of photons by electrons, which allows the electrons to jump to higher-energy orbitals; these transitions tend to be the most diagnostic of different mineral species (Burns 1993). Orbitals are mathematical constructs and only approximate the wave functions for atoms with more than one electron (Scerri 2000). This section will assume that a single-electron model, as discussed in Burns (1993), can be applied to a three-dimensional electron system.

The position, strength, and structure of crystal field features vary according to the coordination number of each transition metal and the geometry of the site it occupies. In meteorites, Fe^{2+}, Fe^{3+}, Ti^{4+}, and Cr^{3+} are the most common transition metal cations, though bands resulting from Ti^{3+}, Mn^{2+}, Mn^{3+}, and Ni^{2+} are sometimes observed. The presence of Fe^{2+} typically causes the strongest absorption features of the transition elements in the visible and near-IR wavelength regions. Olivine and pyroxene (Fig. 5) have very distinctive absorptions in the visible and near-IR due to Fe^{2+}.

First-series transition metals are defined on the basis of having unfilled $3d$ electron orbitals (Burns 1993). The five $3d$ orbitals fall into two distinct groups on the basis of the relationship of their lobes to the x, y, and z axes: the t_2 or t_{2g} orbitals (d_{xy}, d_{yz}, d_{xz}), and the e or e_g orbitals ($d_{x^2-y^2}$, d_{z^2}). If an ion is isolated (i.e., as when floating around unbonded), all of these orbitals are perfectly shaped. When a transition metal is incorporated into a mineral structure, the surrounding anions (oxygens) usually do not form a perfectly spherical distribution of charge around the cation. Instead, the charge is unevenly distributed, with the negative charge being concentrated in the vicinity of the anions at the polyhedral corners. The effect of this non-spherical charge distribution is to destroy the degeneracy, so that the energies of all the orbitals are no longer equal. The electrons in the $3d$ orbitals that are close to the oxygen neighbors are repelled more strongly than those that are farther away from the oxygens. Thus, the energies of the formerly equivalent $3d$ orbitals change—they effectively split. Some will have higher energies (those close to the bonding oxygens) and some will have lower energies (those whose lobes point to areas that are oxygen-free). The difference in energy between the lowest orbitals and the highest orbitals is called crystal field splitting and is represented by the symbol Δ (or sometimes, $10Dq$). The energies of the Δ values are dependent on many factors, including the symmetry and coordination number of the coordination polyhedra; the valence state of the cation; the strength of its bond with the surrounding anions; the distance between the cation
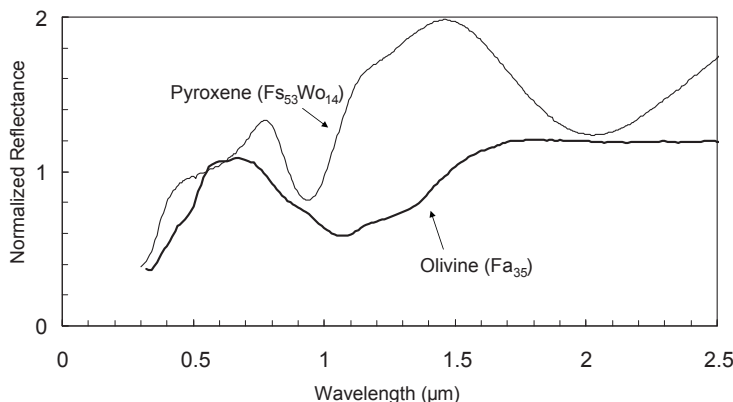
Figure 5. Reflectance spectra of olivine and pyroxene. Olivine spectrum is for EET 99402 (Fa_{35}) (brachinite) (Burbine et al. 2006). Pyroxene spectrum is for Bouvante (eucrite) ($Fs_{53}Wo_{14}$) (Burbine et al. 2001). Spectra are normalized to unity at 0.55 μm.

and the surrounding anions; pressure; and temperature. Within any given mineral group, crystal field splitting energies may also vary as a function of composition, with larger cations tending to move the absorption band minima to longer wavelengths.

The effect of temperature is important to consider when comparing meteorite or mineral spectra to asteroid spectra, since most meteorites and minerals are measured at room temperature while the surface temperatures of main-belt asteroids are much colder (~120-220 K) (Hinrichs et al. 1999). Singer and Roush (1985), Roush and Singer (1987), Moroz et al. (2000), and Sunshine et al. (2000) showed that, with decreasing temperature, the absorption features tend to narrow and band positions generally move to lower wavelengths, with the opposite trends observed with increasing temperatures. These effects are predicted by crystal field theory (Burns 1993), since the thermal motions of atoms should decrease for lower temperatures and, therefore, fewer vibrational modes are available.

The intensities of the crystal field bands are related to the probability that electronic transitions will occur. Spin-allowed transitions do not change the number of unpaired electrons. Spin-forbidden transitions result in a change in the number of unpaired electrons and are much less likely to occur than spin-allowed transitions (Burns 1993). For example, Fe^{2+} would have four unpaired electrons and one pair of electrons before and after a spin-allowed transition while Fe^{2+} would have four unpaired electrons and one pair of electrons in its *3d* orbitals before the transition and could have two unpaired electrons and two pairs of electrons its *3d* orbitals after a spin-forbidden transition. Spin-allowed transitions are much stronger than spin-forbidden ones.

Absorptions can also occur as a result of charge transfer between adjacent cations, in a manner similar to crystal field splitting, except instead of electrons jumping between *orbitals* within the same atom, electrons jump between *atoms*. These intervalence transfers of charge can create intense absorptions from very small numbers of shared electrons. For example, Fe^{2+} and Fe^{3+} ions in adjacent sites pass an electron back and forth. At one instant, the charge is distributed as Fe^{2+} and Fe^{3+}, and the next instant it is Fe^{3+} and Fe^{2+}. The resultant transitions are intense and significantly wider than crystal field bands.

Another type of electronic absorption feature occurs because some minerals, such as sulfides, have two energy levels in which electrons can reside (e.g., Clark 1999). The higher energy level is called the "conduction band," where electrons can move freely. The lower energy level is called the "valence band," where electrons are attached to individual atoms. The difference between the energy levels is called the band gap.

Olivine. Olivine most commonly occurs as a magnesium-iron silicate with the formula $(Mg,Fe^{2+})_2SiO_4$ with minor substitution by Ca, Mn, Fe^{3+}, and Ni. The two endmember compositions are termed fayalite (Fa), Fe_2SiO_4, and forsterite (Fo), Mg_2SiO_4. Olivine compositions are usually given in terms of mole percentages of one of these endmembers. The divalent cations in the olivine structure occupy two different six-coordinated sites that are designated as M1 and M2. The M1 site is smaller than the M2 site by ~0.03-0.05 Å and is the more distorted of the two sites. The M1 site is a tetragonally-elongated octahedron (Burns 1993). The resultant site distortion creates a split in the energies of the two e_g orbitals, giving rise to two distinctive absorptions in the visible region with absorptions at roughly 0.9 and 1.25 μm (~11,000 cm^{-1} and ~8000 cm^{-1}). The M2 site is more like a trigonally elongated octahedron, and this distortion results in the two e_g orbitals being similar in energy. Thus, although there are again two possible transitions to e_g orbitals, their energies (and wavelengths) are so similar (~1.13 and ~1.08 μm, or ~8830 and ~9270 cm^{-1}, respectively) (Burns 1985) that only a single M2 absorption feature is usually observed at ~1.1 μm (~9000 cm^{-1}). Substitution of Fe^{2+} for Mg moves the positions of all three olivine bands to longer wavelengths (e.g., Sunshine et al. 1998).

A number of meteorites have distinctive olivine absorption features (**Fig. 6**). Brachinites are olivine-dominated meteorites containing over ~70 wt% olivine, with compositions of
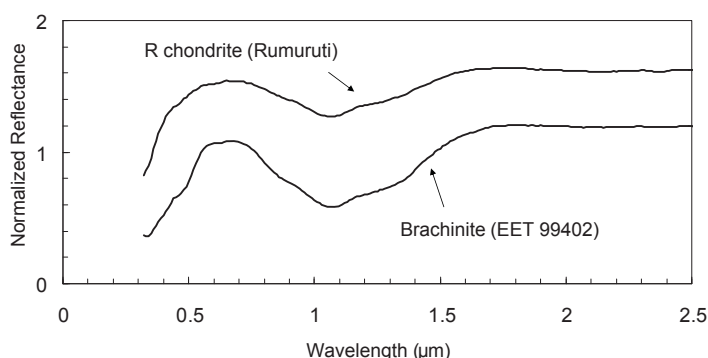
Figure 6. Reflectance spectra of a brachinite (EET 99402) (Burbine et al. 2006) and an R chondrite (Rumuriti) (Burbine et al. 2003). Reflectance spectra are normalized to unity at 0.55 μm and then offset in reflectance by 0.5.

Fa_{30-35} (Mittlefehldt et al. 1998). R chondrites contain about 58-75 vol% olivine, with compositions typically Fa_{37-40} (Brearley and Jones 1998). Pallasites are approximately 50-50 mixtures of olivine and FeNi metal, with olivine compositions between Fa_{10} and Fa_{20} (Mittlefehldt et al. 1998), but very little reflectance spectra of unweathered samples have been obtained on pallasites.

Ni^{2+} can substitute for Mg^{2+} in olivine and can change the spectral properties of olivine (Wood 1974; King and Ridley 1987; Burns 1993). Ni^{2+} has an absorption band centered near 0.7 μm, which causes the reflectance maximum between the UV and 1 μm absorption features to move to shorter wavelengths. The wavelength position of this ~0.7 μm absorption band is dependent on the concentration of Ni in the olivine (e.g., Burns 1993). The presence or absence of Ni in olivine can give information on the initial oxidation state of the assemblage (Gaffey 1998). Olivine in R-chondrites, which formed under relatively oxidizing conditions, tends to be Ni-rich compared to that in other meteorites (e.g., Schulze et al. 1994). The R-chondrite Rumuruti, however, which has a mean NiO concentration of 0.19 wt% (Schulze et al. 1994), does not show any noticeable difference in the position of the reflectance maximum between the UV and 1 μm absorption features relative to the brachinite EET 99402, which does not have any detectable NiO (Mittlefehldt et al. 2003).

Olivine is a major component of many different chondritic (ordinary, carbonaceous, R), achondritic (brachinites, lodranites/acapulcoites), and stony-iron (pallasite) meteorite groups. Among chondrites, the most olivine-rich chondrites tend to have the most fayalite-rich olivine, while the least olivine-rich tend to have fayalite-poor olivine (Sunshine et al. 2007). Iron must be oxidized to enter silicates, so relatively oxidizing conditions, which favor the formation of FeO, lead to more fayalitic compositions, while conditions under which Fe metal is stable lead to more forsteritic compositions (e.g., McCammon 2005). Therefore, the fayalite content of olivine in an asteroid can be an important indicator of its oxidation state. Differentiation, however, also can affect the composition of olivine in an asteroid (Sunshine et al. 2007). The earliest silicate melts from the partial melting of a chondrite are enriched in plagioclase and Fe-rich pyroxene. Thus, with continued melting the residue becomes more olivine-rich and more Mg-rich. It may not be possible to distinguish whether an olivine-rich assemblage with moderate fayalite content (~Fa_{20-40}) was an oxidized chondrite or a chondritic assemblage that has experienced low degrees of partial melting (Sunshine et al. 2007).

Pyroxene. The pyroxene-group minerals share the general formula $M2M1(Si_2O_6)$ (Deer et al. 1997), where the M1 site is octahedral and the M2 site is a quite distorted 6- to 8-

coordinated site. The M1 site is thus smaller, and can be occupied by Al, Mg, Fe^{2+}, Fe^{3+}, Cr and Ti, while the M2 site may contain Ca, Na, Mg, Fe^{2+}, Mn^{2+}, Ni and Li. Some substitution of Al for Si in the tetrahedral sites also occurs. Pyroxene compositions are usually given in mole percentages of enstatite (En; $MgSiO_3$), ferrosilite (Fs; $FeSiO_3$), and wollastonite (Wo; $CaSiO_3$). The low-Ca minerals are usually orthorhombic. When more than 10 mol% Ca is added, the structures all become monoclinic, the pyroxenes are termed clinopyroxenes, and are divided into Li, Na, Ca-Na, Ca, Mn-Mg, and Mg-Fe^{2+} subgroups. There is complete solid solution between the Mg and Fe species, but not with respect to Ca. A miscibility gap exists between pigeonite ($(Ca,Mg,Fe)(Mg,Fe)Si_2O_6$) (low-Ca clinopyroxene) and augite ($(Ca,Na)(Mg,Fe,Al)(Al,Si)_2O_6$) (high-Ca clinopyroxene) (e.g., Longhi and Bertka 1996). When Ca completely fills the M2 sites and Ca makes up more than half of the M-site cations, the pyroxene structure itself is no longer stable because the additional Ca cannot fit into the M1 site. Such minerals are pyroxenoids and are members of the wollastonite group.

In pyroxene, the M1 site is barely distorted; its geometry is that of a nearly perfect octahedron. Crystal field bands arising from Fe^{2+} in M1 sites are similar in nearly all pyroxene-group minerals; they occur in pairs around 1.18 μm (8475-8500 cm^{-1}) and 0.93-0.98 μm (10,200-10,700 cm^{-1}) (e.g., Adams 1975; Cloutis and Gaffey 1991; Straub et al. 1991; Burns 1993; Schade et al. 2004). These bands have been well-studied in pyroxenes such as $CaFeSi_2O_6$ (hedenbergite), where Fe^{2+} occurs solely in the M1 site because the M2 site is filled by Ca. Such high-Ca pyroxenes are usually called "type A." These spectral properties can be seen in the spectra of some angrites (Burbine et al. 2006) (Fig. 7). Angrites are composed predominately of Al-Ti diopside-hedenbergite, Ca-rich olivine (including sub-calcic kirschsteinite; $CaFeSiO_4$), and anorthite ($CaAl_2Si_2O_8$) (Mittlefehldt et al. 2002). (Diopside has the formula $CaMgSi_2O_6$). The exception is Angra dos Reis, the type specimen of the angrites. The Angra dos Reis meteorite is composed almost entirely of Al-Ti diopside-hedenbergite (Prinz et al. 1977) and has the distinctive pyroxene 1 and 2 μm features (Fig. 7).

The M2 site is far more distorted than M1 because the metal-to-oxygen distances around the M2 site vary considerably with composition. Because site distortion increases the band intensity, pyroxene in which Fe^{2+} has substituted for Ca has bands that tend to dominate the spectra; even when Fe^{2+} is concentrated in the M1 site, bands due to a small amount of Fe^{2+} in the M2 will dominate. The features are typically located at 0.9-1 μm (~9600 cm^{-1}), which is called Band I, and 1.9-2 μm (~4400 cm^{-1}), which is called Band II, in Ca-rich compositions (Burns and Huggins 1973; Burns 1993). These two bands are usually thought to be the
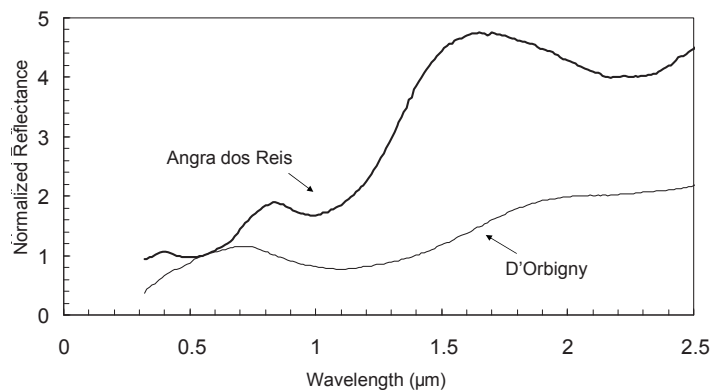
Figure 7. Reflectance spectra of two angrites: Angra dos Reis and D'Orbigny (Burbine et al. 2006). Spectra are normalized to unity at 0.55 μm.

"typical" absorption features for pyroxene. The replacement of larger Ca^{2+} ions by smaller Fe^{2+} ions causes the M2 site to contract slightly and the crystal field bands due to Fe^{2+} in the M2 site to move to shorter wavelengths (Adams 1974; Burns 1993).

These spectral differences are readily apparent when looking at the pyroxene features found in the spectra of HED (howardite, eucrite, diogenite) meteorites (**Fig. 8**). Eucrites are composed primarily of anorthitic plagioclase and low-Ca pyroxene with augite exsolution lamellae, while diogenites are predominately magnesian orthopyroxene (Mittlefehldt et al. 1998). Howardites are polymict breccias containing both lithologic units and are the primary evidence that almost all HEDs come from one parent body, which is thought to be Vesta (McCord et al. 1970).

The band centers for the eucrites, which contain pyroxenes that are generally richer in Ca and Fe than pyroxenes in the howardites and diogenites, tend to be at longer wavelengths than those of howardites and diogenites. The band centers for the diogenites, which contain pyroxenes that are generally depleted in Ca and Fe relative to pyroxenes in the eucrites and howardites, tend to be at shorter wavelengths than other HEDs. Howardites tend to have band positions intermediate between eucrites and diogenites.

Virtually FeO-free enstatite has no distinctive absorption features in the visible or near-IR and is the dominant pyroxene in some meteorite types. Aubrites are composed primarily of this essentially FeO-free enstatite and are distinguished by their lack of distinctive absorption features and very high visual albedos (**Fig. 9**) (Burbine et al. 2002c). Weak absorption features seen in some aubrite spectra are most likely due to terrestrial weathering. Enstatite chondrites are primarily mixtures of FeO-free enstatite and FeNi. As with the aubrites, weak absorption features in enstatite chondrite spectra are also likely due to terrestrial weathering.

FeNi metal. Metallic iron is found in meteorites as either low-Ni kamacite, high-Ni taenite, or an intergrowth of these phases (Mittlefehldt et al. 1998). FeNi metal has moderate albedos (~0.10-0.30), and no absorption features in the visible and near-IR, with a monotonically increasing spectrum (**Fig. 10**) (Cloutis et al. 1990). Although a common constituent of meteorites, it has been difficult to constrain metal abundances of asteroids. This is because there is no obvious correlation between metal abundance and spectral slope, and metal may not be the only cause of the continuum in asteroid spectra. In many studies of asteroid spectra, the continuum is explicitly removed and only the silicate fraction is considered, with the metal fraction ignored. A further complication is the reduction of iron in silicates and the creation of nanophase iron ("space weathering") potentially occurring in asteroid regoliths. The regolith is the surface layer of an asteroid, consisting of fragmentary, incoherent, rocky debris (Price 2004). This causes ambiguity in distinguishing metal-rich mineralogies from space-weathered ones. Contrary to the conclusion of Gaffey (1976), Cloutis et al. (1990) found no correlation between Ni abundance and spectral redness in measured FeNi samples. Cloutis et al. (1990) also found that the spectra of iron meteorites become redder with increasing grain size. One question that has never been fully answered is why FeNi in iron meteorites is spectrally red while FeNi in ordinary chondrites, the most common type of meteorite to fall to Earth, is spectrally flat (Gaffey 1986). H chondrites, which can contain up to ~20% metallic iron, are not spectrally red, while metallic iron separated from ordinary chondrites is spectrally flat (Gaffey 1986). Gaffey (1986) proposed that metal grains in ordinary chondrites are coated with wüstite (FeO).

Feldspars. Feldspars are a series of Al-bearing silicate minerals that are commonly found in meteorites. The ideal chemical formula for feldspar is MT_4O_8 (Smith and Brown 1988). The M site is relatively large and can contain cations such as Na^+, K^+, and Ca^{2+} while the T site contains Si^{4+} or Al^{3+}. Feldspars consist of a three-dimensional network of SiO_4 and AlO_4 tetrahedra with Na^+, K^+ and Ca^{2+} in the voids between the tetrahedra. End-member compositions in the feldspar series are orthoclase ($KAlSi_3O_8$), anorthite ($CaAl_2Si_2O_8$) and albite ($NaAlSi_3O_8$). Plagioclase feldspar comprises a solid solution series between anorthite and albite. The crystal structure of plagioclase allows for the incorporation of only minor
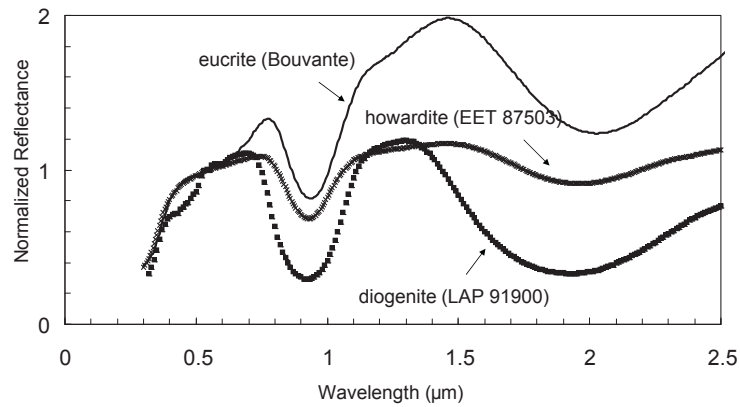
Figure 8. Reflectance spectra of the eucrite Bouvante (Burbine et al. 2001), howardite EET 87503 (Hiroi et al. 1995), and the diogenite LAP 91900 (Burbine et al. 2000). Spectra are normalized to unity at 0.55 μm.
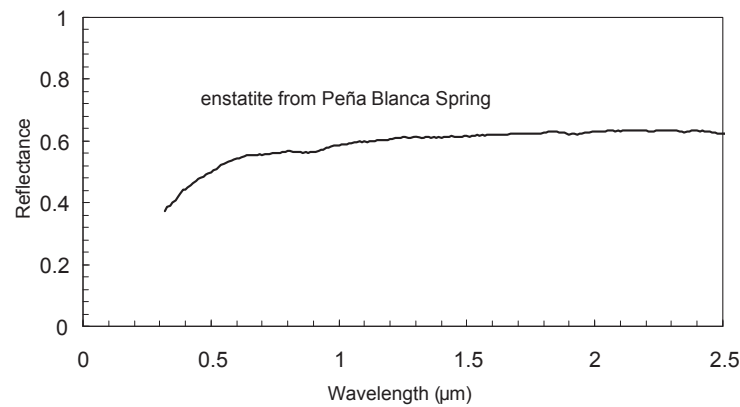
Figure 9. Reflectance spectrum of enstatite from the Peña Blanca Spring aubrite. Spectrum is not normalized to unity at 0.55 μm.
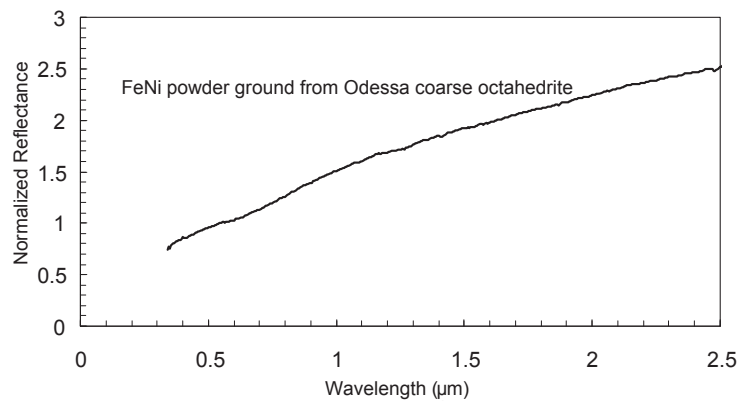
Figure 10. Reflectance spectrum of FeNi powder ground from the Odessa coarse octahedrite (Cloutis et al. 1990). Spectrum is normalized to unity at 0.55 μm.

amounts of Fe^{2+}. Pure samples have a relatively high albedo and an absorption band due to the electronic transition of Fe^{2+} centered between 1.2 and 1.3 μm (Fig. 11). This signature is quickly overpowered in the presence of even small amounts of mafic minerals, however. Thus, plagioclase is difficult to identify in mineral mixtures (Crown and Pieters 1989).

The spectral presence of plagioclase has been attributed to an absorption feature found between 1.2 and 1.3 μm in the spectra of eucrites, which usually contain 30-50 wt% plagioclase (Kitts and Lodders 1998). Klima et al. (2007), however, found that spectral measurements of pure synthetic pyroxenes have a band centered between 1.2-1.3 μm, which they attribute to Fe^{2+} in the M1 site.

Spinels. Spinels are a group of minerals with the general formula of XY_2O_4, where X has a charge of +2 and Y has a charge of +3. Spinels found in meteorites include spinel *sensu stricto* ($MgAl_2O_4$), hercynite ($FeAl_2O_4$), magnetite (Fe_3O_4), and chromite ($FeCr_2O_4$). Mao and Bell (1975) saw that spinel and chromite have an absorption feature centered near 2 μm (Band II) and a weak to non-existent one at 1 μm (Band I). A spectrum of spinel is displayed in Figure 12. Mao and Bell (1975) attributed the 2-μm absorption to octahedral Fe^{2+}. A weaker absorption between 0.6 and 0.7 μm was attributed to spin-forbidden bands of tetrahedral Fe^{2+}. Cloutis et al. (2004) did a spectral study of spinel, hercynite, and chromite from 0.3 to 26 μm. They found a large number of spectral features with some of the band positions of the features correlating with Fe^{2+}, Fe^{3+}, Cr, Mg, or Al contents. Rajan and Gaffey (1984) measured the reflectance spectra of CAIs in the CV chondrite Allende and found that CAIs tend to have a strong Band II and a very weak Band I. They attributed these spectral properties to either spinel and/or a Ti-rich augite (a type A pyroxene). Cloutis and Gaffey (1993) and Cloutis (2001) have done spectral studies of minerals commonly found in CAIs.

Sulfides. Troilite (FeS) is the most common sulfide in meteorites. Other sulfides found in meteorites include oldhamite (CaS), ferromagnesian alabandite ((Mn,Fe,Mg)S), and daubréelite ($FeCr_2S_4$). Sulfides tend to have a very sharp absorption feature in the visible wavelength region (Fig. 13), due to the movement of electrons between the conduction and valence bands. The sulfide with the strongest absorption band is oldhamite (Burbine et al. 2002c), which has strong absorption features at ~0.5 μm and ~0.9 μm. Oldhamite is commonly found in aubrites and enstatite chondrites. Troilite (Burbine et al. 2002c) has a very weak absorption feature in the ultraviolet and usually is treated as an opaque due to its low albedo.

Vibrational absorption features

Photons can also cause molecules to be promoted into vibrational states of higher energies. Water and hydroxyl-bearing minerals have diagnostic features throughout the IR due to vibrational absorptions of H_2O or OH (hydroxyl). Water is a V-shaped molecule with hydrogen atoms at the end of its arms and an oxygen atom at the intersection of the arms (see Criss and Farquhar 200X). The water molecule can undergo three types of vibrations (Gaffey et al. 1989): a bend where the V opens and closes, which occurs at a wavelength of ~6.08 μm; a symmetric stretch where the arms both lengthen or shorten together, which occurs at ~3.05 μm; and an asymmetric stretch, where one arm lengthens or shortens, which occurs at ~2.87 μm. For hydroxyl-bearing minerals, the bond between oxygen and hydrogen can only lengthen or shorten, so absorptions occur at ~2.87 μm. Sulfates also have a number of vibrational absorption bands due to stretching and bending of SO_4 and possibly OH and/or H_2O ions (Cloutis et al. 2006).

A 3-μm absorption feature in hydrated minerals is typically caused by a combination of the very strong OH-radical absorption feature and the very strong first overtone of the 6.08-μm H_2O fundamental at 3.04 μm. Overtones occur at higher frequencies (shorter wavelengths) and are integer multiples of the fundamental frequencies. Adsorbed water has a symmetric stretch mode giving rise to an absorption feature at ~3.05 μm and an anti-symmetric stretch feature at ~2.87
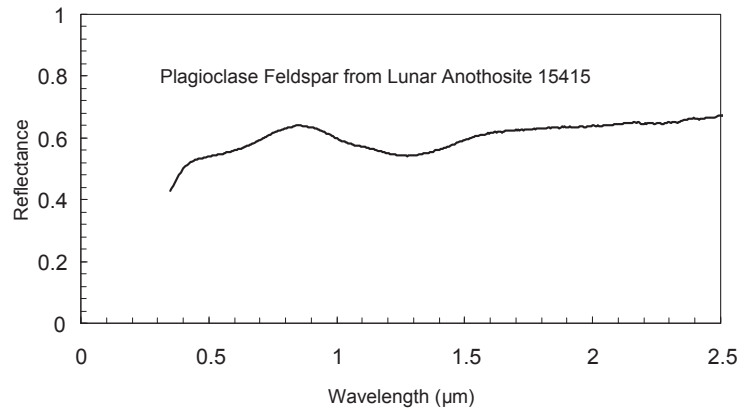
Figure 11. Reflectance spectrum of plagioclase feldspar (An$_{97}$) from lunar anorthosite 15415 (Pieters 1996). Spectrum is not normalized to unity at 0.55 μm.
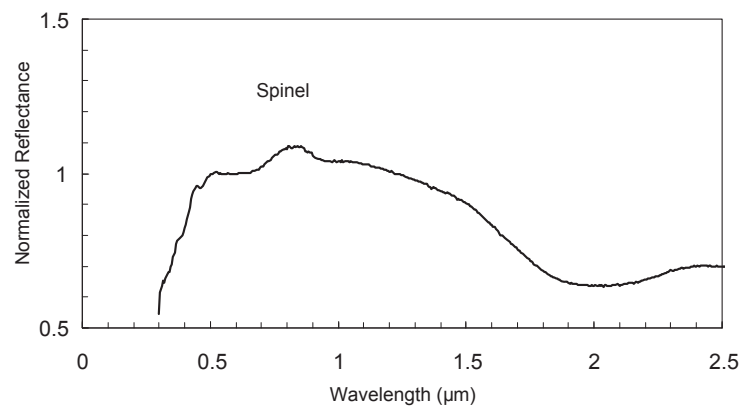
Figure 12. Reflectance spectrum of spinel from Ambatomaninty, Madagascar (Cloutis et al. 2004). Spectrum is normalized to unity at 0.55 μm.
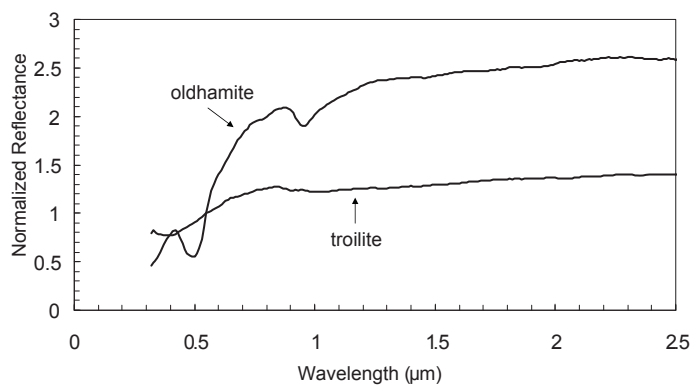
Figure 13. Reflectance spectra of troilite from the Paragould LL5 chondrite and oldhamite from the Norton County aubrite (Burbine et al. 2002c). Spectra are normalized to unity at 0.55 μm.

μm. Structural hydroxyl (OH) that has been incorporated into mineral lattices produces a stretch absorption at ~2.7 μm. The depth of the fundamental H_2O or OH feature depends on many parameters besides the abundance of hydrated material, including particle size and albedo.

Phyllosilicates. Phyllosilicates are composed of sheets of interconnected six-member rings of SiO_4 tetrahedra (e.g., Burns 1993). Phyllosilicates contain hydroxyl (OH⁻) ions in their crystal structure. Phyllosilicates in meteorites (Rubin 1997a) include those in the serpentine group such as cronstedtite, greenalite, and antigorite. Phyllosilicates in meteorites also include clay group minerals such as montmorillonite and saponite. Clays contain H_2O as well as OH⁻. These minerals have silicon:oxygen ratios of 2:5, as three of the four oxygens from each tetrahedron are shared with other tetrahedra.

Phyllosilicates are commonly found in CI, CM, and CR chondrites. The spectrum of a CM chondrite, whose 3-μm feature is primarily due to OH in phyllosilicates, is shown in Figure 14. Both Mg-rich (King and Clark 1989; Calvin and King 1997) and Fe-rich (Calvin and King 1997) phyllosilicates have distinctive spectral absorption features; however, these absorption features tend to be subdued in carbonaceous chondrites due to the high proportion of opaques in these meteorites. Water abundances as low as fractions of a weight percent are observable using 3-μm spectroscopy in the laboratory (Salisbury et al. 1991). Higher-order overtones at shorter wavelengths (1.4 and 1.9 μm) are masked more easily by opaques than the 3-μm feature (Clark 1981), and they are not always seen, even in freshly-fallen phyllosilicate-bearing meteorites (Hiroi et al. 2001b).
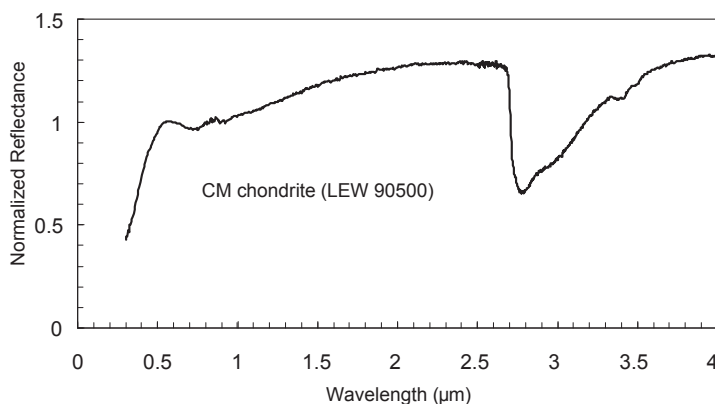
Figure 14. Reflectance spectrum of LEW 90500 CM chondrite (Hiroi et al. 1996b) out to 4 μm. Spectrum is normalized to unity at 0.55 μm.

Determining water contents. Techniques to quantify the amount of OH or hydrogen present on asteroidal surfaces have been developed as a means of comparing the astronomical observations to laboratory studies of meteorites. The first connections between spectroscopy and amount of hydrated minerals were made by Miyamoto and Zolensky (1994), who correlated the H/Si ratio to the integrated intensity of the 3-μm band, and by Sato et al. (1997), who correlated the integrated intensity to two spectral ratios, respectively. Rivkin et al. (2003a) combined these two correlations to determine a relation between spectral ratios and the H/Si ratio and applied it to C-complex asteroids, finding a bimodal distribution of CM-like values and anhydrous objects. (The C-complex contains C-types and objects with similar spectra.) An independent effort by Milliken and Mustard (2005) involving the calculation of normalized path lengths shows promise of being applicable to a wide range of materials, whereas the relations of Rivkin et al. (2003a) are technically only valid for carbonaceous chondrite-like surfaces.

Due to the difficulties of observing in the 3-μm region compared to the visible and near-IR, there has been great effort put toward identifying and establishing an alternate way to detect and measure hydrated minerals on asteroids using proxy bands. Observations by Feierberg et al. (1985) established that the 0.35-0.4 μm spectral slope in low-albedo asteroids was correlated with the 3-μm band depth. This slope is due to an inter-valence charge transfer band (IVCF) in ferric oxide. However, this correlation was not seen to extend to higher-albedo objects that have the 3-μm band. Furthermore, with the popularity of red-optimized CCDs for spectral work over photometers, the 0.35-0.4 μm region is not commonly used and would not confer much advantage over observations in the 3-μm region.

A more promising proxy band is found near 0.7 μm, attributed to a charge transfer absorption involving Fe^{2+} and Fe^{3+} (Vilas and McFadden 1992; Vilas 1994; Fornasier et al. 1999). This band is seen in some phyllosilicates and some carbonaceous chondrites, though not all. It also appears in some anhydrous terrestrial minerals (King and Clark 1997). Cases where the 3-μm band is present but the 0.7-μm band is absent are interpreted as due to the fact that the 0.7-μm band is more sensitive to heating, as shown by Hiroi et al. (1996b). Such objects may have been mildly heated, to the extent that the carrier of the 0.7-μm band is destroyed but some OH still remains. More difficult to understand are objects for which a 0.7-μm band is seen without a 3-μm band. Howell et al. (2001a,b) have shown that those objects display evidence of rotational variation in the 0.7-μm region and uneven coverage by hydrated minerals. Without simultaneous observations in both of these wavelength regions (which can be very difficult to arrange), no definitive answers can be given, but the observations are consistent with the 3-μm and 0.7-μm observations sampling parts of an asteroid with different hydration states. In brief, the presence of a 0.7-μm band almost guarantees the presence of a 3-μm band, while the absence of a 0.7-μm band is not diagnostic for the absence or presence of a 3-μm band.

SPACE WEATHERING

Remote sensing methods, for the most part, do not sample the pristine rocks of the body, but rather the exposed regolith. Exposure to the harsh space environment can alter the physical and optical properties of the regolith in subtle, but important ways, and it is critical to understand these changes in order to properly interpret remote sensing datasets. The term "space weathering" is generally used to describe both the processes and products by which physical and optical changes are incurred by an exposed surface. Solar wind implantation and sputtering, and the melting and vaporization associated with micrometeorite bombardment are the major components of space weathering.

The soil samples returned from the Moon by the Apollo program provide us with a unique opportunity to study the effects of soil formation in the laboratory, and thus our current understanding of space weathering comes largely from lunar soils. There are two major space weathering products found in lunar soils: agglutinates, and grain rims. Agglutinates are glass-welded aggregates created by melting due to micrometeorite impacts (Fig. 15). They are ubiquitous in lunar soil, accounting for as much as 60% of very mature soils (McKay et al. 1991). Grain rims, like the one shown in Figure 16, can be created by both subtractive (radiation damage) and additive (vapor deposition and solar wind sputtering) processes (Keller and McKay 1993, 1997; Wentworth et al. 1999). These rims are quite common in mature lunar soils, with up to 90% of grains bearing rims (Keller et al. 2000).

Effect of space weathering on reflectance spectra

Both rims on grains and agglutinates commonly contain single-domain metallic iron particles that are usually called nanophase iron ($npFe^0$). $npFe^0$ has distinct and predictable effects on the optical properties of lunar soils (e.g., Pieters et al. 1993, 2000; Taylor et al. 2000). The effects on spectra in the visible/near-IR region have traditionally been described as
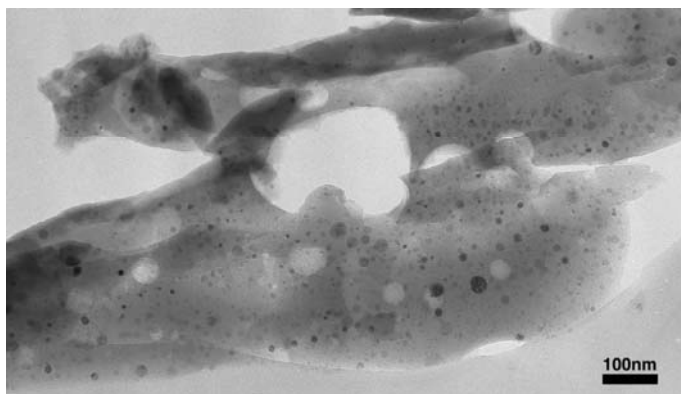
Figure 15. TEM (Transmission Electron Microscope) image of a
nanophase iron-rich agglutinate from lunar soil 10084.
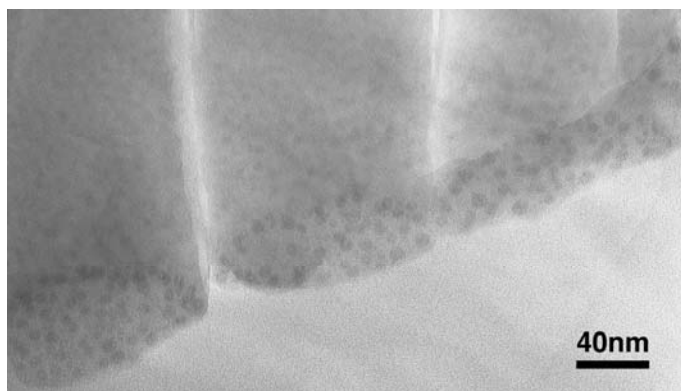
Figure 16. TEM image of a nanophase, iron-rich, vapor-deposited rim
on a cristobalite (SiO_2) grain from lunar soil 10084.

threefold: $npFe^0$ results in an attenuation of the characteristic absorption bands, and also causes the reflectance spectra to darken and redden. The process is actually more complex than simply "reddening" and "darkening", however; as a soil acquires $npFe^0$, its continuum changes in a regular and predictable way (Noble et al. 2001). These trends, first noticed in the finest fractions of lunar soil, are illustrated in Figure 17. Very small amounts of $npFe^0$ result in a steep curvature in the visible while longer wavelengths remain relatively flat (stage 1). As more $npFe^0$ is added, the spectrum remains concave, but becomes very red throughout the visible/near-IR range (stage 2). From this point the spectrum becomes increasingly linear and begins to darken (stage 3), eventually ending up very dark (stage 4—though natural lunar soils never reach this stage). These stages have also been seen experimentally (Allen et al. 1996; Noble et al. 2003) and have been modeled (Hapke 2001). Hendrix and Vilas (2006) found that space weathering causes the spectra of asteroids to appear bluer at near-ultraviolet wavelengths, in contrast to the reddening that occurs at longer wavelengths. Space weathering is complex, and the exact weathering effects of these various processes will be dependent on both composition and environment, and thus will vary from body to body. For silicate materials, we can extrapolate what we have learned from lunar space weathering and apply that knowledge to silicate asteroids. Much less is known about space weathering of carbonaceous material.
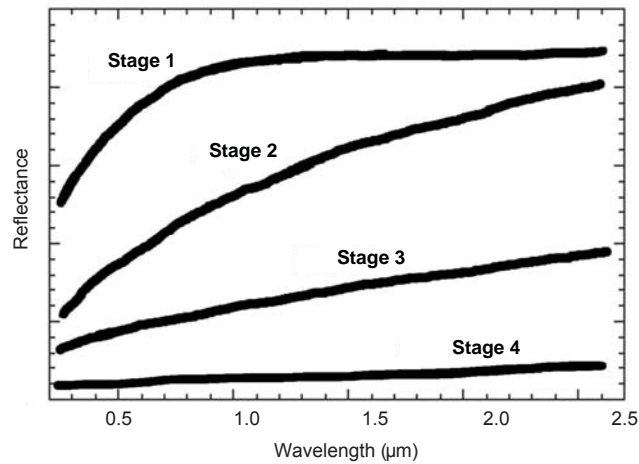
Figure 17. Schematic diagram of the weathering trends seen
in the visible and near-IR spectra of lunar soils.

Space weathering environment of asteroids

The space environment at the asteroid belt is significantly different than at the Moon. In particular, the greater distance from the Sun means that less solar wind reaches asteroids in the main belt, and therefore, less sputtering should occur, and the lower average impact velocity should result in less melting and vaporization as compared to the Moon. Given those conditions, the rate of space weathering is expected to be significantly slower than the lunar case. Though the velocity of impacts is lower, the rate of impact is greater in the asteroid belt as compared to lunar conditions. Therefore, the turnover rate for soils at the surface should be higher and weathering products will not build up as they do in lunar soils. Alteration of silicate asteroid regoliths then should be most similar to the stage 1 described above, with reddening concentrated in the visible region of the spectrum.

Experimental studies

In recent years, several groups have tried to re-create space weathering in the laboratory using either ion irradiation to simulate the solar wind, or lasers to simulate micrometeorite impacts. The classic sputtering experiments were performed by Hapke in the 1970s (Hapke 2001), but more recent experiments have used a variety of techniques on a variety of materials to expand our knowledge of ion-induced alteration. Strazzulla et al. (2004) irradiated an H5 meteorite with Ar^{++} ions and concluded that, for NEAs, solar wind irradiation may be a very efficient process, with the ability to alter OC material to S-complex spectra on timescales of 10^4-10^6 yr. (The S-complex contains S-type asteroids and objects with similar spectral properties.) Further work (Brunetto and Strazzulla 2005; Marchi et al. 2005a) also suggests that not only $npFe^0$, but the simple amorphization of the uppermost layer can redden and darken asteroidal surfaces. Recently, Moretti et al. (2006) tried to duplicate the effects of micrometeoroid impacts on the reflectance spectra of ordinary chondrites.

Moroz et al. (1996) was the first to attempt to simulate micrometeorite bombardment using lasers. Unfortunately, it was found that the pulse length of their laser was too long, resulting in more material melting than vaporizing in their experiments. Spectral changes in their samples resulted largely from the creation of glass phases. Sasaki et al. (2001) developed a system utilizing a Nd-YAG (λ = 1064 nm) laser capable of nanosecond pulses, which more closely mimic the vaporization associated with micrometeorite bombardment. TEM

(Transmission Electron Microscopy) analyses of their samples confirm the production of $npFe^0$ from both olivine and pyroxene. Furthermore, it was demonstrated that it is more difficult to redden the spectrum of pyroxene than olivine in this manner (Yamada et al. 1999). Hörz et al. (2005) point out, however, that lasers cannot reproduce the shock conditions of actual impacts and little is known about shock-induced vaporization. Recently, alteration experiments on powdered silicates using a UV excimer laser were performed by Brunetto et al. (2006a). Their results also show reddening and darkening, but they attribute these alterations to changes in the morphological structure of the sample surface rather than the creation of $npFe^0$. Vernazza et al. (2006b) were able to redden and darken the Bereba eucrite using ion irradiation.

A few ion irradiation and laser experiments have also been performed on carbonaceous material. Moroz et al. (2004a) found that complex organics, which are spectrally red by nature, lose their red slope when exposed to ion irradiation, due to irradiation-induced carbonization. Ion irradiation of carbonaceous chondrites (Lazzarin et al. 2006) reddened their spectral slope. Laser experiments were performed by Moroz et al. (2004b) on a CM2 chondrite using a Nd-YAG laser with a microsecond pulse duration. Their results (Shingareva et al. 2004) produced significant melting and vitrification (conversion into glass) of their samples. The resulting spectra (Moroz et al. 2004b) showed dehydration, an overall smoothness, and a red spectral slope.

Evidence of space weathering on asteroids

There is growing evidence of space-weathering alteration of S-complex asteroids. Images from the Galileo spacecraft appear to show color changes with time on the asteroids Ida and Gaspra, i.e., fresh craters appear "bluer" than older surfaces, exactly the effect predicted from space weathering models (Chapman 1996). Binzel et al. (1996) demonstrated using SMASS data that, among S-complex NEAs, a continuum exists from bodies that spectrally resemble ordinary chondrites to those with classic S-complex spectra. This result is also consistent with an ongoing alteration process. Spacecraft data for S-type 433 Eros suggest that it is compositionally an ordinary chondrite (Trombka et al. 2000). A recent study by Nesvorny et al. (2005) found, using SDSS data, that over time the spectra of S-complex asteroids become redder and their absorption bands become shallower. Brunetto et al. (2006b) estimated that the time needed to space-weather asteroid 832 Karin is similar to the age (~5.8 Ma) estimated for the formation of the Karin asteroid family (Nesvorný and Bottke 2004). A spectral study of Karin family members by Vernazza et al. (2006a) in the visible and near-IR found that the observed objects had spectral slopes slightly redder than ordinary chondrites, which they argue is consistent with only a small degree of spectral alteration due to the young age of the family.

There have been fewer efforts expended towards understanding space weathering effects on other types of asteroids. Though their age data were limited, the Nesvorny et al. (2005) study did find a correlation between ages and colors for the C-complex asteroids in their survey. Interestingly, it suggests the opposite trend from S-complex objects. Spectra of the C-complex asteroids become "bluer" with age. In addition, Lagerkvist et al. (2005) found that red D-asteroids among the Cybele group (3.3-3.5 AU) tended to be smaller than the more spectrally neutral P-asteroids and C-complex objects. They suggest that this difference may be due to weathering effects where the collisional disruption of the larger (and more "mature") objects creates smaller objects with freshly exposed (redder) surfaces. More work is clearly needed, but these initial studies are consistent in suggesting that carbon-rich material loses redness as it is exposed to the space environment.

Implications for visible/near-IR remote sensing

The biggest consequence of space weathering for interpretation of spectral data for silicates is the attenuation (reduction of strength) of absorption bands. Weaker bands are more difficult to distinguish, and subtle inflections can be lost. Further, bands at different wavelengths may attenuate at different rates. For example, there is evidence that the 1-μm band (Band I) may attenuate faster than the 2-μm band (Band II), impacting the apparent olivine/pyroxene ratio

(Ueda et al. 2002a). Band centers do not generally appear to be influenced by space weathering processes. Weathering will also result in a reddening of the spectral slope, particularly at visible wavelengths. For carbon-rich asteroids, the effects of space weathering are still somewhat unclear, though dehydration, with the accompanying attenuation of water-related bands, is likely to be a major consequence. The amount of weathering required to significantly impact or completely eliminate water-related bands, however, is not well constrained.

ORDINARY CHONDRITES, LODRANITES/ ACAPULCOITES, AND UREILITES

The most common meteorites are the ordinary chondrites (H, L, LL), and identification of their parent bodies has been a significant part of asteroid studies for over 30 years. Ordinary chondrites are primarily mixtures of olivine, pyroxene, and FeNi metal. H (high-iron) chondrites contain the highest abundances of metallic iron, L (low-iron) have lower metallic iron abundances, and LL (very-low iron) have the lowest abundances. The ordinary chondrites follow Prior's Rules (e.g., Hutchison 2004), so the LL chondrites have the highest iron abundances in their silicates, L chondrites have lower abundances, and H chondrites have the lowest. H chondrites usually contain approximately equal percentages of olivine and pyroxene, L chondrites usually contain slightly more olivine than pyroxene, and LL chondrites generally have twice as much olivine as pyroxene.

Pyroxene tends to spectrally dominate any olivine-pyroxene mixture. These effects can be seen in the spectral properties of ordinary chondrites (Fig. 18). H chondrites have the most distinctive pyroxene absorptions while LL chondrites have the most distinctive olivine absorptions, with L chondrites intermediate between H and LL chondrites.

There are a number of other meteorites with distinctive olivine and pyroxene bands. Lodranites/acapulcoites are primarily mixtures of orthopyroxene and olivine and have experienced partial melting (e.g., McCoy et al. 2000). Spectral measurements (Fig. 19) of these meteorites (Hiroi and Takeda 1991; Burbine et al. 2002a) show that their spectra are dominated by orthopyroxene. Besides olivine and pyroxene, ureilites contain 10% or less dark interstitial material that consists of varying amounts of carbon, metal, and sulfides (Mittlefehldt et al. 1998). Ureilites have absorption features (Fig. 19) due to pyroxene and olivine that are subdued in strength (Cloutis and Hudon 2004).
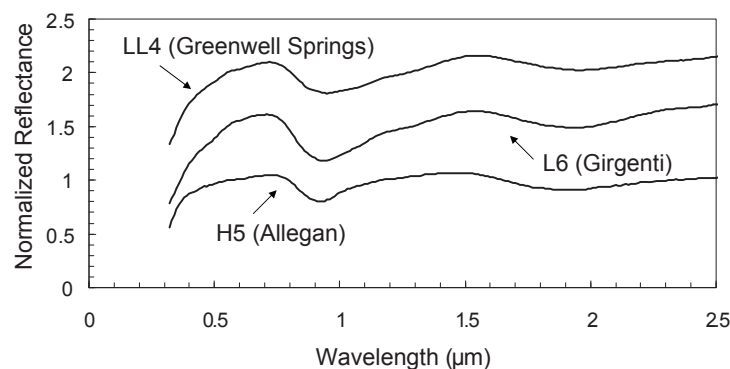
Figure 18. Reflectance spectra of Allegan H5 chondrite, Girgenti L6 chondrite, and Greenwell Springs LL4 chondrite (Burbine et al. 2003). Reflectance spectra are normalized to unity at 0.55 μm and then offset in reflectance by 0.5.
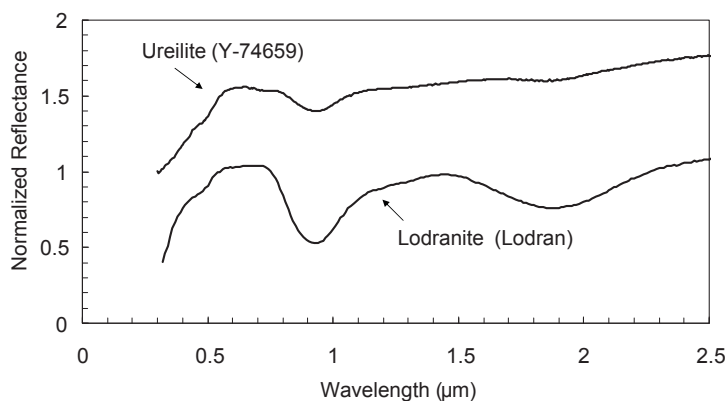
Figure 19. Reflectance spectra of the Lodran lodranite (Burbine et al. 2002a) and the Y-74659 ureilite (Hiroi unpublished). Reflectance spectra are normalized to unity at 0.55 μm and then offset in reflectance by 0.5.

DETERMINING MINERAL CHEMISTRIES

Gaffey et al. (2002) developed a number of formulas for determining average pyroxene compositions from their Band I and Band II centers. Band centers are the band minima observed when the continuum (either red- or blue-sloped) has been divided out. The formulas for molar contents of *Fs* and *Wo*, with uncertainties, are:

$$Fs \ (\pm 5) = 268.2 \times Band \ II \ center \ (\mu m) - 483.7 \quad (Wo < 11) \tag{2}$$

$$Fs \ (\pm 5) = 57.5 \times Band \ II \ center \ (\mu m) - 72.7 \qquad (Wo = 11\text{-}30; Fs < 25 \ excluded) \tag{3}$$

$$Fs \ (\pm 4) = -12.9 \times Band \ II \ center \ (\mu m) + 45.9 \quad (Wo = 30\text{-}45) \tag{4}$$

$$Fs \ (\pm 5) = -118.0 \times Band \ II \ center \ (\mu m) + 278.5 \ (Wo > 45) \tag{5}$$

$$Wo \ (\pm 3) = 347.9 \times Band \ I \ center \ (\mu m) - 313.6 \quad (Fs < 10; Wo \approx 5\text{-}35 \ excluded) \tag{6}$$

$$Wo \ (\pm 3) = 456.2 \times Band \ I \ center \ (\mu m) - 416.9 \quad (Fs = 10\text{-}25; Wo \approx 10\text{-}25 \ excluded) \tag{7}$$

$$Wo \ (\pm 4) = 418.9 \times Band \ I \ center \ (\mu m) - 380.9 \quad (Fs = 25\text{-}50) \tag{8}$$

The values in parentheses after each formula are the compositional ranges where the equation is valid. These formulas were derived from the spectra of minerals, and can only be directly used for reflectance spectra of pyroxene-dominated assemblages with little to no spectral component due to olivine. These formulas work well for predicting the pyroxene mineralogy of assemblages with one pyroxene. For assemblages with low- and high-Ca pyroxenes, Gaffey et al. (2002) argue, from the analysis of the spectra of ordinary chondrites, which contain two pyroxenes, that the Band II position is an almost-linear function of the abundances of these two types of pyroxenes. To calculate the average pyroxene compositions from the spectrum of an olivine-orthopyroxene mixture, the displacement in the Band I center position due to olivine must be corrected for by using a correction factor from Gaffey et al. (2002). The amount of displacement will increase with increasing abundance of olivine.

Determining the ratio of olivine to pyroxene

Cloutis et al. (1986) found that the ratio of the area of Band II (2-μm feature) to the area of Band I (1-μm feature), which is called the Band Area Ratio or *BAR*, was related to the ratio of olivine to orthopyroxene. This ratio is usually written as *ol*/(*ol+opx*) and was derived from the analysis of physical mixtures of olivine and orthopyroxene. The equation can be written as *ol*/(*ol+opx*) = (0.417 × *BAR*) + 0.052 or *ol*/(*ol+opx*) = (−0.417 × *BAR*) + 0.948,

and is valid for the interval 10-90% orthopyroxene (Gaffey et al. 2002). Using the reflectance spectra of primarily ordinary chondrite meteorites, Burbine et al. (2003) derived the equation $ol/(ol+opx) = (-0.228 \times BAR) + 0.768$. The pyroxene component contains both orthopyroxene and clinopyroxene. The mineralogies of Burbine et al. (2003) were determined from CIPW (Cross, Iddings, Pirsson, Washington) norms, which are theoretical mineralogies calculated from bulk elemental compositions. Gastineau-Lyons et al. (2002) noted systematic offsets between modal (mineralogic maps of thin sections) and normative (theoretical calculations of mineralogy) $ol/(ol+opx)$ ratios for meteorites and that CIPW norms may not accurately estimate mineral abundances of silicates in chondrites.

Modified Gaussian Modeling

The Modified Gaussian Model (MGM) is a numerical tool for modeling the component absorption bands in the visible and near-IR spectral regions. Developed by Sunshine et al. (1990), MGM has been demonstrated to be a physically realistic model of electronic transition absorption bands that are well understood from crystal field theory (Burns 1993). The model was created as an improvement over the use of Gaussians to deconvolve the spectra features, which Sunshine et al. (1990) found could not adequately model olivine and pyroxene absorption bands. Sunshine et al. (1990) found that absorption bands were best fit with a modified Gaussian, $m(x)$, which uses a power law such as $m(x) = s \times \exp\{-(x^n\text{-}\mu^n)^2/2\sigma^2\}$, where n was found to be -1 for room temperature measurements.

MGM can be used to model meteorite and asteroid spectra. The spectra are modeled as a number of absorption bands superimposed onto a linear continuum in log reflectance and energy (Sunshine 1997). Due to the overlapping absorption features of minerals commonly found in meteorites and asteroids (low-Ca pyroxene, high-Ca pyroxene, olivine), however, it is difficult to apply MGM to mixtures that are not primarily monomineralic. In addition, asteroid data tend to have lower resolution and larger error bars than laboratory spectra, which leads to more uncertainties in the resulting fits.

Studies using MGM look primarily at the positions and strengths of the fitted absorption bands. MGM has been used to fit the spectral features of minerals (e.g., Sunshine et al. 1990, 2000; Sunshine and Pieters 1993, 1998) and meteorites (e.g., Schade and Wäsch 1999; Schade et al. 2004; Mayne et al. 2006). A number of asteroid spectra have also been fit using MGM for mineralogical analyses (e.g., Hiroi et al. 1996a; Ueda et al. 2002b; Sunshine et al. 2004, 2007; de León et al. 2004, 2006; McFadden et al. 2005) or to determine a ratio of band areas (e.g., Rivkin et al. 2004a). This ratio of band areas is used for objects that do not have full spectral coverage of both Bands I and II, which does not allow for a Band Area Ratio to be determined but does allow for MGM to fit the absorption features. The resulting areas from the MGM fit can be ratioed and appear to be proportional to the Band Area Ratio.

ASTEROID TAXONOMY

Asteroid taxonomies group objects with similar spectral properties into classes with the hope that objects with the same classification have similar surface mineralogies. Most taxonomies are based on extended visible ($\sim$0.4 to $\sim$1.0 μm) reflectance spectra because these data are the easiest to obtain, and mineralogically significant absorption features occur in this wavelength region. Asteroid classifications started as simple systems that classified objects as stony or carbonaceous (e.g., Zellner et al. 1975). The stony and carbonaceous designations evolved into a letter-based system using the S, C, or U (unusual) designations (Chapman et al. 1975). As more objects were observed, more classes (and letters) were used to distinguish between objects with different spectral properties.

The classification system that was most widely used in the late 1980s and 1990s is the asteroid taxonomy developed by Tholen (1984). Tholen (1984) grouped objects into fourteen

classes (**Table 2**) using a minimal-tree analysis of seven colors from eight broad-band filters from 0.34 to 1.04 μm and visual albedo, when available. Most classified asteroids have estimated diameters of 20 km or greater. This classification system was primarily based on the strengths of the UV and 1-μm absorption bands, which were the only features apparent in this spectral region and at this spectral resolution.

The X-class had a wide range of albedos and its members were divided into the E- (high albedo), M- (intermediate albedo), and P- (low albedo) classes. E-, M-, and P-types are generally thought to have experienced distinctly different heating histories, with the E-types linked with the high-albedo and enstatite-rich aubrites, M with metallic iron cores, and P with low-albedo, carbon and/or organic-rich asteroids. All three types of material would be expected to have similar spectral properties when observed using the limited resolution of the ECAS filters, but they would have strongly contrasting albedos.

The drawback with using taxonomic letters that are often derived from the first letter of a specific inferred composition is that it is often assumed that all members of a class have that composition even though the classification just indicates specific spectral properties. The M-class was derived from the word "metallic" because members of this class have spectral properties similar to those of metallic iron, with flat to slightly red, featureless visible spectra and moderate albedos (~0.11-0.30). Many researchers assume that all M-types have metallic

Table 2. A listing of Tholen (1984) and other commonly used classes.

Tholen Class	IRAS Albedo	Spectral Properties in the Visible
A	0.17-0.60	very strong UV feature, strong 1 μm feature
B	0.06-0.16	weak UV feature, blue past 0.4 μm, subclass of C complex
C	0.03-0.20	weak UV feature, flat to reddish past 0.4 μm
D	0.03-0.08	very red spectrum
E	0.50-0.55	flat to slightly red, featureless spectrum, higher albedo than P- and M-types
F	0.03-0.10	very weak UV feature, flat to bluish past 0.4 μm. subclass of C complex
G	0.05-0.11	strong UV feature, flat past 0.4 μm, subclass of C complex
M	0.11-0.30	flat to slightly red, featureless spectrum, albedo between P- and E-types
P	0.02-0.07	flat to slightly red, featureless spectrum, lower albedo than M- and E-types
Q	(0.21)[a]	strong UV and 1 μm features
R	0.38	strong UV and 1 μm features
S	0.05-0.50	strong UV feature, usually has 1 μm feature
T	0.05-0.10	weak UV feature, reddish past 0.4 μm
V	0.42	strong UV and 1 μm features

Other Classes		Spectral Properties
K (Bell 1989)	0.14	spectrum intermediate between S and C asteroids
J (Binzel and Xu 1993)	?	deeper 1 μm feature than a V-type spectrum
O (Binzel et al. 1993)	?	weak UV feature out to 0.44 μm, very strong 1 μm feature
W (Rivkin et al. 1995)	0.16-0.25	M-type with 3 μm feature

[a]The albedo for 1862 Apollo is from Lebofsky et al. (1981b).

iron compositions even though a number of different types of material could have these spectral properties.

A few classes initially had only one member. The Q-class was used to classify NEA 1862 Apollo, the R-class was used for 349 Dembowska, and the V-class was used for asteroid 4 Vesta. The Q-class has become synonymous for asteroids with spectra similar to ordinary chondrites because Apollo has a visible spectrum (McFadden et al. 1985) similar to LL chondrites. A number of objects were discovered near Vesta with similar spectral properties to Vesta and the HEDs (howardites, eucrites, and diogenites) (e.g., Binzel and Xu 1993), and these objects were also called V-types.

A few more classes (Table 2) were subsequently proposed to describe objects with distinctive spectra whose spectral properties were not adequately described in the Tholen (1984) taxonomy. K-types have spectra intermediate between S- and C-types (Bell 1988); this classification was initially used to describe members of the Eos family. The J class was used to classify asteroids that had UV and 1-μm features of similar strength to diogenites (Binzel and Xu 1993; Xu et al. 1995). The O-class was used to describe the visible spectra of 3628 Božněmcová (Binzel et al. 1993; Xu et al. 1995), which has a weak UV feature and very strong 1-μm feature. Božněmcová was interpreted as having similar spectral properties to LL chondrites (Binzel et al. 1993). The W-class was proposed for M-types with 3-μm absorption features (Rivkin et al. 1995). The presence of a 3-μm absorption feature is consistent with hydrated silicates on the surface and is not consistent with a surface of metallic iron.

Near-IR spectra tend, for the most part, to confirm the basic interpreted compositions for the asteroid classes. S-types usually have absorption features in the near-IR due to olivine and/or pyroxene (e.g., Gaffey et al. 1993a). V-types usually have near-IR spectra similar to HEDs (e.g., Burbine et al. 2001b). A-types usually have spectra consistent with olivine-dominated surfaces. B-, C-, F-, and G-types usually have low albedos and relatively featureless spectra out to 2.5 μm and are usually linked with carbonaceous chondrites (e.g., Burbine 1998) or thermally altered carbonaceous chondrites (Hiroi et al. 1993, 1996b). The relatively featureless spectra of E-types out to 2.5 μm and their high albedos are consistent with aubrites. D- and P-types usually have extremely red near-IR spectra and low albedos, which are consistent with the spectral properties of organic-rich primitive material.

Almost every Tholen (1984) class appears to contain objects with a variety of compositions. Gaffey et al. (1993a) did a study of the visible and near-IR spectra of a number of S asteroids and grouped them into seven subtypes (I through VII) based on the interpreted ratios of olivine to pyroxene from the analysis of Band Area Ratios and Band I minima. At the two compositional extremes, S(I) objects had spectra consistent with silicate assemblages that were almost entirely olivine while S(VII) objects had silicate assemblages almost entirely composed of pyroxene. With increasing subtype number, the proportion of pyroxene at the surface tends to increase. S(IV)-types had interpreted mineralogies consistent with ordinary chondrites. The range of meteorite types that may derive from the S-type asteroids includes the pallasites, ureilites, brachinites, lodranites/acapulcoites, ordinary chondrites, winonaites, and mesosiderites (Gaffey et al. 1993a,b). Near-IR observations of X-types (E, M, P) by Clark et al. (2004b) appear to be consistent with more than three types of assemblages. Observations in the 3-μm region e.g., (Jones et al. 1990; Rivkin et al. 1995) also show that a variety of assemblages exist within a number of Tholen (1984) asteroid classes, because many classes (e.g., E, M, C) contain objects with and without 3 μm bands.

The most recent asteroid taxonomy (Bus 1999; Bus and Binzel 2002b) extends the taxonomy of Tholen (1984) to the CCD spectra of Bus and Binzel (2002a). Bus (1999) found that the Tholen (1984) taxonomy could not adequately distinguish the spectral variations in their high-resolution CCD spectra, so 26 taxonomic types and subtypes were defined (Table 3 and Fig. 20) to classify ~1400 main-belt and NEAs. These types included the Tholen (1984) A,

Table 3. Bus (1999) and Bus and Binzel (2002b) taxonomic classes.

Class	Spectral Properties in the Visible
A	Very steep red slope shortward of 0.75 μm and a moderately deep absorption longward of 0.75 μm
B	Linear, featureless spectrum over interval of 0.44-0.92 μm with negative (bluish) to flat slope
C	Weak to medium UV absorption shortward of 0.55 μm, flat to slightly reddish longward of 0.55 μm
Cb	Linear, featureless spectrum from 0.44-0.92 μm with a flat to slightly reddish spectral slope
Cg	Strong UV feature shortward of 0.55 μm and flat to slightly reddish slope longward of 0.55 μm
Cgh	Similar to Cg spectrum, except for addition of broad, shallow absorption band centered near 0.7 μm
Ch	Similar to C spectrum, except for addition of broad, shallow absorption band centered near 0.7 μm
D	Relatively featureless spectrum with a very steep red slope
K	Moderately steep red slope shortward of 0.75 μm, flat to slightly negative slope longward of 0.75 μm
L	Very steep red slope shortward of 0.75 μm and then becoming approximately flat
Ld	Very steep red slope shortward of 0.7 μm, becoming approximately flat longward of 0.75 μm
O	Red slope from 0.44-0.54 μm, less sleep from 0.54 to 0.7 μm, deep absorption longward of 0.75 μm
Q	Moderately steep red slope shortward of 0.7 μm and deep, rounded absorption longward of 0.75 μm
R	Very steep red slope shortward of 0.7 μm and a deep absorption longward of 0.75 μm
S	Steep, reddish slope shortward of 0.7 μm and a moderate to deep absorption longward of 0.75 μm
Sa	Spectrum intermediate between S and A types
Sk	Spectrum intermediate between S and K types
Sl	Spectrum intermediate between S and L types
Sq	Spectrum intermediate between S and Q types
Sr	Spectrum intermediate between S and R types
T	Moderately steep red slope shortward of 0.75 μm, becoming flat longward of 0.85 μm
V	Moderate to very steep red slope shortward of 0.7 μm with a deep absorption longward of 0.75 μm
X	Generally featureless spectrum with a slight to moderate reddish slope
Xc	Slightly reddish spectrum, generally featureless except for gentle curvature
Xe	Slight to moderate reddish slope with series of absorption features such as one shortward of 0.55 μm
Xk	Moderately red slope shortward of about 0.75 μm and generally flat longward of 0.75 μm

B, C, D, Q, R, S, T, and X classes plus the K class (Bell 1988), the newly defined L class, and the O class (Binzel et al. 1993). The "L" designation was chosen to stress the apparent spectrum continuum that these objects have with K asteroids. Over half of the asteroids classified by Bus (1999) have diameters of less than 20 km.

The Bus (1999) taxonomy used the presence or absence of a number of specific spectral features to classify the CCD spectra. The letter "h" was used for objects that had a 0.7 μm feature (Fig. 20). This feature is usually assumed to be due to the presence of oxidized iron in phyllosilicates; King and Clark (1997), however, found that this feature is present in the spectra of other types of minerals. The letter "g" was used for C objects that had deep UV features because the Tholen (1984) G class was not defined in the Bus (1999) taxonomy. Some objects were classified as Cgh-types. The letter "e" was used for X-types that had a feature centered at ~0.49 μm (Fig. 20).

Bus (1999) also found that a number of objects have spectra intermediate between the S and the A, K, L, Q, and R classes. These intermediate classes were designated as the Sa,
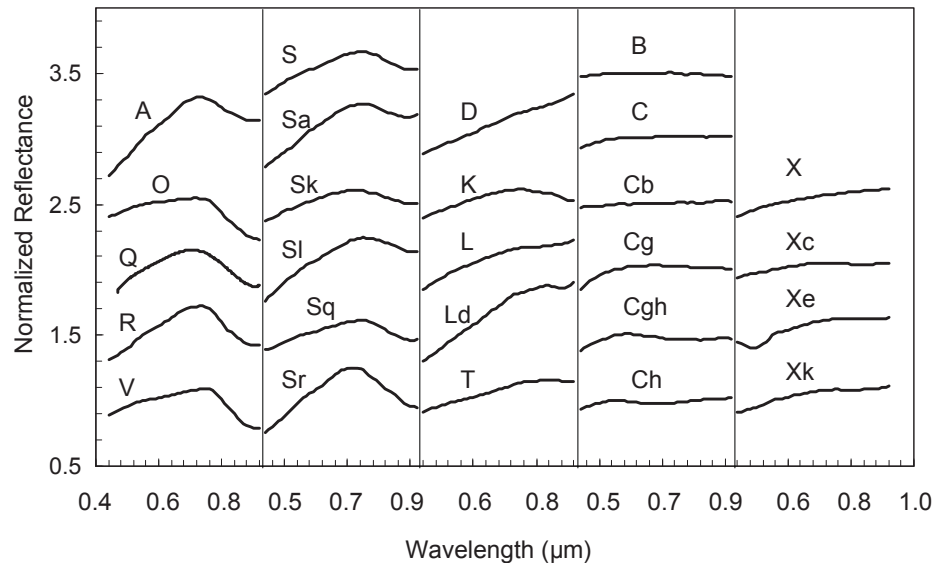
Figure 20. Reflectance spectra of Bus (1999) taxonomic classes.
The wavelength range for each spectrum is ~0.44 to ~0.92 μm.

Sk, Sl, Sq, and Sr classes (Fig. 20) and are considered part of the S-complex, consisting of the S class plus the A, K, L, O, Q, and R classes. Spectra intermediate between C and B objects were called Cb, and those between L and D objects were called Ld. The C-complex contains the B, C, Cb, Cg, Ch, and Cgh classes. The X-complex includes the X and Xe class plus Xc (intermediate between the X and C classes) and the Xk (intermediate between the X and K classes) classes. Other authors (e.g., Binzel et al. 2004), however, have defined these complexes differently, by including different Bus (1999) classes in each complex.

X-type asteroids span a wide range of albedos, and contain a large range of interpreted mineralogies. In the Tholen (1984) taxonomy, the albedos are used to separate the X class into the E- (high albedo), M- (moderate albedo) and P- (low albedo) subclasses, while the separation in the Bus taxonomy into X-, Xe-, Xk-, and Xc-classes is based on inflections and absorptions not visible at the low spectral resolutions available to Tholen (1984). Care must be taken in being clear which taxonomy is used, as the classes and subclasses are not perfectly matched, and results derived from studying one group (the E class, for instance) cannot be strictly applied to another group (Xe in this case).

The significance of these intermediate classes is unknown. Bus (1999) found a continuum of asteroid spectral properties. Spectral differences between asteroids are probably due to a combination of factors (e.g., composition, degree of space weathering, grain size), which are very hard to constrain, so it is difficult to impossible to know what is actually causing small spectral variations between objects.

A number of asteroids (Table 4) have had their mineralogies interpreted from analyses of their reflectance spectra and/or comparison to mineral or meteorite spectra. The following sections will discuss the mineralogical interpretations of a number of taxonomic classes.

A-types

A-types have visible spectra indicative of silicate compositions dominated by olivine. Their near-IR spectra tend to confirm that these objects have olivine-dominated surfaces

Table 4. Mineralogical characterizations of asteroids. This table is
an expanded version of the one in Gaffey et al. (2002).

Asteroid	Class[a]	a (AU)[b]	Interpreted Composition [c]	Reference
1 Ceres	G, C	2.77	hydrated silicates	Vernazza et al. (2005)
2 Pallas	B	2.77	hydrated silicates	Larson et al. (1979)
3 Juno	S, Sk, S(IV)	2.67	ol/(ol+pyx) ≈ 0.70, L chondrite	Gaffey et al. (2002)
4 Vesta	V	2.36	howardite, eucrite, diogenite	Gaffey (1997)
6 Hebe	S, S(IV)	2.43	ol/(ol+pyx) ≈ 0.6, H chondrite	Gaffey and Gilbert (1998)
7 Iris	S, S(IV)	2.39	ol/(ol+pyx) ≈ 0.70, L chondrite	Gaffey et al. (2002)
8 Flora	S, S(III)	2.20	ol/(ol+pyx) ≈ 0.75, FeNi	Gaffey (1984)
9 Metis	S, S(I)	2.39	ol/(ol+pyx) ≈ 0.88, FeNi	Kelley and Gaffey (1997)
11 Parthenope	S, Sk, S(IV)	2.45	ol/(ol+pyx) ≈ 0.66	Gaffey et al. (2002)
12 Victoria	S, L, S(II))?	2.33	ol/(ol+pyx) ≥ 0.86	Gaffey et al. (2002)
13 Egeria	G, Ch	2.58	CM chondrite	Burbine (1998)
15 Eunomia	S, S(III)	2.64	ol, pyx, FeNi	Reed et al. (1997)
16 Psyche	M	2.92	FeNi metal	Ostro et al. (1985)
17 Thetis	S	2.47	low-Ca and high-Ca pyx	Sunshine et al. (2004)
18 Melpomene	S, S(V)	2.30	ol/(ol+pyx) ≈ 0.53	Gaffey et al. (2002)
19 Fortuna	G, Ch	2.44	CM chondrite	Burbine (1998)
20 Massalia	S, S(VI)	2.41	ol/(ol+pyx) ≈ 0.34	Gaffey et al. (2002)
21 Lutetia	M, Xk	2.44	CO3/CV3 chondrite	Birlan et al. (2006)
25 Phocaea	S, S(IV)	2.40	ol/(ol+pyx) ≈ 0.70	Gaffey et al. (2002)
26 Proserpina	S, S(II)	2.66	ol/(ol+pyx) ≈ 0.70	Gaffey et al. (2002)
27 Euterpe	S, S(IV)	2.35	ol/(ol+pyx) ≈ 0.75	Gaffey et al. (2002)
37 Fides	S, S(V)	2.64	ol/(ol+pyx) ≈ 0.28	Gaffey et al. (2002)
39 Laetitia	S, S(II)	2.77	ol/(ol+pyx) ≈ 0.74	Gaffey et al. (2002)
40 Harmonia	S, S(VII)	2.27	ol/(ol+pyx) ≈ 0.11	Gaffey et al. (2002)
42 Isis	S, L, S(I)	2.44	ol/(ol+pyx) ≈ 1.00, FeNi	Gaffey et al. (2002)
43 Ariadne	S, Sk, S(III)	2.20	ol/(ol+pyx) ≈ 0.80-0.87	Gaffey et al. (2002)
44 Nysa	E	2.42	enstatite	Clark et al. (2004)
63 Ausonia	S, Sa, S(II-III)	2.40	ol/(ol+pyx) ≈ 0.73, FeNi	Gaffey et al. (2002)
64 Angelina	E, Xe	2.68	aubrite	Zellner et al. (1977)
67 Asia	S, S(IV)	2.42	ol/(ol+pyx) ≈ 0.54	Gaffey et al. (2002)
68 Leto	S, S(II)	2.78	ol/(ol+pyx) ≈ 0.82	Gaffey et al. (2002)
69 Hesperia	M, X	2.98	low-Fe, low-Ca pyx, FeNi	Hardersen et al. (2005)
80 Sappho	S, S(IV)	2.30	ol/(ol+pyx) ≈ 0.70	Gaffey et al. (2002)
82 Alkmene	S, Sq, S(VI)	2.77	ol/(ol + pyx) ≈ 0.39	Gaffey et al. (2002)
110 Lydia	M, X	2.73	low-Fe, low-Ca pyx, FeNi	Hardersen et al. (2005)
113 Amalthea	S, S, S(I-II)	2.38	ol/(ol+pyx) ≈ 0.87, FeNi	Kelley and Gaffey (1997)
115 Thyra	S, S, S(III-IV)	2.38	low- and high-Ca pyx	Gaffey et al. (2002)
125 Liberatrix	M, X	2.74	low-Fe low-Ca pyx, FeNi	Hardersen et al. (2005)
130 Elektra	G, Ch	3.12	organic-bearing	Cruikshank and Brown (1987)
138 Tolosa	S	2.45	low-Ca pyx	Hardersen et al. (2006)
201 Penelope	M, X	2.68	low-Fe low-Ca pyx, FeNi	Hardersen et al. (2005)
216 Kleopatra	M, Xe	2.77	FeNi	Ostro et al. (2000)
221 Eos	S, K	3.01	CO3 chondrite	Bell (1988)
			partially differentiated	Mothé-Diniz and Carvano (2005)
246 Asporina	A	2.70	ol	Sunshine et al. (2007)
289 Nenetta	A	2.87	ol	Sunshine et al. (2007)
306 Unitas	S	2.36	low-Ca pyx, ol	Hardersen et al. (2006)
308 Polyxo	T	2.75	Tagish Lake	Hiroi and Hasegawa (2003)
			CO3 chondrite	Dotto et al. (2004)
346 Hermentaria	S	2.80	low-Ca and high-Ca pyx	Hardersen et al. (2006)
349 Dembowska	R	2.93	ol/(ol + pyx) ≈ 55	Abell and Gaffey (2000)
354 Eleonora	S, Sl, S(I)	2.80	ol with 5-10% pyx	Sunshine et al. (2007)
387 Aquitania	S, L	2.74	spinel on surface	Burbine et al. (1992)
433 Eros	S, S(IV)	1.46	ordinary chondrite	McCoy et al. (2001)
434 Hungaria	E, Xe	1.94	enstatite	Kelley and Gaffey (2002)
446 Aeternitas	A	2.79	ol with 5-10% pyx	Sunshine et al. (2007)

480 Hansa	S	2.64	low-Ca pyx, ol	Hardersen et al. (2006)
532 Herculina	S, S(III)	2.77	low- and high-Ca pyx	Gaffey et al. (2002)
584 Semiramis	S, Sl, S(IV)	2.37	ol/(ol+pyx) ≈ 0.74, FeNi	Gaffey et al. (2002)
599 Luisa	S, K	2.77	CV3 chondrite	Burbine et al. (2001a)
624 Hektor	D	5.22	carbon, pyx	Cruikshank et al. (2001)
653 Berenike	S, K	3.01	CO3 chondrite	Burbine et al. (2001a)
			partially differentiated	Mothé-Diniz and Carvano (2005)
674 Rachele	S, S(VII)	2.92	ol/(ol+pyx) ≈ 0-0.32	Gaffey et al. (2002)
808 Merxia	Sq	2.75	basaltic	Sunshine et al. (2004)
832 Karin	S	2.86	ordinary chondrite	Sasaki et al. (2004)
847 Agnia	S	2.78	basaltic	Sunshine et al. (2004)
863 Benkoela	A	3.20	ol with 5-10% pyx	Sunshine et al. (2007)
980 Anacostia	SU, L	2.74	spinel on surface	Burbine et al. (1992)
984 Gretia	Sr	2.80	ol with 5-10% pyx	Sunshine et al. (2007)
1036 Ganymed	S, S(VI-VII)	2.66	ol/(ol+pyx) ≈ 0.18-0.36	Gaffey et al. (2002)
1273 Helma	V	2.39	eucrite/howardite	Burbine et al. (2001b)
1459 Magnya	V	3.15	eucrite-like	Hardersen et al. (2004)
1862 Apollo	Q	1.47	LL chondrite	McFadden et al. (1985)
1906 Naef	V	2.37	eucrite/howardite	Burbine et al. (2001b)
1929 Kolla	V	2.36	eucrite	Kelley et al. (2003)
1933 Tinchen	V	2.35	eucrite/howardite	Burbine et al. (2001b)
1951 Lick	A	1.39	ol	de León et al. (2004)
2045 Peking	V	2.38	eucrite/howardite	Burbine et al. (2001b)
2442 Corbett	J	2.39	eucrite/howardite	Burbine et al. (2001b)
2501 Lohja	A	2.42	ol with 5-10% pyx	Sunshine et al. (2007)
2579 Spartacus	V	2.21	eucrite/howardite, ol?	Burbine et al. (2001b)
2590 Mourào	V	2.34	eucrite/howardite	Burbine et al. (2001b)
2653 Principia	V	2.44	eucrite/howardite	Burbine et al. (2001b)
2763 Jeans	V	2.40	eucrite/howardite	Burbine et al. (2001b)
2851 Harbin	V	2.48	eucrite/howardite	Burbine et al. (2001b)
2867 Steins	E	2.36	enstatite	Barucci et al. (2005)
3103 Eger	E, Xe	1.41	enstatite	Gaffey et al. (1992)
3200 Phaethon	F	1.27	hydrated silicates	Licandro et al. (2007)
3268 De Sanctis	V	2.35	eucrite/howardite	Burbine et al. (2001b)
3376 Armandhammer	Sq	2.35	eucrite/howardite	Burbine et al. (2001b)
3551 Verenia	V	2.09	eucrite/howardite	Cruikshank et al. (1991)
3657 Ermolova	J	2.31	eucrite/howardite	Burbine et al. (2001b)
3819 Robinson	Sr	2.77	ol with 5-10% pyx	Sunshine et al. (2007)
3908 Nyx	V	1.93	eucrite/howardite	Cruikshank et al. (1991)
3944 Halliday	V	2.37	eucrite/howardite	Burbine et al. (2001b)
3968 Koptelov	V	2.32	eucrite/howardite	Burbine et al. (2001b)
4005 Dyagilev	J	2.45	eucrite/howardite	Burbine et al. (2001b)
4055 Magellan	V	1.82	eucrite/howardite	Cruikshank et al. (1991)
4147 Lennon	V	2.36	eucrite/howardite	Burbine et al. (2001b)
4188 Kitezh	V	2.34	eucrite/howardite	Burbine et al. (2001b)
4215 Kamo	J, V	2.42	eucrite/howardite	Burbine et al. (2001b)
4900 Maymelou	V	2.38	eucrite/howardite	Burbine et al. (2001b)
4979 Otawara	S	2.17	ordinary chondrite	Fornasier et al. (2003)
6178 1986 DA	M	2.81	FeNi	Ostro et al. (1991)
6611 1993 VW	Q	1.70	ordinary chondrite	Di Martino et al. (1995)
9969 Braille	Q	2.35	equal amounts of ol and pyx	Buratti et al. (2004)
25143 Itokawa	S	1.32	LL chondrite	Binzel et al. (2001)
69230 Hermes	S	1.66	L/LL chondrite	Rivkin et al. (2004a)
2002 NY40	Q	2.05	LL chondrite	Rivkin et al. (2003b)

[a] The classes (where available) are from Tholen (1984), Tholen (1989), Xu et al. (1995), Bus and Binzel (2002b), and Gaffey et al. (1993a).

[b] Semi-major axes for main-belt asteroids are from the AstDyS website (*http://hamilton.dm.unipi.it/cgi-bin/astdys/astibo?proper_elements:0;main*) and for near-Earth asteroids are from the Minor Planet Center website (*http://cfa-www.harvard.edu/iau/lists/Unusual.html*).

[c] Abbreviations: ol = olivine; pyx = pyroxene; and plag = plagioclase.

(**Fig. 21**). Approximately 20 A-types have been identified, including 289 Nenetta, 246 Asporina, 446 Aeternitas, and 863 Benkoela. Olivine-dominated asteroids also exist among S-types, but are not classified as A-types because they have weaker absorption features in the visible.

The identification of only a small number of A-types has been a mystery because the presence of ~10 magmatic iron groups and a number of ungrouped irons, which may represent ~50 parent bodies (Burbine et al. 2002b), implies a large number of disrupted differentiated objects. The mantle-derived debris would be expected to be olivine-rich. One possible explanation for the "absence" of this mantle material is that the differentiated assemblages were disrupted early in the history of the Solar System and the mantle material has been subsequently broken down to sizes that are not spectrally observable (Burbine et al. 1996).

The focus of much of the research on the mineralogy of A-types has been on determining the fayalite content of their olivine, since olivine-dominated meteorites with different thermal histories tend to have distinctive iron contents. A-types are commonly linked to either pallasites (Fa_{10-20}) or brachinites (Fa_{30-35}), but R-chondrites (Fa_{37-40}) also appear to be possible spectral analogs. These meteorite types have experienced very different thermal histories. Pallasites are believed to be from the core-mantle boundaries of differentiated bodies, brachinites are thought to be derived from objects that partially differentiated, and R-chondrites have been heated but not melted. Compensating for temperature effects, Sunshine et al. (2007) analyzed the spectra of six A-types using MGM. They found that one A-type was Mg-rich (iron-poor) (1951 Lick, ~Fa_{20}), two objects were more Fe-rich (246 Asporina and 289 Nenetta, ~Fa_{40}), and three objects (446 Aeternitas, 863 Benkoela, 2501 Lohja) were Mg-rich with 5-10% pyroxene. Asporina and Nenetta are consistent with an R-chondrite assemblage or the partial melting of an R-chondrite, while the other objects are consistent with differentiated assemblages (e.g., pallasite).

C-complex

C-complex asteroids include the B, C, F, and G asteroids of the Tholen (1984) taxonomy and the C-complex objects of the B-, C-, Cg-, Ch-, and Cgh-types of the Bus (1999) taxonomy. These asteroids are typically linked with carbonaceous chondritic material because, like the latter, they have low albedos and relatively featureless spectra, with only weak absorption bands in the visible and near-IR.

Asteroid 1 Ceres, a member of the C-complex, is the largest object in the main belt (975 by 909 km) (Thomas et al. 2005). Although one of the first asteroids to be observed spectroscopically, the details of Ceres' surface composition are still not agreed upon. Its visible and near-IR spectrum places it in the C complex in the Bus (1999) taxonomy, with a basically flat spectrum. Ceres' albedo is higher than those of most other C-complex objects, with an IRAS albedo of 0.11 (Tedesco et al. 2002) and a visual albedo of 0.09 (Li et al. 2006). Ceres was classified as a G-type in the Tholen (1984) taxonomy due to its strong UV feature. Larson et al. (1979) originally interpreted a low-resolution 3-μm spectrum along with Ceres' visible and near-IR spectrum (**Fig. 22**) as indicating a CI chondritic composition.

Higher-resolution spectra of Ceres in the 3-μm region (Lebofsky et al. 1981a) show a band shape due to water, with a minimum near 3.05 μm. This band minimum was confirmed by King et al. (1992), Rivkin et al. (2003a), and Vernazza et al. (2005). The interpretations have varied dramatically. Lebofsky et al. (1981a) considered a water ice frost to be responsible, though such a frost is only stable near the poles of Ceres. This interpretation seemed to be bolstered by the observation of OH emission off the sunlit pole of Ceres by A'Hearn and Feldman (1992) using International Ultraviolet Explorer (IUE) satellite observations. King et al. (1992) attributed the 3.05-μm band (Fig. 22) to ammonium (NH_4^+) ions in clays. Such minerals are found in hydrothermal systems on Earth, and were considered possible on asteroids by Lewis and Prinn (1984), who postulated NH_4^+-bearing brines. The presence of an ammoniated clay
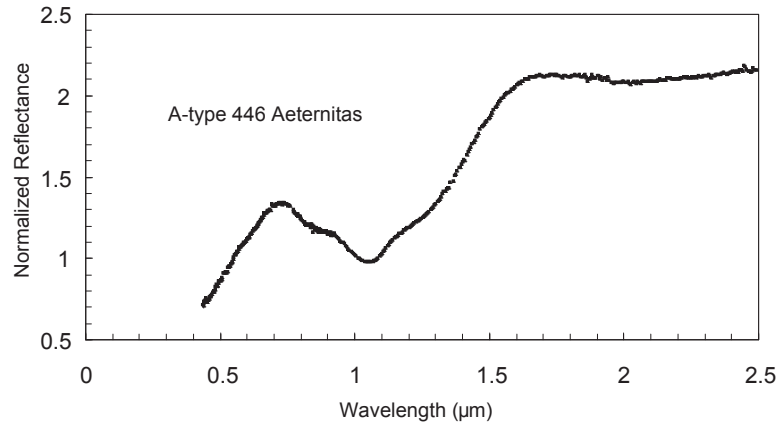
Figure 21. Reflectance spectrum of 446 Aeternitas (Bus and Binzel 2002a; Binzel personal communication). Spectrum is normalized to unity at 0.55 μm. Error bars are one-sigma, but are smaller than the points for most of the spectrum.
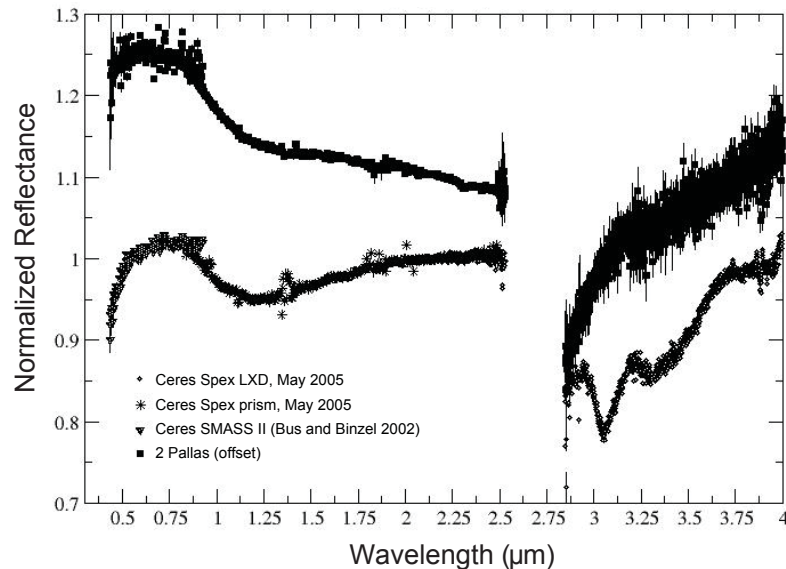
Figure 22. The lower spectrum, of Ceres, was constructed from three different datasets, showing how full spectral coverage requires piecing together information from multiple sources. The upper spectrum, of Pallas, was constructed the same way. Evident in both spectra is the local maximum near 0.75 μm. Shortward of 0.5 μm is an absorption due to oxidized iron. A local minimum is seen in both objects near 1.2 μm; this feature is also seen in clay minerals and carbonaceous chondrites. The two objects differ in obvious ways, however: Pallas has an overall blue slope to its spectrum (lower reflectance with increasing wavelength) compared to Ceres' relatively flat continuum. Also, Ceres and Pallas have very different band shapes near 3 μm. Pallas' band shape is similar to that found in CM meteorites, while Ceres' is unknown in meteorites and has been interpreted several different ways. C-types that have been surveyed tend to have Pallas-like band shapes, though Ceres-like shapes are also seen. Error bars are one-sigma.

assemblage on Ceres would place tight constraints on the highest temperature experienced because temperatures higher than 400K lead to deammoniation of clays.

Vernazza et al. (2005) found that a spectral minimum near 3.05 μm could be generated in macromolecular organic materials irradiated in the presence of water ice. Recent work by Thomas et al. (2005) found that the shape of Ceres is inconsistent with a homogeneous body, and postulates the existence of a subsurface ocean (though perhaps currently frozen). McCord and Sotin (2005) show that such an ocean is a natural outcome of thermal models, and suggest that Ceres is 17-27% water by mass, beneath a ~10 km-thick, unmelted crust. The presence of large amounts of water could plausibly resupply a frost, though modeling has not been done. Rivkin et al. (2006b) identified absorption features in Ceres' spectrum that appear to be due to carbonates and Fe-rich clays.

In the near-IR, Ceres also can be seen to have a very broad (~1 μm in width), relatively shallow (~5% band depth) band centered near 1.2 μm. This band is also seen in carbonaceous chondrites and is likely due to phyllosilicates. Ceres' band shape, with a minimum near 3.05 μm, is shared by several other asteroids, including 10 Hygiea, 24 Themis, and 375 Ursula (Rivkin et al. 2003a; 2004b). If all of these objects have similar mineralogies, looking at their common properties should help distinguish between the competing theories of Ceres' composition.

As with Ceres, early work associated Pallas with carbonaceous chondrite meteorites (Larson et al. 1983). The main spectral difference between Ceres and Pallas is the shape of their 3-μm bands (Fig. 22), and the significant blue slope in the spectrum of Pallas in the visible and near-IR. Pallas was seen as being potentially poor in Fe^{2+}, with evidence for low-Fe hydrated and anhydrous silicates. Pallas' band shape in the 3-μm region is commonly found among low-albedo objects, and is reminiscent of the band shapes of the CM chondrite Murchison. However, Pallas' IRAS albedo (0.16) is much higher than the visual albedos of CM chondrites (~0.05). The cause of spectral continua is not well-understood, and while blue slopes are uncommon, they are not unknown.

Rivkin et al. (2003a) found an H/Si ratio of ~1.6 for Pallas, with an equivalent water content of ~7.5%, assuming 30% SiO_2. This is lower than what is seen for CM meteorites by roughly one third, but is still well within the range that could be expected for hydrated meteorites. Given what we currently know about Pallas spectroscopically, we might expect a CM-like object. The calculated density of Pallas (4.2 ± 0.3 g/cm³) (Hilton 1999), however, is considerably higher than the average bulk density of CM chondrites (~2.1 g/cm³) (Britt and Consolmagno 2003).

A number of C-complex asteroids have been linked to CM chondrites. Asteroid 19 Fortuna (**Fig. 23**) has a reflectance spectrum that is very similar to CM2 chondrite LEW 90500 (Burbine 1998). Asteroid 13 Egeria was also found to be spectrally similar to CM2 chondrites. Both objects have the 0.7 μm feature that is found in the spectra of CM chondrites. Both asteroids have diameters greater than 200 km and are located near the meteorite-supplying 3:1 resonance.

Hiroi et al. (1993, 1996b) found that a number of thermally metamorphosed CI and CM chondrites had no 0.7 μm bands and weaker UV and 3-μm features compared to unmetamorphosed CI and CM chondrites. Heating to temperatures of ~400 °C and above destroys the original aqueous minerals in the carbonaceous chondrites. Nakamura (2006) has identified one metamorphosed CM chondrite (Y-793221) as being a regolith breccia of a hydrous asteroid, based on evidence of the effects of impact, heating, dehydration, and solar-wind implantation. A number of large C-complex asteroids (Hiroi et al. 1993, 1996b) have spectra similar to these metamorphosed carbonaceous chondrites.

D- and P-types

A large number of outer-belt objects are classified as D- and P-types due to their red-sloped, featureless spectra and low albedos. Cybele asteroids observed by Lagerkvist et al. (2005) in the visible wavelength region tended to be primarily X-, D-, and P-types. Visible reflectance spectra
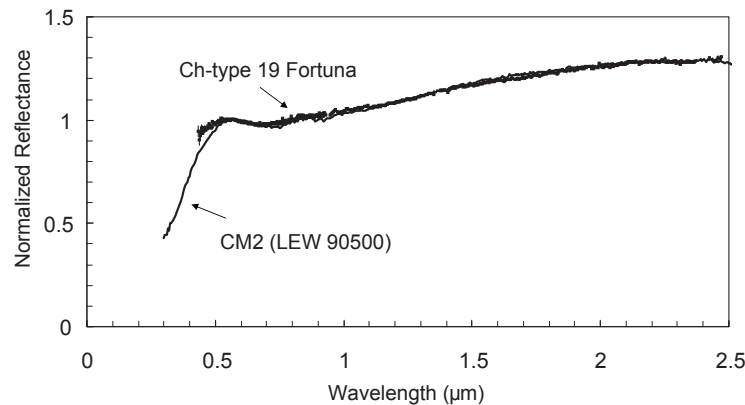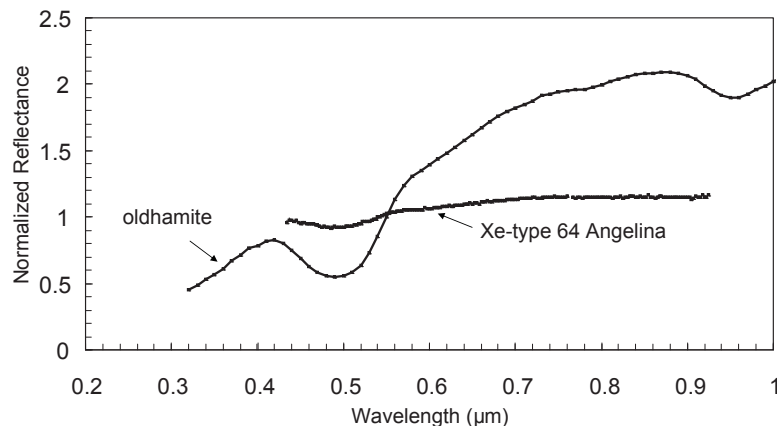
Figure 23. Reflectance spectra of 19 Fortuna (Bus and Binzel 2002a; Binzel personal communication) and CM2 chondrite LEW 90500 (Hiroi et al. 1993). Spectra are normalized to unity at 0.55 μm. Error bars are one-sigma, but are smaller than the points for most of the spectrum.

of asteroids in the Hilda group (3.70-4.20 AU) by Dahlgren et al. (1997) show that these objects are mostly D-types with very few C- and P-types. Measured albedos of these objects range from 0.03 to 0.11. Visible and near-IR observations of Trojans have found no clear evidence of 0.7-μm bands (Jewitt and Luu 1990; Barucci et al. 2002; Bendjoya et al. 2004; Fornasier et al. 2004; Dotto et al. 2006b), possibly indicating that these objects are not similar to CM chondritic material. Hiroi et al. (2004) were able to duplicate the spectral properties of P-types in the visible and near-IR, however, using mixtures of altered and unaltered CI/CM meteoritic material and the unusual chondrite Tagish Lake. The material was altered through heating with a pulsed laser.

Jewitt and Luu (1990) observed 32 Trojan asteroids in the visible wavelength region and found that they have a range of spectral slopes from relatively flat to slightly red. They noted the possible presence of absorption features in the 0.5-0.6 μm range in the spectra of two Trojans, 1870 Glaukos and 5028 Halaesus, which resembled features found in porphyrins of organic materials. Fornasier et al. (2004) observed 26 Jupiter Trojans at the L_5 Lagrangian point in the visible wavelength region. No discernible absorption features were found to be present in any of the Fornasier et al. (2004) spectra. Observations with the Spitzer Space Telescope by Emery et al. (2005) found that the mid-IR spectra of Trojan asteroids are most consistent with anhydrous silicates; however, Kanno et al. (2003) has detected a 3-μm band in the spectra of main-belt D-type asteroid 773 Irmintraud. Irmintraud was classified as D-type by Tholen (1984), but as a T-type by Bus and Binzel (2002b).

E- and Xe-types

E-types have relatively featureless spectra and high albedos. These spectral properties are consistent with aubrites (Zellner et al. 1977), which consist almost entirely of FeO-free enstatite (Burbine et al. 2002c). Bus (1999) did not use albedo information in his classification scheme, so he grouped objects (E, M, P) that Tholen (1984) subdivided by albedo into the X-complex. High-resolution spectra of these objects (Bus and Binzel 2002a) show that a number of these asteroids also have features centered at ~0.49 μm, and Bus (1999) classified them as Xe-types (**Fig. 24**). This ~0.49-μm feature has been linked to oldhamite (CaS) (Burbine et al. 2002c), which is commonly found in aubrites. These E- and Xe-types have been found in high numbers in the Hungaria region, such as 434 Hungaria (Kelley and Gaffey 2002). E-type NEA 3103 Eger has been postulated as the source body of the aubrites (Gaffey et al. 1992). Other E- or Xe-type objects, such as 64 Angelina, are found further out in the belt. E- and Xe-type

Figure 24. Reflectance spectra of 64 Angelina (Bus and Binzel 2002a; Binzel personal communication) and oldhamite from the Norton County aubrite (Burbine et al. 2002) out to 1 µm. Spectra are normalized to unity at 0.55 µm. Error bars are one-sigma, but are smaller than the points for most of the spectrum.

44 Nysa has a high albedo (0.49), but also has a 1-µm feature that indicates the presence of a Fe^{2+}-bearing silicate (Gaffey et al. 1989; Clark et al. 2004a). This interpreted composition is different from that found in aubrites, which have silicates that are virtually Fe^{2+}-free.

K- and L-types

Asteroids in the Eos family have long been noted to have spectral properties intermediate between the S- and C-types in the visible wavelengths (Gradie and Zellner 1977). The Eos family (extending from 2.97 to 3.07 AU) (Zappalà et al. 1994) has over 3,200 members (Mothé-Diniz et al. 2005). Bell (1988) found that these objects tend to have relatively flat spectral slopes in the near-IR with shallow silicate absorption bands, and labeled these objects as K-types. Asteroids outside the Eos family have also been classified as K-types. Burbine et al. (2001a) noted the spectral similarities between Eos family members (221 Eos and 653 Berenike) and a CO3 chondrite and a non-Eos family member (599 Luisa) with a CV3 chondrite. Recently, Mothé-Diniz and Carvano (2005) noted spectral similarities between Eos and Divnoe (Petaev et al. 1994), an ungrouped olivine-rich achondrite, and argue that Eos family members have been extensively heated.

The L-class asteroids (Bus 1999) have stronger UV slopes than K-types. L-types include 387 Aquitania and 980 Anacostia, which were identified as having anomalous spectra (Burbine et al. 1992), because their 2-µm features are stronger than their 1-µm features. Burbine et al. (1992) postulated that these spectral properties are consistent with the spectra of spinel in CAIs. Burbine (2000) noted that there appears to be a number of different mineral assemblages among L-types. For example, L-type 42 Isis has distinctive olivine absorption bands and was labeled as an S(I)-subtype by Gaffey et al. (1993a).

M-types

M-type asteroids have spectra consistent with FeNi metal in the visible region plus relatively moderate visual albedos (0.10-0.30). These spectral properties are consistent with FeNi being the only constituent present, as in iron meteorites or, if other constituents beside FeNi are present, they are spectrally transparent (e.g., enstatite chondrites).

Extended spectral coverage has increased the number of possible mineralogies present in the M-class. Observations in the 3-µm region by Jones et al. (1990) and Rivkin et al. (1995,

2000) all show that some M-types have absorptions interpreted as due to hydrated minerals. Rivkin et al. (2000) classified these "wet" M-objects as W-types in order to separate different mineralogies from one another. The amount of water implied by these minerals is still a matter of some debate, as relations appropriate to M-types have not been determined. However, these observations show that many of the asteroids first classified as M are not consistent with iron meteorites, as an iron composition cannot be reconciled with hydrated minerals in spectrally observable amounts. Rivkin et al. (2000) found that roughly 1/3 of the M-types had a 3-μm band. The largest asteroids were found to be much more likely to have the 3-μm band than smaller ones, with the breakpoint at a diameter of ~65 km. They argued that this was consistent with the idea that larger M-types were too large to be disrupted cores, as their implied parent body sizes were very large compared to the sizes of objects expected to be disrupted over the course of Solar System history. Hardersen et al. (2005) also found spectral diversity in the M class, interpreting some objects as having reduced silicate mineralogy consistent with core-mantle boundaries, smelting-type reactions, or Bencubbinite-like mineralogies. This latter group does have some hydrated minerals, though direct comparisons are frustrated by the lack of available CB or CH spectra.

Other data support the diversity of mineralogies among M-types. Radar observations of 216 Kleopatra (Mitchell et al. 1995) show a high radar albedo consistent with a surface of metallic iron. The radar albedo is the radar cross section per unit of projected surface area (Ostro et al. 2000). The observations of 16 Psyche also show a somewhat high radar albedo. Asteroid 21 Lutetia, conversely, has a radar albedo typical of C-types. Barucci et al. (2005) found that Lutetia, one of the spacecraft targets of the Rosetta mission, has spectral properties similar to carbonaceous chondrites. Magri et al. (1999, 2007) found that main-belt M-types have higher mean radar albedos and a wider range of radar albedos than other taxonomic types, implying that both metal-rich and metal-poor M-types exist.

Polarimetric and photometric data from Lupishko and Belskaya (1989) also indicate that the largest M-types are not pure metal. Available densities also show variation through the M class: observations of the orbit of the satellite of 22 Kalliope give a density of 2.37 g/cm^3 (Margot and Brown 2003), inconsistent with an iron meteorite, but consistent with the 3-μm observations of Rivkin et al. (2000), while 16 Psyche has had reported densities that range from 1.8 ± 0.4 g/cm^3 (Viateau 2000) to 6.98 ± 0.58 g/cm^3 (Kuzmanoski and Kovacevic 2002), the latter consistent with an iron meteorite mineralogy. Because densities of metallic iron are ~7.3-7.7 g/cm^3, the bulk porosity of Psyche would have to be around ~70% for it to be composed entirely of metallic iron if its density is 1.8 g/cm^3 (Britt et al. 2002). This degree of porosity seems implausible for a metallic iron body.

M-type 16 Psyche has been long thought to be the FeNi core of a disrupted differentiated body. Psyche has a relatively high radar albedo among main-belt asteroids, which appears consistent with both a metallic regolith having typical lunar values of porosity and an enstatite chondrite-type regolith (~30% metal) with a porosity slightly below the lunar range (Ostro et al. 1985; Magri et al. 1999). Lupishko and Belskaya (1989) noted that the ECAS spectra of Psyche appeared to show a weak absorption feature in the 0.8 to 0.9-μm range. Hardersen et al. (2005) has also observed a weak absorption feature at ~0.9 μm that they attribute to orthopyroxene. The presence of Fe^{2+}-bearing silicates on the surface of Psyche is consistent with a differentiated metallic core with orthopyroxene on the surface, and not with an enstatite chondrite composition (Hardersen et al. 2005). Binzel et al. (1995) found no significant changes in the visible rotation spectra of Psyche, implying no large-scale variations in the content of the silicates (if present) on the surface.

M- and Xe-type 216 Kleopatra has been proposed to be the FeNi core of a disrupted differentiated body. Kleopatra has an extremely high radar albedo that is consistent with a metallic regolith having typical lunar porosity values (Mitchell et al. 1995). Hardersen et al.

(2005) observed a weak absorption feature at ~0.9 μm for Kleopatra that they attribute to orthopyroxene on the surface.

O-types

O-type 3628 Božněmcová has been previously linked with the ordinary chondrites due to its spectral similarities with these meteorites in the visible wavelength region (Binzel et al. 1993). Božněmcová is located near the 3:1 resonance and has a diameter of ~7 km. In the visible wavelength region, Božněmcová has a relatively flat to slightly red reflectance from 0.5 to 0.8 μm and a very deep 1-μm absorption feature, similar to the characteristics of the L6 and LL6 chondrites. A near-IR spectrum (out to 1.65 μm) of Božněmcová, however, does not resemble spectra of ordinary chondrites (Fig. 25) (Burbine and Binzel 2002).

Q-types

Q-type 1862 Apollo has long been known (McFadden et al. 1985) to have spectral properties similar to LL chondrites (Fig. 26). Apollo and LL chondrites have similarly-shaped, asymmetric 1-μm features and weak 2-μm features. Additional Q-type asteroids were identified in spectroscopic surveys of NEAs (e.g., Bus and Binzel 2002b). Binzel et al. (2004) defined a Q-complex containing Q- and Sq-types and found that one-quarter of classified NEAs were of this complex. This observation appears to be consistent with the dominance of ordinary chondrite material in our meteorite collections.

R-types

Asteroid 349 Dembowska has long been known to have a unique reflectance spectrum (Fig. 27) (e.g., Feierberg et al. 1980), which is unlike any known meteorite. From analyses of its visible and near-IR spectrum, Abell and Gaffey (2000) derive an *ol*/(*ol*+*opx*) ratio of ~0.45-55 with a pyroxene composition of ~$Fs_{25}Wo_{10}$. They interpret this composition as indicating that Dembowska only experienced small degrees of partial melting. Bus (1999) also identified 1904 Massevitch, 2371 Dimitrov, and 5111 Jacliff as being R-types.

S-complex

Approximately 40% of the objects observed by Bus (1999) were classified as part of the main S-complex (S, Sa, Sk, Sl, Sq, Sr). As mentioned earlier, asteroids classified as part of the
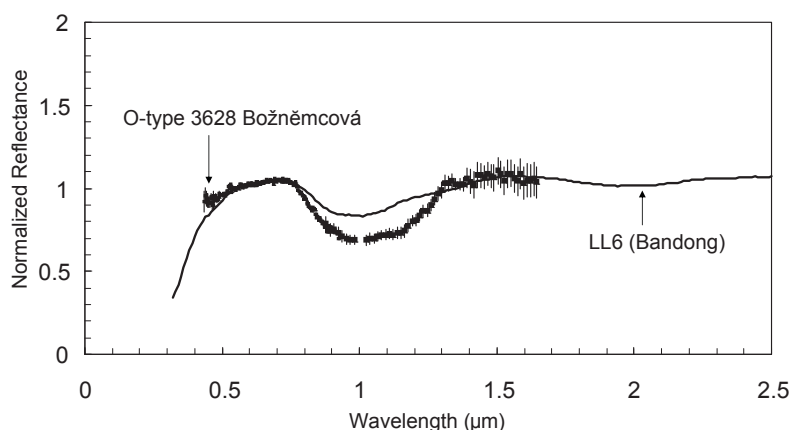
Figure 25. Reflectance spectra of 3628 Božněmcová (Bus and Binzel 2002a; Burbine and Binzel 2002) and LL6 chondrite Bandong (Burbine et al. 2003). Spectra are normalized to unity at 0.55 μm. Error bars are one-sigma.

S-complex span a continuum of compositions from olivine-dominated to pyroxene-dominated (Gaffey et al. 1993a). This range of compositions has caused S-types to be subdivided on the basis of visible (Bus 1999; Bus and Binzel 2002a) and near-IR spectra (Gaffey et al. 1993a; Howell et al. 1994). Meteorite types possibly derived from S-type asteroids include the pallasites, ureilites, brachinites, lodranites/acapulcoites, ordinary chondrites, winonaites, and mesosiderites. Hardersen et al. (2006) has also found a number of S-types that have spectral properties consistent with partially differentiated assemblages that do not appear to be present in our current meteorite collections.

The prevailing question concerning S-type asteroids is: what percentage of them have mineralogies similar to ordinary chondrites, the most common type of meteorite to fall to Earth? A number of authors (e.g., Binzel et al. 1996; Chapman 1996, 2004) argue that S-types are predominantly ordinary chondrites. Binzel et al. (1996) found that S-complex NEAs tend to have spectral properties intermediate between those of ordinary chondrites
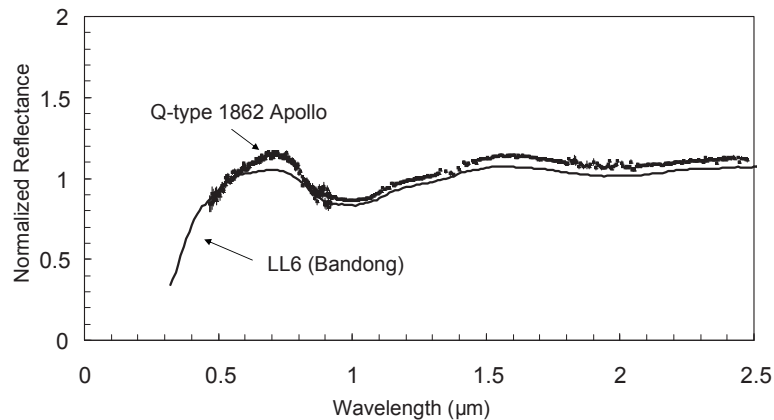
Figure 26. Reflectance spectra of 1862 Apollo (Binzel et al. 2006) and LL6 chondrite Bandong (Burbine et al. 2003). Spectra are normalized to unity at 0.55 μm. Error bars are one-sigma.
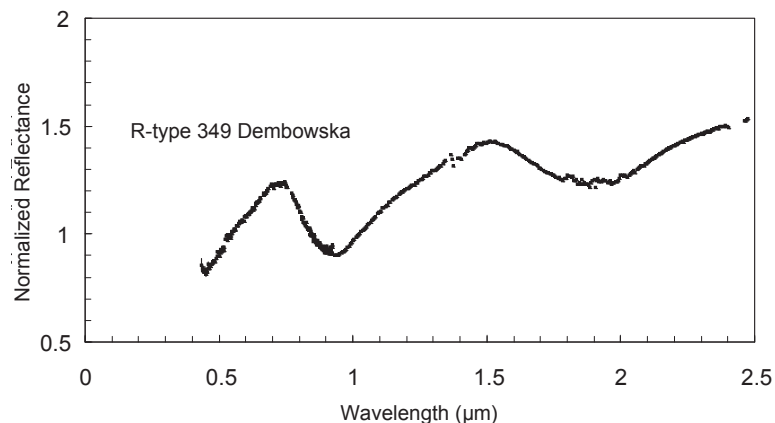
Figure 27. Reflectance spectrum of 349 Dembowska (Bus and Binzel 2002a; Binzel personal communication). Spectrum is normalized to unity at 0.55 μm. Error bars are one-sigma, but are smaller than the points for most of the spectrum.

and main-belt asteroids, implying a spectral continuum, which was consistent with reddening and reduction of the band strength of spectra of ordinary chondrite assemblages by space weathering. Alternatively, a number of authors (e.g., Gaffey et al. 1993a; Hardersen et al. 2006; Gaffey 2006) argue that S-types are primarily partially differentiated objects, on the basis of observation of a number of asteroids with interpreted mineralogies that are not consistent with ordinary chondrite assemblages.

The S-asteroid that is most closely linked with a meteorite type is 6 Hebe, which has been proposed as the parent body of the H chondrites (Gaffey and Gilbert 1998). Calculated Band Area Ratios and Band I minima for Hebe are consistent with H chondrites, with an interpreted *ol*/(*ol*+*opx*) ratio of 0.6 (Gaffey et al. 2002). However, Hebe's spectrum is reddened compared to ordinary chondrite spectra. Gaffey and Gilbert (1998) propose that sheets of metallic iron on the surface, produced by impact heating, are the cause of this reddening. Evidence for impact melting and sheets of metallic iron on the H-chondrite parent body are found in the IIE iron Watson (Olsen et al. 1994), which contains silicates with chemical and oxygen isotopic compositions similar to H chondrites, and Portales Valley, a metal-veined H6 chondrite (Ruzicka et al. 2005). As mentioned earlier, however, ambiguities in interpreting the spectrum of FeNi metal make this interpretation non-unique. For example, a space-weathered ordinary chondritic surface could yield a similar spectrum (Pieters et al. 2000).

T-types

T-type asteroids, as defined by Bus (1999), have visible spectra intermediate between Xk-, L-, and D-types. T-types have been linked with a variety of compositions, including mixtures of organics and hydrated silicates (Gaffey et al. 1993b) and troilite-rich surface compositions (Britt et al. 1992). One of the most-studied T-type asteroids is 308 Polyxo, due to its relatively large estimated size of ~141 km. Hiroi and Hasegawa (2003) noted the spectral similarity of Polyxo in the visible and near-IR with the unusual carbonaceous chondrite Tagish Lake, while Hiroi et al. (2005) noted the spectral similarity of Polyxo and the ungrouped C2 chondrite WIS 91600. Dotto et al. (2006a) analyzed spectra from 7 to 26 μm for 308 Polyxo and found that, in this wavelength region, Polyxo was similar to CO3 chondrite Ornans and was not spectrally similar to Tagish Lake.

V-types

V-type 4 Vesta is the asteroid that has been most persuasively argued to be a meteorite parent body (e.g., Pieters et al. 2005). McCord et al. (1970) discovered that the Vesta spectrum has absorption bands in the visible wavelength region that are similar in structure, wavelength position, and strength to the bands found in HED spectra. Larson and Fink (1975) found that these spectral similarities continue into the near-IR. Hiroi et al. (1994) found that the spectrum of a very fine-grained howardite, EET 87503, was a good match for the spectrum of Vesta (**Fig. 28**). Vesta is a relatively large object (560 by 544 by 454 km) (Thomas et al. 1997b), and is part of the Vesta family, which has over 4000 members (Mothé-Diniz et al. 2005). About 75% of the classified asteroids in the Vesta family are V-types. In the Vesta family, objects with V-class designations generally have diameters less than 10 km, while objects with other designations tend to have sizes greater than 10 km (Burbine 2000).

The proposed linkage between Vesta and the HEDs was strengthened by Binzel and Xu (1993), who found of a number of small objects (< 10 km across) with spectra similar to those of HEDs in the Vesta family, and located between Vesta and the 3:1 resonance. These objects are typically called "Vestoids." Additional main-belt V-types have been identified by Bus and Binzel (2002b) and Florczak et al. (2002). A 460-km crater near the south pole of Vesta has been identified using Hubble Space Telescope Images (Thomas et al. 1997a) and has generally been linked to the formation of the Vestoids. Near-IR spectra of Vestoids (e.g., Burbine et al. 2001b; Kelley et al. 2003; Duffard et al. 2004) confirm their spectral similarities to HEDs (**Fig. 29**). A near-IR spectral study (Duffard et al. 2004) of nineteen V-types near Vesta confirms

the presence of different kinds of basalts, but with no clear correlation between mineralogies and membership to the Vesta's dynamical family.

Vestoids tend to have a relatively large spread in semi-major axis and much tighter distributions in inclination and eccentricity because it is dynamically easier to change the semi-major axis of a body than its inclination or eccentricity (Binzel et al. 1999). Objects randomly ejected from Vesta would be expected to have such a distribution. Dynamical modeling of the migration of some inner main-belt Vestoids (Carruba et al. 2005) suggests that some of these objects could be fragments of Vesta. Roig and Gil-Hutton (2006) have identified ~500 possible Vestoids in the belt using SDSS colors. Approximately half of these possible Vestoids are part of the Vesta dynamical family while most of the other possible Vestoids are located in the inner main belt and are most likely fragments of Vesta. Roig and Gil-Hutton (2006) identified six possible Vestoids in the middle/outer part of the belt that appear quite isolated in proper element space.
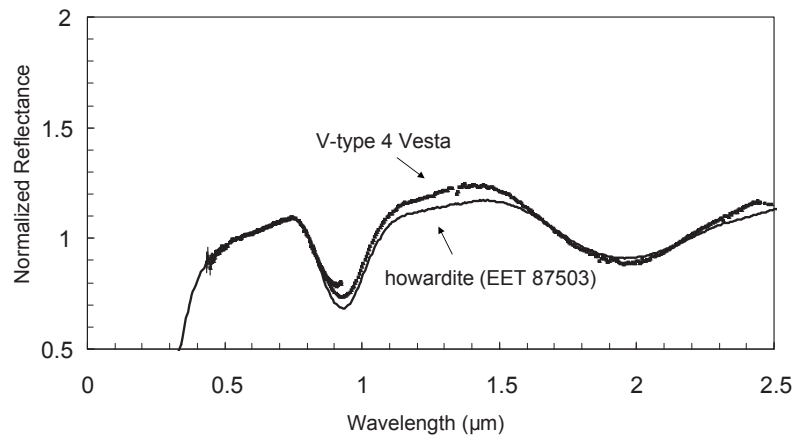
Figure 28. Reflectance spectra of 4 Vesta (Bus and Binzel 2002a; Binzel personal communication) and howardite EET 87503 (Hiroi et al. 1994). Spectra are normalized to unity at 0.55 μm. Error bars are one-sigma, but are smaller than the points for most of the spectrum.
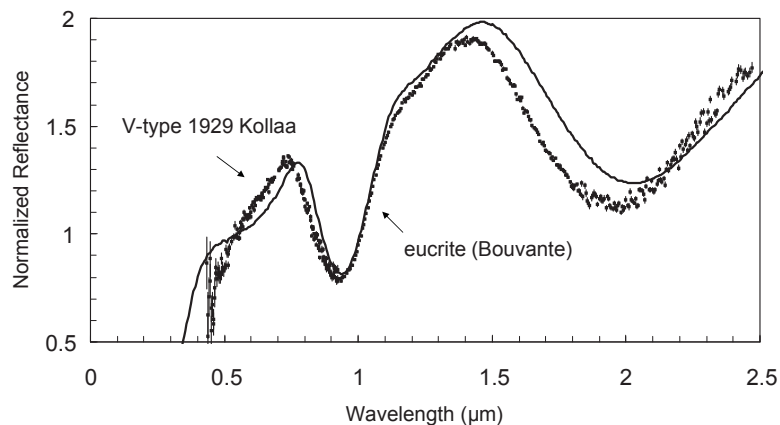
Figure 29. Reflectance spectra of 1929 Kollaa (Bus and Binzel 2002a; Binzel personal communication) and eucrite Bouvante (Burbine et al. 2001b). Spectra are normalized to unity at 0.55 μm. Error bars are one-sigma.

Asteroid 1459 Magnya (Fig. 30) was the first V-type to be identified in the outer main belt (a = 3.15 AU) (e.g., Lazzaro et al. 2000). Dynamically, it is very difficult to derive Magnya from Vesta (Michtchenko et al. 2002). Magnya's recently obtained albedo is 0.37 ± 0.06 (Delbo et al. 2006), which is consistent with HEDs and is much higher than its previously determined IRAS albedo (0.12 ± 0.03). Magnya's diameter was calculated to be 17 ± 1 km (Delbo et al. 2006). Hardersen et al. (2004) found Magnya to be a basaltic assemblage with an average pyroxene composition of $En_{55-57}Fs_{36}Wo_{7-9}$.

Cochran and Vilas (1997, 1998), Vilas et al. (2000), Sykes and Vilas (2001), and Cochran et al. (2004) have found a weak feature at 0.5065 μm in their high-resolution CCD spectra of Vesta and some, but not all, Vestoids. All HEDs appear to have this feature (Hiroi et al. 2001a).

Hasegawa et al. (2003) reported a 3-μm absorption feature in their spectrum of Vesta at about the 1% level. They proposed that this feature may be due to solar wind implantation, with protons reacting with oxygen atoms to form hydroxylated minerals in glasses, and/or the impact of CM2 material. Further observations of Vesta by Vernazza et al. (2005) and Rivkin et al. (2006a) in the 3-μm region do not confirm the presence of this 1% feature. Rivkin et al. (2006a) note that a 1% drop in reflectance is consistent with HED laboratory data, all of which have been affected by terrestrial water. More laboratory study of HEDs under conditions optimized for 3-μm spectroscopy is necessary before the continuum behavior is known to the 1% level near 3 μm.

HELIOCENTRIC DISTRIBUTIONS OF TAXONOMIC CLASSES IN THE MAIN BELT

From the earliest observations of asteroids using UBV (ultraviolet, which peaks at ~0.36 μm; blue, which peaks at ~0.44 μm; and visible, which peaks at 0.55 μm) filters, it has been known that there are systematic spectral differences between inner and outer main-belt asteroids (e.g., Chapman et al. 1971; Gradie et al. 1989). Inner-belt objects tend to have redder (reflectance increasing with increasing wavelength) UBV spectra than the bluer ("flatter" spectra), outer-belt objects. This spectral trend was also apparent when the first asteroid taxonomies were developed (e.g., Chapman et al. 1975), because asteroids classified as S-types were found to dominate in the inner part of the asteroid belt while C-types dominated
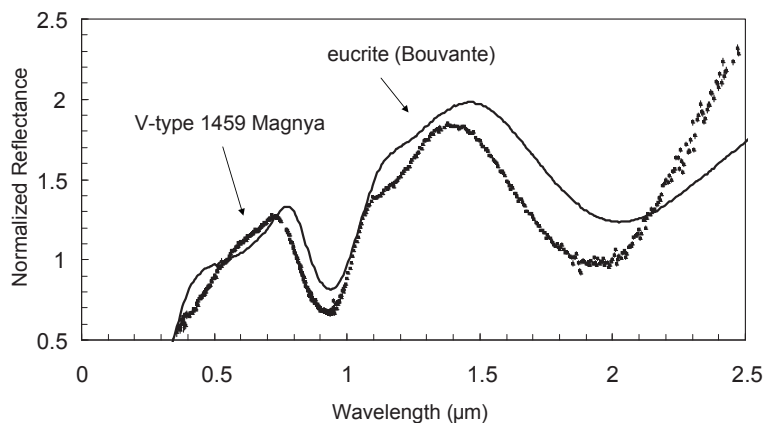
Figure 30. Reflectance spectra of 1459 Magnya (Binzel personal communication) and eucrite Bouvante (Burbine et al. 2001b). Spectra are normalized to unity at 0.55 μm. Error bars are one-sigma.

the outer part. Since Chapman et al. (1975), researchers have carried out various analyses with increasingly larger datasets using different taxonomies, applied to different data sets.

For albedo, the main source is the IRAS (Tedesco 1986) and TRIAD (Tucson Revised Index of Asteroid Data) (Bender et al. 1978) catalogs. For visible spectral data, the surveys available are the ECAS (Zellner et al. 1985b), SMASS I (Xu et al. 1995) and II (Bus and Binzel 2002a), and S3OS2 (Lazzaro et al. 2004). It is important to note that all observational surveys are naturally biased towards bright objects, and to the particular scientific focus of the survey. Therefore, in order to analyze the true heliocentric distribution of classes, it is necessary to correct for observational bias. The research that attempted this kind of analysis differs slightly in the details of how the bias correction is performed, and mainly in the total amount of numbered asteroids known at the time of the analysis.

Zellner (1979) used a variety of observations of over 700 objects available in TRIAD to investigate the distribution of the C-, S-, M-, E-, and R- types, as defined by Bowell (1978). Gradie and Tedesco (1982) accomplished the same kind of analysis using the major classes of Bowell (1978) plus the additional D-, F-, and P-classes, since the Tholen (1984) classification had not been published yet. Gradie and Tedesco (1982) mainly used albedos from the preliminary results of the 10- and 20-μm radiometric survey (Gradie and Tedesco 1988) and ECAS spectra (Zellner et al 1985b). In both of the latter two works, the classified sample objects were bias-corrected according to the population of ~1,400 numbered objects. The availability of IRAS data (Matson et al. 1986), which yielded albedos for more than 1,700 numbered asteroids, allowed Gradie et al. (1989) to reanalyze the taxonomic distribution of asteroids, using their extended 18-class taxonomy based on Tholen's (1984) taxonomy.

Zellner (1979) separated the asteroids into 15 orbital element zones. Four of these zones were associated with dynamical families (Eos, Koronis, Nysa, Themis); six of them represented dynamical associations like the Flora clan, and the Apollo-Amor, Hungarias, Phocaeas, Hildas, and Trojans; four zones were natural separations of the main belt from 2.06 to 3.65 AU according to major mean motion resonances (3:1 at ~2.5 AU, 5:2 at ~2.83 AU and the 2:1 at ~3.27 AU); and one zone was called "exceptional", covering all objects that could not fit into one of the previous groups. The Gradie and Tedesco (1982) zones were slightly different, based on the twelve regions defined by Kiang (1971): nine zones corresponding to the Kirkwood gaps and other commensurability points; the range $1.0 < a < 2.0$ AU; the Hildas; and the Trojans. Gradie et al. (1989), on the other hand, bias-corrected their data using the 19-zone system of Zellner et al. (1985a).

To perform the bias correction in either work, only asteroids with mean opposition magnitudes less than 16.5 were retained in the sample, and each zone was then divided into half-magnitude bins. Then, the bias factor f was computed as the ratio of the number of asteroids present in the zone to the number sampled. It was assumed that for each classified asteroid A, with a bias factor f, there are $f−1$ additional objects of identical type and diameter in the same zone. Additionally, Gradie and Tedesco (1982) identified and discarded members of asteroid families (Flora, Nysa, Koronis, Eos, Themis). To account for the oversampling of these objects, each dynamical family has been represented by a single object of the most common type found in that family. They also discarded the planet-crossing objects because their formation locations are different from where they are found today.

The main result of these works is that the heliocentric distribution of taxonomic types is not uniform. This agrees with the earlier work of Chapman et al. (1975), who performed a bias-corrected analysis of the physical properties of a set of ~80 asteroids with $D > 90$ km. Moderate-albedo S-types prevailed in the inner belt ($a < 2.4$ AU) while low-albedo objects dominated the outer belt ($a > 2.4$ AU). Zellner (1979) found that, for the whole main belt population, ~75% are C-types, ~15% S-types, and ~10% are other types.

Gradie and Tedesco (1982) showed that the main belt is highly structured, with at least six major compositionally distinct regions, and a particular class or set of classes dominating each region. They proposed that the asteroids formed at or near their present locations, because this distinct zoning of the distribution could not be explained by random transport of objects over large distances of the Solar System. In particular, the S-types peak at ~2.3 AU and make up 40% of the local population, while the C-types have their maximum at ~3.0 AU, accounting for 80% of the local population.

Assuming the usual linkages between taxonomic classes and particular asteroids, the distribution of objects found by Gradie and Tedesco (1982) mimics part of the equilibrium condensation sequence (Table 1), with enstatite-rich bodies being found in the inner belt and asteroids becoming more oxidized with larger heliocentric distances. High-albedo E-types (linked with the enstatite-rich aubrites) are found in the innermost part of the belt. S-types, which tend to contain ferrous olivines and pyroxenes, are most abundant in the inner part of the belt. The low-albedo C-complex objects (usually linked with some type of carbonaceous chondritic material) peak in the middle of the belt. Lower-albedo P- and D-types, believed to be organic-rich, peak in the outermost part of the belt.

In the Chapman et al. (1975) analysis, the same general characteristic was seen: moderate-albedo objects dominate the inner belt and the low-albedo objects were preferably found in the outer belt. The main difference between the results of Chapman et al. (1975) and the work of Gradie and Tedesco (1982) concerns the distribution of C-class objects in the main belt. Gradie and Tedesco (1982) see a peak in the distribution at around 3.0 AU, which is not as apparent in the Chapman et al. (1975) distribution.

Since the last decade, high throughput long-slit spectrographs employing charge-coupled devices (CCDs) have become widely used in measuring the visible spectra of asteroids. Initiated in 1991, data from SMASS II (Bus and Binzel 2002a) became available in 2001, and produced an internally consistent dataset of spectra for over 1,400 asteroids in the 0.44-0.92 μm spectral range. The SMASS II survey focused on regions surrounding the asteroid 4 Vesta, and between 2.69 and 2.82 AU, with detailed investigations of dynamical families in these regions.

Initiated some years later, another survey, S3OS2 (Lazzaro et al. 2004), was completed and obtained visible spectra for over 700 asteroids from 0.5-0.92 μm. Like SMASS II, S3OS2 is also biased, because part of the survey focused on some large asteroid families or clans like Flora, Eunomia and Themis, as well as the "Magnya region" around 3.14 AU, and the regions around some resonances. Another focus of the S3OS2 was on asteroids located at high eccentricities and inclinations. Asteroid spectra in both surveys were classified according to Bus' (1999) taxonomy, which is based on the Tholen's (1984) taxonomic system. Therefore, most of the objects belonging to one of the classes of Tholen are also members of one of the Bus (1999) complexes.

Bus (1999) used ~1,200 objects located between 2.10 and 3.278 AU, with most objects having D < 20 km, to determine the heliocentric distribution of the Bus (1999) classes. The diameters of the objects were estimated using the mean IRAS albedos for each spectral class. He divided the belt into three zones, with limits of $2.100 \leq a < 2.501$ AU, $2.501 \leq a < 2.825$ AU, and $2.825 \leq a < 3.278$ AU. These boundaries were defined according to the locations' major mean motion resonances. As in the earlier works, the correction factor, f, for a particular zone was calculated as the ratio between the total number of asteroids in that bin to the number of classified asteroids in the bin. Then, given an asteroid belonging to a taxonomic class, and with a correction factor f, the remaining $f-1$ asteroids of the same class were distributed around the semi-major axis of a, according to a normal distribution, with a standard deviation of ±0.1 AU. This procedure was adopted in order to avoid the creation of large concentrations of asteroids in regions where the bias correction factors were large.

Mothé-Diniz et al. (2003) used ~2,000 classified objects from both the SMASSII and S3OS2 surveys with semi-major axes between 2.064 and 3.278 AU. Only asteroids with magnitude H < 13.0 were used in the analysis. This corresponds to objects larger than 7 km in the S-complex, 13 km in the C-complex and 10 km in the X-complex, considering a mean albedo for each complex derived as the average of the median albedo of the subclasses of the complex. To account for the bias correction, Mothé-Diniz et al. (2003) used small refinements of the method used by Bus (1999), with the belt divided into 6 zones, according to the major mean-motion resonances with Jupiter (at ~2.50, ~2.823, ~2.956 AU). Two additional divisions were placed at 2.70 and 3.08 AU for a better correction. Also, the distribution of the *f−1* asteroids in semi-major axis was made according to a standard deviation (σ) derived empirically: $\sigma = 0.008 \times f$, if $0.008 \times f \leq 1/6\Delta a$; and $\sigma = 1/6\Delta a$ otherwise. As in the work of Bus (1999), this procedure was adopted in order to minimize the effects of large bias factors in some regions.

Mothé-Diniz et al. (2003) studied the taxonomic distribution according to different criteria: using the whole debiased population; considering each asteroid family as one body of the most common class in the family, plus the "interlopers;" considering only objects larger than 13 km (to study the influence of very small objects in the distribution) and removing the effects of families; and, finally, all the preceding analysis techniques, but for asteroids in the Low Main Belt (LMB) and in the High Main Belt (HMB) separately. The HMB was composed of asteroids with high eccentricities ($e > 0.15$) or high inclinations ($i > 15°$), and the LMB contained the remaining objects. The authors did not study the distribution of the "outlying classes" V, O, T, D, and Ld of Bus (1999), because the relative frequencies of these classes were significant only in very narrow regions of the main belt. Figure 31 shows the percentage of each complex versus heliocentric distance for the whole sample, while Figures 32a,b shows
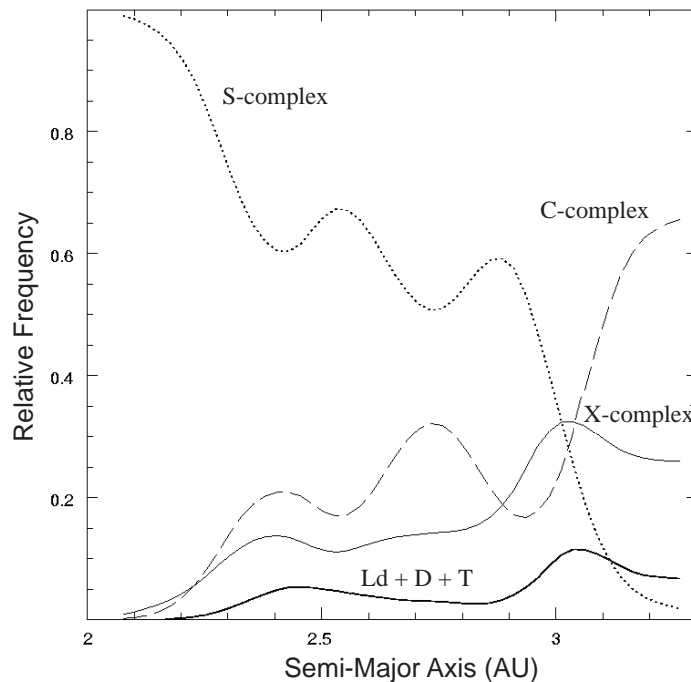
Figure 31. Plot reproduced from Mothé-Diniz et al. (2003) data, showing the fraction of bias-corrected SMASSII and S3OS2 objects per semi-major axis, from 2.064 to 3.78 AU, for the major S-, C-, and X-complexes and the outlying Ld-, D-, and T-classes.
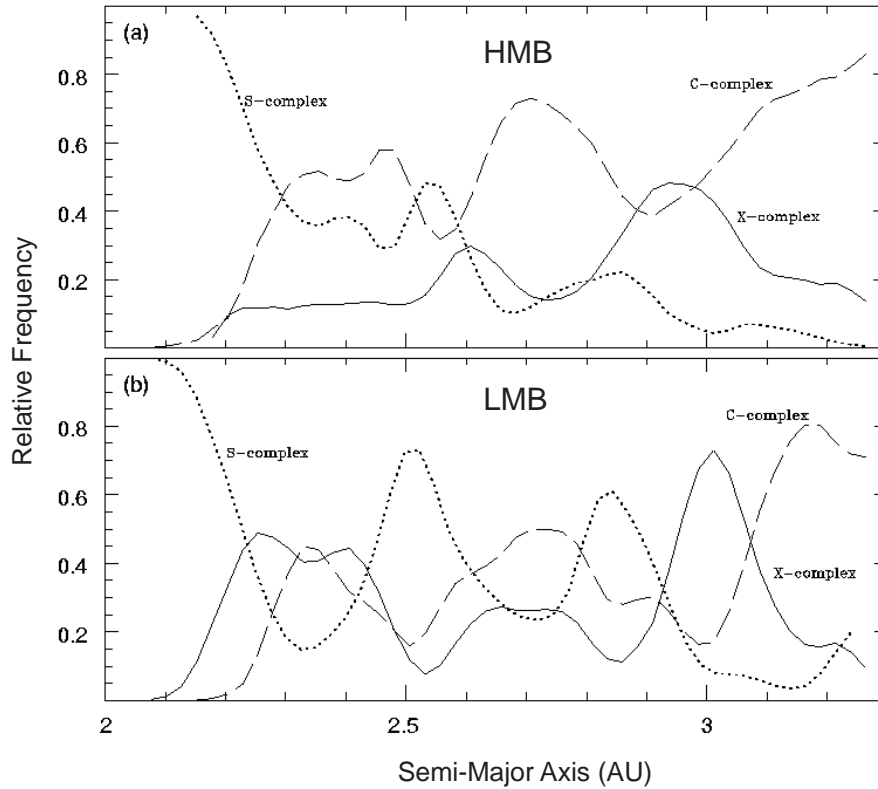
Figure 32. (a) Plot reproduced from Mothé-Diniz et al. (2003) data, removing asteroid families as described in the text, and considering only objects in the high main belt (HMB). (b) The same as in Figure 32a, but considering only objects in the low main belt (LMB).

the percentages for the HMB and LMB, respectively. The outlying classes Ld, D, and T, which are not presented by Mothé-Diniz et al. (2003), have been added to Figure 31 for a better comparison with the distributions produced by Bus (1999).

The results of Bus (1999) confirm the main results of Gradie and Tedesco (1982). Considering only objects larger than 20 km, they found that the percentage of objects of the C-complex increases from ~25% in the inner to almost 65% in the outer main belt. On the other hand, the percentage of asteroids in the S-complex decreases from about 55% to 5% in the same interval of semi-major axis, while the distribution of asteroids in the X-complex is quite flat, at a level of 20%.

The results of Mothé-Diniz et al. (2003) are also similar to the previous works of Gradie and Tedesco (1982) and of Bus (1999), but only if they used a "restricted sample:" either the objects larger than 30 km diameter, or those with high inclinations or eccentricities (HMB) (Fig. 32a). Using the entire database, the distribution of taxonomic classes is significantly different from previous work because it does not show a steep decrease of S-types with semi-major axis. The S-types are rather evenly distributed along the main belt, even when families and small asteroids are not included in the analysis (smaller than 13 km, which represents the size above which the population of asteroids in the three complexes of Bus (1999) is complete). By studying the spatial distribution (HMB vs. LMB) of the asteroidal population, Mothé-Diniz et al. (2003) noticed that the distribution in the LMB (Fig. 32b) is very different from that in

the HMB (Fig. 32a), with the latter distribution being similar to the results of previous authors. These results indicate that the LMB seems more "mixed" than the HMB.

In addition to the new spectroscopic data, an enormous database of asteroid spectrophotometric data from SDSS has been released (Ivezić et al. 2001). Five-color CCD photometry was determined almost simultaneously in five bands: u, g, r, I, and z, centered respectively at 0.3557 μm, 0.4825 μm, 0.6261 μm, 0.7672 μm, and 0.9097 μm, that have 0.1-0.3 μm band widths (Fukugita et al. 1996). This catalogue provides important information on asteroids because it has a detection limit much fainter ($V \approx 21.5$) than other asteroid surveys ($V \approx 18$) (Ivezić et al. 2002) (Fig. 33). Using SDSS observations, Ivezić et al. (2002) estimated that 90% of asteroids in the main belt are parts of families. They found that objects that did not belong to the most populous families and are usually thought of as background objects did show color clustering. One flaw in this argument is that just because objects have similar colors does not mean that they are genetically related.

The main limitation of any study of the distribution of taxonomic classes is the availability of spectral data. The observations that allow taxonomic classifications cover only a small fraction of the numbered asteroids. This leads to large bias factors in some regions that have not been well-sampled. Another limitation is the incompleteness of the numbered population, presently starting at about absolute magnitude 11.75 in the external part of the main belt (3.0-3.5 AU), 12.25 in the intermediate main belt (2.6-3.0 AU), and 12.75 in the inner main belt (2.0-2.6 AU) (Jedicke and Metcalfe 1998).

One could also expect a limitation caused by the magnitude cutoff, i.e. the diameter cutoff, which is a function of heliocentric distance, and is different for each class. In fact, this causes the bias analysis to be limited to diameters larger than the cutoff diameter of the most distant zone.
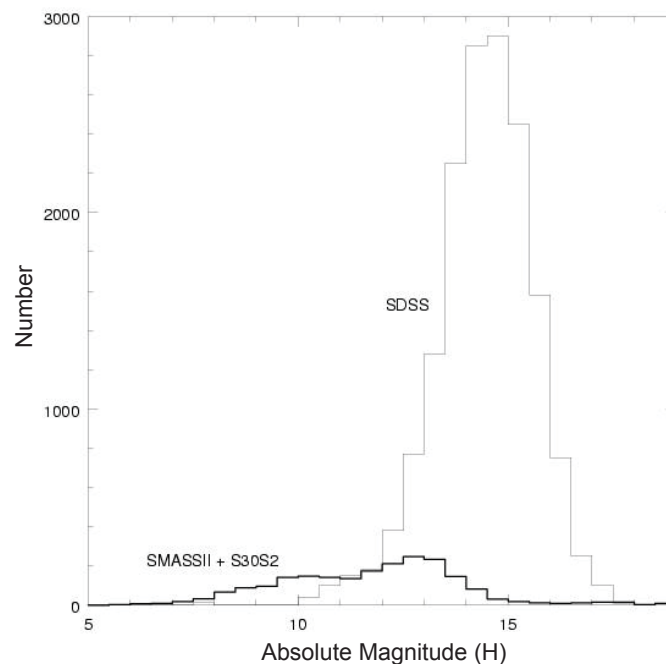
Figure 33. Histograms showing the number of objects observed in SMASSII and S3OS2, compared to those observed in SDSS, per half-magnitude bin.

This point does not represent a real limitation, because most of the small objects come from the breakup of larger bodies, and in all analyses, the asteroid families were considered as one single body. Therefore, most of the small objects in the sample were not taken into account.

The meaning of some taxonomic classes has changed significantly from the first classification scheme of Chapman et al. (1975) and the first work on the distribution of classes of Zellner (1979). However, the cores of some classes have suffered little change. This is the case of the S and C classes, which were recognized very early as distinct groups. In the Bus taxonomy, all the S-types, and their subtypes according to other taxonomies, are included in the S-complex. The same is true for the C-complex. Thus, the conclusions from research on the C- and S-complexes should be directly comparable to previous studies that involved the C- and S-types.

The same is not true for X-types. The X-complex of Bus (1999) is composed of, among others, objects from the earliest E-, M-, and P-classes, which are subtypes of Tholen's (1984) X-class. As discussed earlier, objects from the E-, M- and P-classes have similar, featureless visible spectra, but have been separated according to their albedo. However, even if an old X-type object belongs to the X-complex, it is difficult to compare the distribution of this complex from 2.064 to 3.278 AU to previous studies. These earlier works included the heliocentric distributions of types E, M and P individually, and because albedo data are not used in the Bus (1999) taxonomic scheme, we cannot say whether or not the distribution of the X-complex or of one of its subtypes is similar to that of earlier works.

There are definite trends in the distribution of X-types in the far inner and outer main belt regions that appear consistent with mineralogical differences. Asteroids in the Hungaria group (1.78-2 AU) are known to contain a considerable number of asteroids classified as E (Clark et al. 2004a), X, and Xe (Carvano et al. 2001). The distribution of different classes in the Cybele region was found to be a function of size, with the spectrally red D-type asteroids generally more numerous at small diameters, while larger asteroids tended to be more spectrally neutral (flatter spectral slopes), such as X-types. The number of P-types decreases with increasing distance from the Sun. Dahlgren et al. (1997) found that objects in the Hilda group (3.70-4.20 AU) are typically D types, with very few C- and P-types, and with relatively low albedos (0.03-0.11). Still farther out, Fornasier et al. (2004) found that Trojan asteroids (~5.2 AU) are predominantly D-types with only a few P-types.

Taxonomic classifications are based on spectral features which, among ground-based spectroscopic measurements, are the best indicators of an asteroid's underlying composition. Therefore, they should provide some indication of an asteroid's mineralogy, as well as an interpretation of their distribution along the main belt. Based on the results of Gradie and Tedesco (1982), Bell et al. (1989) attempted to relate the distribution of classes with mineralogy, by proposing a scenario in which the "igneous" asteroids (objects formed from a melt and represented by the classes V, R, S, A, M and E) were in the inner part of the main belt; the "metamorphosed" (those that have been sufficiently heated to exhibit spectral changes, represented by the classes B, F, G, and T) in the middle; and the "primitive" (those that have undergone little or no heating, with representatives in the classes D, P, C, K, and Q) in the outer part of the belt. These three large groups were called "superclasses" and agreed with the intuitive picture of a heliocentric heating gradient. This interpretation is dubbed the "Big Picture."

The main complaint with the "Big Picture" is the mineralogical interpretation of the igneous classes. Bell et al. (1989) considered the S-types as igneous since, at that time, they were commonly associated with achondrites and stony-iron meteorites, even if an alternative association with ordinary chondrites was already postulated through dynamical studies and meteorite fall rates. With the increase of the quantity and quality of the observations, as well as a better understanding of the space weathering phenomenon, however, this paradigm has changed. There is now stronger evidence linking some S-types to ordinary chondrites and a

better understanding of space weathering processes (e.g., Chapman 1996; Binzel et al. 1996; Pieters et al. 2000; Chapman 2004). There is evidence for partially differentiated S-complex asteroids (e.g., Gaffey et al. 1993a; Hardersen et al. 2006; Gaffey 2006), but it is still unclear whether chondritic or partially differentiated objects predominate among the S-types.

Sunshine et al. (2004) suggest that some members of the Merxia and Agnia families might be differentiated. However, the location of these two "differentiated" families in the main belt (around 2.74 AU and 2.78 AU, respectively) does not seem to support the kind of heating gradient in the asteroid belt that Bell et al. (1989) suggested. Another question is the absence of differentiated families associated with M-types. Such families were to be expected if M-types are metallic cores of differentiated parent bodies that formed locally and were shattered by catastrophic collisions. Moreover, the discovery of hydration bands in some M-types (Rivkin et al 2002) suggests that many M-types are not metallic. Finally, a basaltic V-type (1459 Magnya) was found in the outer belt, without any apparent dynamical relation with the Vesta family (Lazzaro et al. 2000; Michtchenko et al. 2002). This discovery is inconsistent with the strict zoning of the belt proposed by Bell et al. (1989). Mothé-Diniz et al. (2003) showed that S-types are almost as abundant in the outer part of the belt as in the inner belt.

In summary, the scenario of the "Big Picture" is no longer valid but, on the other hand, at present no clear and/or intuitive geological scenario for the distribution of the taxonomic classes can be proposed. In fact, a picture emerges of a main belt where both the dynamical and thermal evolution is much more complex than what is depicted in the Bell et al. (1989) "Big Picture." There seems to be much more mixing than was previously proposed, specifically among small asteroids.

This mixing is consistent with the knowledge that Yarkovsky effects can lead to considerable semi-major axis mobility for small asteroids (Bottke et al. 2002, 2006b). The Yarkovsky effect is a non-gravitational thrust produced when small bodies absorb sunlight, heat up, and then re-radiate the energy after a short delay due to the thermal inertia of the surface. In this context, we can suggest a possible explanation for why the taxonomic distribution in the upper main belt is more similar to what is seen when only bigger asteroids are considered: in general, high-eccentricity asteroids can move only through a small range in semi-major axis before hitting a resonance and being removed.

The abundance of high-albedo objects with featureless spectra consistent with aubrites in the interior Hungaria region of the belt appears to indicate that objects in this region were heated to temperatures high enough for them to melt. The abundance of C-complex asteroids in the outer part of the belt and D- and P-objects still farther out indicates that asteroids in these regions were not significantly heated. But without knowing how ordinary chondrites, partially-differentiated, and fully-differentiated asteroids are distributed in the S-complex population, it is very difficult to understand how the heating gradient varied throughout most of the belt. Was there a sharp dropoff in heating with heliocentric distance, or was the dropoff more gradual?

DISTRIBUTION OF HYDRATED ASTEROIDS IN THE MAIN BELT

Looking at the belt as a whole, it is clear that there is a correlation between semi-major axis and various measures of hydrated mineral concentration. Figure 34 shows the fraction of objects testing positive for hydrated minerals using the 0.7-μm and 3-μm regions. An understanding of the distribution of water in the asteroid belt is inevitably shaped by an understanding of how meteorite samples are delivered to Earth. The fraction of hydrated meteorites found on Earth is skewed by many factors, including the relatively low strength of hydrated meteorites relative to other meteorites, and the observation that impacts into carbonaceous chondrites seem to generate fewer large pieces of ejecta and a greater mass of dust (Tomeoka et al. 2003). When combined with the greater contribution made to the meteorite population by objects in
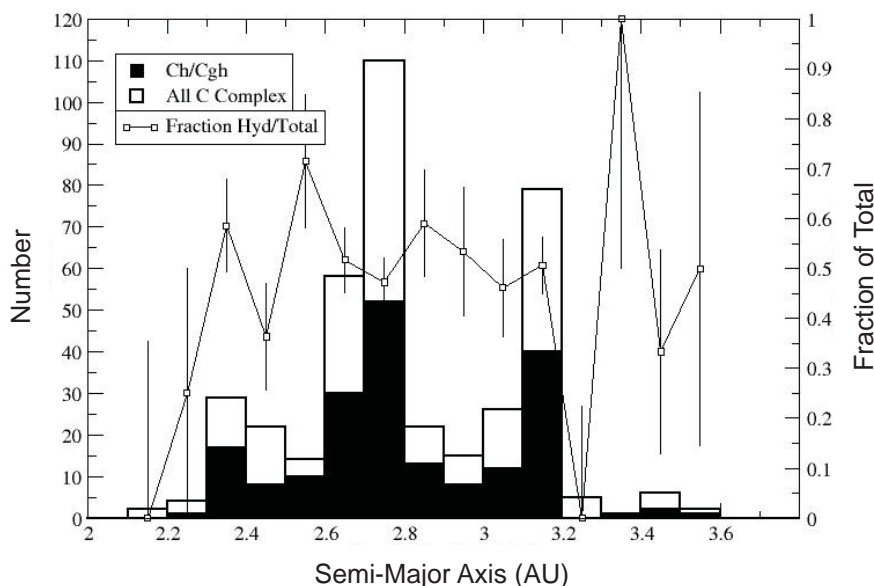
Figure 34. Hydrated C-types in the main belt. The histogram shows the number of C-complex (shaded) and Ch/Cgh-subclass (solid) objects in the belt vs. semi-major axis (AU). In areas with good statistics, the Ch/Cgh objects represent roughly half of the C-complex. The open symbols represent this fraction, using the axis on the right. It is uncertain whether the increase from 2.1-2.3 is an artifact due to small number statistics. Given that some C-types can be hydrated without having a 0.7-μm band (which would make them Ch/Cgh), the true fraction of hydrated C asteroids is higher than 0.5.

the inner asteroid belt and near resonances, it is unlikely that the meteorite collection is a true measure of the relative proportions of materials present in the asteroid belt, and furthermore some unsampled mineralogies may easily be present. As discussed by Burbine et al. (2002b), there is a huge difference between the number of distinct parent bodies (~100-150) that we have evidence for in our meteorite collections and the number of asteroids in the main belt. In terms of the carbonaceous chondrites, roughly 2/3 of falls are hydrated. This ratio is in good agreement with observations of main-belt C-types, of which roughly 2/3 show a 3-μm band (Rivkin et al. 2002).

Nearly 400 different objects in the C-complex have been identified in the SMASS and S2OS3 surveys (Bus and Binzel 2002b; Lazzaro et al. 2004). Figure 34 shows a histogram of this population and its Ch/Cgh fraction as a function of semi-major axis. In addition, the fraction of the C-complex sample that appears hydrated (Ch- and Cgh-subclasses) is shown. The fraction of hydrated C-types, by this measure, is 0.51 ± 0.07 between 2.3 and 3.2 AU, where the majority of this class is found.

The majority of hydrated C-types have spectra with band shapes similar to those of the CM chondrites. However, roughly 1/3 of the objects have band shapes like Ceres, which differs significantly from the typical CM-like shape (Rivkin et al. 2004b). It appears that within a given asteroid family, all members tend to share the same hydration state (Bus 1999). However, several objects have been seen to have varying 0.7- or 3-μm bands with rotation (Howell et al. 2001a), which is not obviously consistent with the family observations.

In the outer belt, the number (and fraction) of objects which show evidence of hydrated minerals drops dramatically. Observations at 3 μm by Jones et al. (1990), Lebofsky et al. (1991), Howell (1995), and Emery and Brown (2003) found no clear-cut evidence of any Trojan with a

3-µm band. Given the position of the Trojans, between hydrated C-types and the icy satellites of Jupiter, this is particularly surprising. Jones et al. (1990) interpreted this to mean that the Trojans, which presumably formed from water ice and anhydrous silicates, never got hot enough to create hydrated minerals, and that any ice present would be found beneath the surface. Cruikshank et al. (2001) obtained data on 624 Hektor and analyzed it using a Hapke mixing model. They placed a relatively high upper limit of 40% for phyllosilicates mixed with low-albedo constituents, and noted that the lack of a 3-µm band did not rule out surficial hydrated minerals *per se*. They also reinterpreted the trend of decreasing frequency of hydrated minerals with increasing solar distance as due to an increase in macromolecular carbon compounds, which could mask the spectral signature of hydrated minerals.

The Trojan asteroids are an interesting contrast to the moons of Jupiter. The Galilean satellites (other than Io) appear to not only have copious amounts of water ice, but also hydrated non-ice material (McCord et al. 1997; McCord et al. 1999). The small, irregular moons of Jupiter also show evidence of hydrated minerals: a 3-µm band is present on Amalthea (Takato et al. 2004) and a 0.7-µm band is seen on Himalia, along with a possible 3-µm band (Jarvis et al. 2000; Chamberlain and Brown 2004). Recent work (Morbidelli et al. 2005) suggests that the Trojans may have been captured from the Kuiper Belt during the period of planetary migration. In that case, the connection between the Trojans and main-belt asteroids becomes more confusing, and the lack of hydrated minerals even more puzzling.

The inner asteroid belt is dominated by objects that are usually interpreted as the parent bodies of anhydrous meteorites, such as the ordinary chondrites and achondrites. There is some evidence of aqueous alteration in ordinary chondrites, with the identification of phyllosilicates (Hutchison et al. 1987) and fluid inclusions in halite (NaCl) (Zolensky et al. 1999) in some ordinary chondrites. We may expect some inner belt S-types to show 3-µm bands. Indeed, 6 Hebe, proposed as the H chondrite parent body by Gaffey and Gilbert (1998), has been found to have a weak 3-µm band (Rivkin et al. 2001). About 1/3 of the M-types reported by Rivkin et al. (2000) have a 3-µm band, as do 4 of the 6 E-types surveyed (Rivkin et al. 1995; Rivkin 1997). The mineralogies of hydrated M-types, labeled as the W-class by Rivkin et al. (1995), and of hydrated E-types have not been fully understood, perhaps representing objects with mineralogies not present in our meteorite collections, such as having large concentrations of high-albedo salts. Hardersen et al. (2005) included bencubbinites as a possible interpretation of a number of M- and W-types using 0.8–2.5 µm data, which may be a preferred interpretation because some of these meteorites contain hydrated minerals (Krot et al. 2002).

The hydrated E-types have no obvious analogs among meteorites, although hydrated enstatite chondrite clasts exist in the Kaidun meteorite (e.g., Zolensky and Ivanov 2003). The hydrated E-types are all in the main part of the asteroid belt rather than the Hungaria region, which dominates the inner edge of the belt and is where the majority of E-types are found. This is consistent with the Hungaria-region objects being different mineralogically from the E-type asteroids further out in the belt.

NEAR-EARTH ASTEROIDS

Near-Earth asteroids, or NEAs, are asteroids with perihelia less than 1.3 AU. Over 4,000 NEAs are currently known. Because of their short dynamical lifetimes, resupply from the main belt is necessary to provide the number of NEAs currently seen. Mars-crossers (MCs) are objects whose orbits cross that of Mars and are thought to be in the process of being dynamically pushed out of the main belt into the NEA population. Binzel et al. (2004) looked at the classifications and spectral properties of ~400 NEAs. The NEAs tend to be dominated by objects that are part of the S- (S, Sa, Sk, Sl, Sr, K, L, and Ld) and Q- (Q and Sq) complexes, as defined by Binzel et al. (2004), with approximately 2/3 of all objects belonging to one of those

two complexes. More recent surveys (Lazzarin et al. 2004) have results that are consistent with Binzel et al. (2004). Marchi et al. (2005b), de León et al. (2006), Duffard et al. (2006), and Davies et al. (2007) have also identified a number of NEAs with V-type spectra.

Marchi et al. (2006a) found a correlation between the visible spectral slope and perihelion distance. They found that the average spectral slope decreases with decreasing perihelion distance, which means that Q- and Sq-types are more abundant at smaller perihelion distances. NEAs with small perihelion distances are more dynamically evolved, meaning that they have had more close encounters with planets. Nesvorný et al. (2005) proposed that close encounters with planets should change the optical properties of a surface through tidal effects that can remove a significant proportion of space-weathered material or can bury the space-weathered material under fresher subsurface material.

There appears to be fewer hydrated NEAs than one would expect from looking at either the main-belt or meteorite data. Because of the faintness of typical NEAs, 3-μm observations are difficult, and those which are observable typically require much larger thermal corrections than are necessary for main-belt objects. Therefore, these objects are obvious candidates for use of the 0.7-μm proxy band. Binzel et al. (2004) found 18 NEAs belonging to the C complex, including objects with and without the 0.7-μm band. Because of their comparable albedos, observing biases between hydrated and anhydrous objects should be minimal or nonexistent.

In contrast to the fraction of hydrated C-types found in the main belt and the fraction of hydrated carbonaceous chondrites, only one Ch-type has been found among the NEAs, and the Cgh-class was the only Bus (1999) class absent from the NEO population in this sample. The C-complex objects on Mars-crossing orbits are more evenly split (3 Ch-types out of 7). While this result is based on a relatively small sample, the numbers are surprising, because 9 Ch/Cgh NEAs would be expected if there were the same correlation between the 0.7- and 3-μm bands as seen in the main belt. Even assigning a 50% correlation, much lower than that seen among the main-belt objects, 6 objects would be expected. It is unclear what the cause is for this difference. The temperature (~400 $^{\circ}$C) needed for the 0.7-μm band to disappear (Hiroi et al. 1996b) is much higher than the sub-solar temperatures for even very low-albedo objects at 1.0 AU, which may reach 150 $^{\circ}$C at the most. However, because the Hiroi et al. (1996b) result is an upper bound on this band's disappearance, heating due to solar radiation still may play a role. Heating due to micrometeorite impacts could also dehydrate carbonaceous chondritic material. In addition, the C-complex population of NEAs may contain a contribution from extinct comets (e.g., Binzel et al. 2004). Binzel and Lupishko (2005) estimate that 15 ± 5% of NEAs may be extinct or dormant comets, although most of these are on short-lived, Jupiter-crossing orbits (Bottke et al. 2002). The extinct comet population might not contain hydrated minerals, or at least may not show evidence for them based on the available spectra (e.g., Abell et al. 2005). Near-IR spectra of 1373 Cincinnati and 2906 Caltech, which have cometary orbits, have spectral properties (Ziffer et al. 2005) roughly consistent with cometary nuclei and primitive asteroids.

SPACECRAFT MISSIONS

The exploration of NEA 433 Eros by the Near Earth Asteroid Rendezvous (NEAR)-Shoemaker mission opened another chapter in linking asteroids and meteorites. Like previous ground-based and fly-by measurements, NEAR-Shoemaker relied heavily on the multi-spectral imager (MSI) and near-IR spectrometer (NIS), which provided reflectance spectra from 0.45-2.6 μm, for mineralogical interpretation and asteroid-meteorite linkages. Ground-based observations (Murchie and Pieters 1996) were interpreted to indicate that Eros was heterogeneous in composition, with an olivine-rich side and a pyroxene-rich side. Despite high spatial resolution, however, little color variation was observed by NEAR-Shoemaker, although significant variations in albedo are present on Eros (McFadden et al. 2001). As had also been observed from

numerous telescopic studies of other S-types, NEAR-Shoemaker reflectance spectra of Eros are a relatively poor fit to the ordinary chondrites, although the band centers and Band Area Ratios are similar to those of ordinary chondrites. McFadden et al. (2001) calculated an ol/(ol+pyx) ratio of 0.58 ± 4% for Eros. This mismatch between spectral matching and derived band parameters has plagued much of asteroid spectroscopy and, for the first time, NEAR-Shoemaker provided the tools to resolve this issue in the form of X-ray and gamma-ray spectrometers.

Eros was the first asteroid where *in situ* geochemical measurements (Trombka et al. 2000) have been made. These measurements provided not only a seemingly solid link between S-types and ordinary chondrites, but also provided some unexpected insights into the processes occurring on asteroid surfaces. Evans et al. (2001) used gamma-ray data and Nittler et al. (2001) used x-ray data to determine the geochemistry of the surface of Eros. Calculated elemental weight ratios (Mg/Si, Al/Si, Ca/Si, Fe/Si), determined from x-ray data, and Si/O and the K abundance are all within the range of ordinary chondrites. However, the calculated S/Si, Fe/Si (determined from gamma-ray data), and Fe/O elemental weight ratios are low compared to values for ordinary chondrites.

The two most plausible explanations for these differences are small degrees of partial melting and space weathering. Nittler et al. (2001) rejected the former hypothesis, because, while removal of metal and sulfide could explain the apparent fractionation of these components relative to silicates, studies of partially melted meteorites universally find non-chondritic Al/Si ratios in meteorites depleted in metal and troilite. Instead, it appears that a combination of space weathering and mechanical metal-silicate separation are responsible for the aberrant S/Si, Fe/Si (determined from gamma-ray data), and Fe/O ratios. Depletion of S likely results from dissociation of FeS due to solar wind exposure and micrometeorite bombardment, with loss of the volatile S. In contrast, separation of metal from silicates to explain the low Fe/Si and Fe/O ratios likely results from the physical processes operating in the regolith to separate the dense metal from the lighter silicates. These interpretations have been bolstered by recent determinations of chondritic Cr/Fe, Mn/Fe, and Ni/Fe ratios from X-ray spectra (Foley et al. 2006).

While these interpretations paint a dynamic picture of the regolith of an asteroid, they were only possible because of the coupling of mineralogical information from reflectance spectra and chemical information from X-ray and gamma-ray spectroscopy. Even with this powerful combination, uncertainties in the data prevented the NEAR-Shoemaker team from definitively linking 433 Eros to one of the chemical subgroups of ordinary chondrites (H, L, LL) (McCoy et al. 2001, 2002). It appears theoretically possible to use remotely-sensed Si/O ratios to determine the olivine/pyroxene ratio with a level of uncertainty that, coupled with precise mineralogical information, would allow one to remotely determine the f_{O_2} of formation of an asteroid. Such information and a definitive meteorite-asteroid link at the subgroup level, while theoretically possible, may well have to await sample return.

NEA 25143 Itokawa was the target of the Hayabusa mission, which orbited Itokawa and attempted to retrieve a sample. A reflectance spectrum of Itokawa by Binzel et al. (2001) appears similar to a reddened LL chondrite (**Fig. 35**), with MGM modeling of the spectrum also consistent with an LL chondrite composition. Burbine et al. (2003) interpreted the resulting Band Area Ratio of Itokawa to imply an *ol/(ol+pyx)* ratio of ~0.70. Folco et al. (2005) argued that Itokawa could possibly be an impact-melted H or L chondrite where olivine has been enriched in the surface after impact melting. A mineralogical analysis by Abell et al. (2006) of their spectrum of Itokawa indicates a pyroxene composition of $Wo_{16\pm5}Fs_{44\pm5}$, which is much more FeO-rich than the average composition of pyroxene in ordinary chondrites, and an ol/(ol+pyx) ratio of ~0.70. Abell et al. (2006) believe that Itokawa is a partially differentiated object.

Results from Hayabusa's near-IR spectrometer confirm the presence of olivine and pyroxene on Itokawa's surface (Abe et al. 2006). Abe et al. (2006) find that Itokawa's surface is olivine-rich and that Itokawa's 1-μm band is most similar in shape to those of LL5/LL6 chondrites.
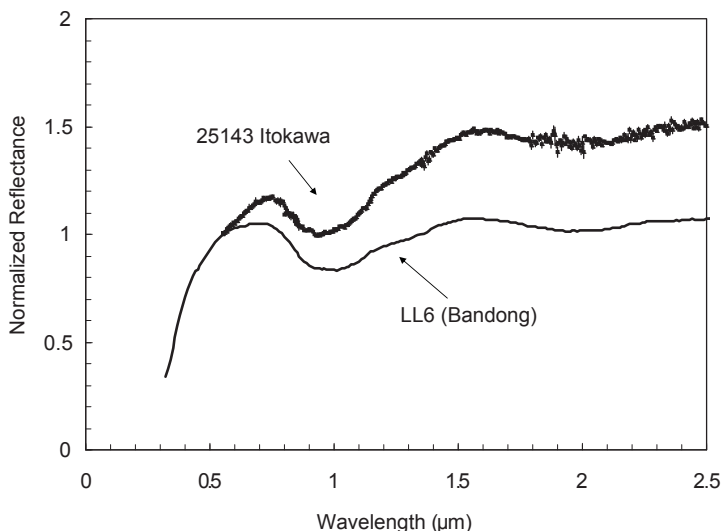
Figure 35. Reflectance spectra of S-type NEA 25143 Itokawa (Binzel et al. 2001) and LL6 chondrite Bandong (Burbine et al. 2003). Spectra are normalized to unity at 0.55 μm.

Results from Hayabusa's X-ray spectrometer are consistent with L and LL chondrites (Okada et al. 2006). Using near-IR spectra data, Hiroi et al. (2006) found that one dark region on Itokawa was significantly more space-weathered than a nearby bright region. They also found that the spectra of the two regions were consistent with LL5/LL6 chondrites with the spectral continuum removed, and that the spectral difference between the dark and bright region was consistent with a higher abundance of nanophase iron particles for the dark region.

Sample collection was attempted, with Hayabusa twice landing on Itokawa's surface. It is unclear at this writing if a metal projectile was successfully fired to cause Itokawa fragments to be ejected from the surface and into the sample return canister. Due to thruster problems, the plan is now for the Hayabusa spacecraft to return to Earth in 2010.

COLLISIONAL AND DYNAMICAL EVOLUTION OF ASTEROIDS

The collisional and dynamical history of the main belt is strongly linked with the growth and evolution of the planets, with the events occurring during this primeval era recorded in the orbits, sizes, and compositional distributions of the asteroids and in the meteorites reaching Earth. By studying asteroids and meteorites and placing them into the appropriate geologic context, we can use these objects as probes into the processes by which planetesimals and planets formed from the solar nebula over 4.5 Ga ago. Hence, to understand the constraints provided by asteroids, we need to first understand how the asteroid belt was affected by planet formation.

The classical view of planet formation in the inner Solar System, which involves the gradual coalescence of many tiny bodies into rocky planets, can be divided into four stages: (i) the accumulation of dust in the solar nebula into km-sized planetesimals; (ii) runaway growth of the largest planetesimals via gravitational accretion into numerous protoplanets isolated in their feeding zones; (iii) oligarchic growth of protoplanets fed by planetesimals residing between their feeding zones; and (iv) mutual perturbations between Moon-to-Mars-sized planetary embryos and Jupiter, causing collisions, mergers, and the dynamical excitation of small body populations not yet accreted by the embryos (e.g., Greenberg et al. 1978). It is

believed that runaway growth occurs over a timescale of 0.01-1.0 m.y. while the latter stages required a few tens of m.y.

During this time, the main belt probably contained perhaps as much as an Earth-mass of material, enough to allow the planetesimals in the main belt region to accrete on short timescales. Eventually, most of the mass was agglomerated into planetary embryos on the scale of Moon- to Mars-size bodies (e.g., Wetherill 1992; Chambers and Wetherill 1998). In turn, these protoplanets dynamically excited the smaller bodies in the main belt region enough to cause some degree of radial mixing (Petit et al. 2001). This likely explains the semi-major axis distribution of large S- and C-types observed by Chapman et al. (1975) and Gradie and Tedesco (1982). At the same time, the dynamical excitation of these bodies increased their collision velocities enough to terminate accretion among most planetesimals and initiate fragmentation (Bottke et al. 2005a,b).

The elimination of planetary embryos and numerous planetesimals from the primordial main belt was triggered by the formation of Jupiter several m.y. after the birth of the Solar System (e.g., Petit et al. 2002). Numerical simulations indicate that combined perturbations of Jupiter and the embryos dynamically ejected more than 90% of the bodies out of the main belt zone. The main belt may have experienced a second dynamical depletion event associated with the so-called Late Heavy Bombardment that took place roughly 3.9 Ga ago (Gomes et al. 2005; Strom et al. 2005). Together, both events depleted the main belt not only of planetary embryos but also of over 99% of its population. At the same time, collisions during this phase produced numerous disruption events. Bottke et al. (2005a,b) argued that the wave-like shape of the main belt size distribution observed today is mostly a "fossil" left over from this early comminution phase.

After the Late Heavy Bombardment, the main belt population took on its current characteristics. Over the last 3-4 Ga, small bodies have been slowly lost from the main belt through a combination of collisions, dynamical evolution via Yarkovsky thermal forces, and resonances (e.g., Bottke et al. 2006a). The Yarkovsky effect compels asteroids smaller than 30-40 km to drift in semi-major axis over long time scales. In some cases, bodies can drift far enough that they enter a powerful mean motion or secular resonance. From here, their eccentricities can be pumped up to planet-crossing (and Earth-crossing orbits), where a small fraction (1-2%) are delivered to Earth. This process tends to keep the NEA and meteoroid (asteroids too small to observe) populations in a quasi-steady-state, though they can be affected by large breakup events or smaller stochastic breakups occurring near resonances. This quasi-steady-state explains why the lunar and terrestrial cratering rate appears to have been relatively constant (within a factor of 2) over 0.5-0.8 to 3 Ga ago (e.g., McEwen et al. 1997). Dynamical and collisional simulations based on this scenario have allowed us to glean insights into the nature of the asteroids and meteorites discussed above.

DELIVERY OF METEOROIDS TO EARTH

One intriguing question is how well calculated fall percentages, the percent of the falls that belong to each meteorite group, correlate with abundances of asteroids in the main belt or NEO population. Meteorite falls are heavily biased toward ordinary chondrites, with approximately 80% of the roughly 1,000 meteorites that have been observed to fall being ordinary chondrites.

While the Yarkovsky effect is a "democratic" process in that it allows small objects across the main belt to drift into main belt resonances, this does not necessarily mean that the meteorite record itself represents a uniform sample of material from all main-belt regions. This idea was tested by Bottke et al. (2006a), who tracked the delivery efficiency of test bodies started from various main-belt resonances to strike the Earth (**Fig. 36**). Their results indicate that meteoroids
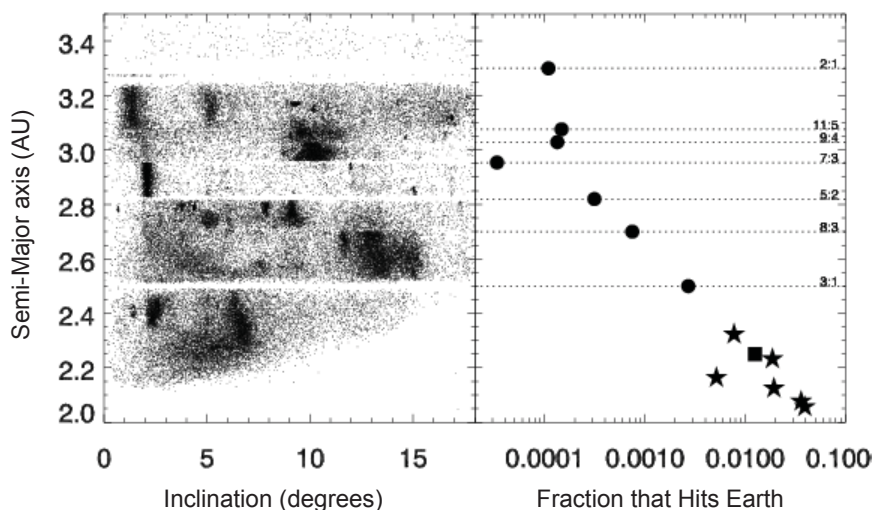
Figure 36. The delivery efficiency of test bodies from various main belt resonances striking the Earth. To create this plot, we updated the work of Gladman et al. (1997) and tracked the dynamical evolution of thousands of test bodies started in all major main-belt resonances. For reference, we have also plotted the proper semi-major axis (*a*) (AU) and inclination (*i*) (degrees) of 71,323 numbered asteroids with absolute magnitude *(H) < 14*. The stars represent values taken from test bodies started in the ν_6 secular resonance. In order of increasing *a*, we gave them *i = 2.5, 5.0, 7.5, 10.0, 12.5,* and *15.0* (Bottke et al. 2002). The filled square represents test bodies placed in the intermediate-source Mars-crossing region located adjacent to the main belt between *a = 2.0-2.5 AU* (Bottke et al. 2002). The filled circles are values from tests bodies placed in numerous mean motion resonances with Jupiter. Objects escaping the main belt with *a < 2.3 AU* are more than 2 orders of magnitude more likely to strike Earth than those with *a > 2.8 AU*. This implies that our meteorite collection is significantly biased toward the innermost regions of the main belt.

escaping the main belt from resonances located at (semi-major axis) *a* < 2.3 AU have a 1-4% chance of striking the Earth. This fraction drops by two orders of magnitude, however, as we move to resonances with *a* >2.5 AU. Because the fluxes of material escaping out of various main-belt resonances are thought to be comparable to one another (Bottke et al. 2002), the known meteorite collection is likely to be biased in favor of samples from the inner main belt. With the dominant taxonomic type found in the inner main belt being S-type asteroids, this may imply that S-types are primarily ordinary chondritic material.

There may also be additional biases in the fall statistics. For example, Gaffey (2006) argues that ordinary chondrites (H, L, LL) are derived from just three parent bodies (one being Hebe) that are located favorably near meteorite-delivering resonances (though this may be an oversimplification of a more complicated problem in terms of meteorite delivery; see Bottke et al. 2005c). Gaffey (2006) argues that partially-differentiated asteroids are more abundant in the main belt. The argument of Gaffey (2006) is a combination of theoretical calculations that predict that most asteroids were not raised to high enough temperatures to fully melt, and mineralogical analyses of a number of main-belt S-types (e.g., Gaffey et al. 1993a; Hardersen et al. 2006). They show that most of these objects do not have interpreted mineralogies consistent with ordinary chondrites, but rather with partially differentiated assemblages. Partially differentiated meteorites (primitive achondrites), however, are less than 1% of known falls.

If the Gaffey (2006) idea is true, then the spectral trends found by Binzel et al. (2004) and Marchi et al. (2006b) would not necessarily imply space weathering. The S, Sq, and Q NEAs and the main-belt S-types would tend to have different mineralogies, with NEAs tending to have ordinary chondrite mineralogies and main-belt S-types tending to be partially differentiated. The

assumed dominance of ordinary chondritic material in the NEA population may also be due to the location of the "three" ordinary chondrite parent bodies favorably near meteorite-delivering resonances. Also, CI and CM chondrites are extremely friable (Sears 1998) and are significantly less likely to make it through the atmosphere than the much stronger ordinary chondrites.

THE EFFECTS OF PLANETARY EMBRYOS AND RADIAL MIXING IN THE MAIN BELT

In the main belt evolution scenario above, we described how planetesimals undergoing gravitational interactions with planetary embryos are the likely explanation for the radial mixing seen among the large S- and C-complex asteroids. The implications of this idea, however, have yet to be fully explored. For example, recall that planetary embryos were also present in the terrestrial planet region, such that they, too, could have scattered planetesimals. To test this idea, Bottke et al. (2006a) used numerical simulations (Fig. 37) to track thousands of test bodies evolving amid a swarm of Moon/Mars-sized planetary embryos spread between 0.5-3.0 AU. They found that planetary embryo perturbations produce the same kinds of radial displacement of bodies observed in the main belt (Chapman et al. 1975; Gradie and Tedesco 1982).

The more interesting part of the Bottke et al. (2006a) simulation, however, was concerning the objects scattered into the main belt zone through a combination of resonant interactions and close encounters with planetary embryos. They found that 0.01-0.1%, 1%, and 10% of
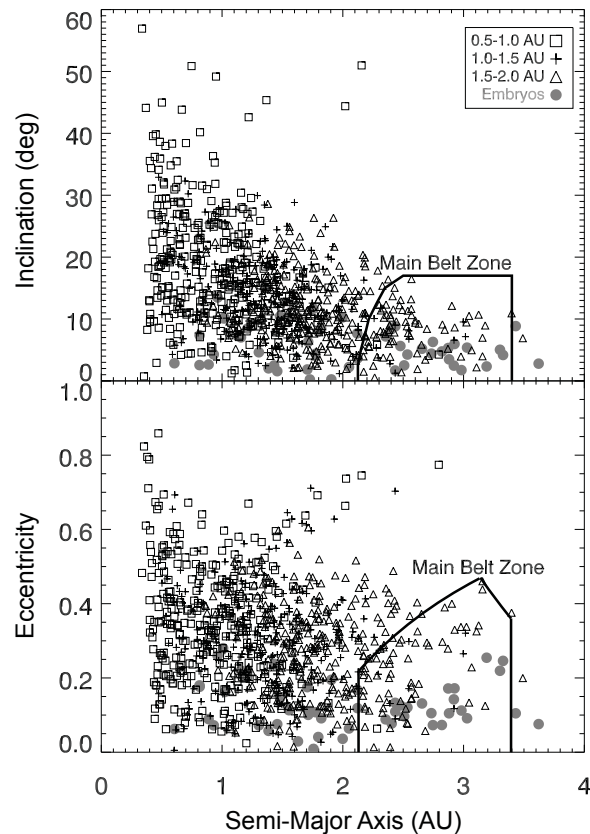
Figure 37. A snapshot of inner Solar System planetesimals and planetary embryos after 10 m.y. of dynamical evolution (Bottke et al. 2006a). The starting conditions and methods used were the same as those used by Levison and Agnor (2003). Here we tracked a set of 100 embryos (grey dots) distributed between 0.5-3.0 AU. Interspersed among the embryos, we placed 1,000 test bodies with uniform semi-major axes between 0.5-2.0 AU and low initial eccentricities and inclinations. The squares, crosses, and triangles show what happens to 1,000 planetesimals started with 0.5-1.0, 1.0-1.5, and 1.5-2.0 AU, respectively. The black line represents the location of the main asteroid belt. Bottke et al. (2006a) found that numerous planetesimals (one square, several crosses and triangles) were driven into the main belt by gravitational interactions with embryos, with the highest concentration in the inner main belt region, the same region that is more likely to deliver meteorites to Earth.

the particles that started with a = 0.5-1.0, 1.0-1.5, and 1.5-2.0 AU, respectively, achieved main belt orbits. Once there, Bottke et al. (2006a) found that these objects were dynamically indistinguishable from the rest of the main belt population. Even though many of these "interlopers" should be ejected over time via interactions with planet embryos, resonances, etc., the proportion of "interlopers" to indigenous material in the main belt should stay the same. Finally, Bottke et al. (2006a) found that most of the "interloper" material was emplaced into the inner main belt, the same region that is most likely to deliver meteorites to Earth. This implies that "interloper" material should be an important component in the meteorite collection.

COULD IRON METEORITES HAVE COME FROM THE TERRESTRIAL PLANET REGION?

If planetesimal material from the terrestrial planet region can actually be found in the main belt, what would it look like? Observations show a broad-scale taxonomic stratification among large main belt asteroids, with S-complex asteroids dominating the inner main belt and C-complex asteroids dominating the outer main belt. This trend, if followed inward toward the Sun, implies that inner Solar System planetesimals experienced significantly more heating than main belt asteroids (with the most plausible planetesimal heat source being short-lived [26]Al; halflife of 0.73 m.y.) (Bizzarro et al. 2005). Hence, bodies that accrete quickly stand the best chance of undergoing differentiation. While precise accretion timescales across the inner Solar System are unknown, modeling work suggests they vary with swarm density and distance from the Sun, such that accretion timescales increase with increasing heliocentric distance. Accordingly, if main belt interlopers are derived from regions closer to the Sun (Bottke et al. 2002), their shorter accretion times would lead to more internal heating, and thus they would probably look like heavily-metamorphosed or differentiated asteroids.

At this point, a reasonable connection can be made between the putative interlopers and iron meteorites. Cooling rate and textural data from irons indicate that most come from the cores of small ($D \approx$ 20-200 km) differentiated asteroids (Mittlefehldt et al. 1998). Isotopic chronometers also indicate that core formation among iron meteorite parent bodies occurred 1-2 m.y. before the formation of the ordinary chondrite parent bodies (e.g., Kleine et al. 2005; Baker et al. 2005). The paradox is that if small asteroids differentiated in the main belt at such early times, it would be reasonable to expect larger bodies forming near the same locations to have differentiated as well (e.g., Grimm and McSween 1992). Hence, if iron meteorites are indigenous to the main belt, large numbers of differentiated bodies and their fragments should reside there today. This is not observed. Instead, Bottke et al. (2006a) argued that a more probable formation location for many iron meteorite parent bodies was the terrestrial planet region, where accretion occurred quickly, and thus differentiation was more likely to occur among small bodies. The protoplanets emerging from this population not only induced collisional evolution among the remaining planetesimals but also scattered some of the survivors into the main belt, where they resided for billions of years until escaping via a combination of collisions, Yarkovsky thermal forces, and resonances. If true, this means that some asteroids are main-belt interlopers, with a select few possibly being remnants of the long-lost precursor material that formed the Earth.

High-temperature condensates (Table 1) would also be expected to be scattered into the inner main-belt. Some of these "interlopers" may be enstatite chondritic and aubritic material, which are believed to have initially condensed very near the Sun (e.g., Rubin and Wasson 1995). The inner-belt Hungaria region has a high proportion of X-types (Clark et al. 2004a), which includes the high-albedo E-types, the more moderate albedo M-types, and the Xe-types. X-types have spectral properties similar to aubrites, enstatite chondrites, and iron meteorites, which are all bodies that would be expected to have formed in the inner Solar System and scattered into the inner main belt in the Bottke et al. (2006a) model.

SUMMARY

Remote sensing can determine the presence of Fe^{2+} and Fe^{3+} and water (H_2O or OH) on asteroid surfaces. Distributions among different asteroid classes can be seen in the asteroid belt; however, we currently do not know how well each asteroid class groups objects of similar surface compositions. It is also difficult to determine what these distributions actually mean due to the effects of space weathering, which appears to affect the reflectance spectra of the surfaces of asteroids, and dynamical mixing, which affects the orbital distribution of objects. Sample return missions should allow us to better determine how well we can derive the surface compositions of asteroids from remote sensing.

ACKNOWLEDGMENTS

REFERENCES

Abe M, Takagi Y, Kitazato K, Abe S, Hiroi T, Vilas F, Clark BE, Abell PA, Lederer SM, Jarvis KS, Nimura T, Ueda Y, Fujiwara A (2006) Near-infrared spectral results of asteroid Itokawa from the Hayabusa spacecraft. Science 312:1334-1338

Abell PA, Fernández YR, Pravec P, French LM, Farnham TL, Gaffey MJ, Hardersen PS, Kusnirák P, Sarounová L, Sheppard SS, Narayan G (2005) Physical characteristics of comet nucleus C/2001 OG$_{108}$ (LONEOS). Icarus 179:174-194

Abell PA, Gaffey MJ (2000) Probable geologic composition, thermal history, and meteorite affinities for mainbelt asteroid 349 Dembowska. Lunar Planet Sci XXXI:1291

Abell PA, Vilas F, Jarvis KS, Gaffey MJ, Kelley MS (2006) Mineralogical composition of (25143) Itokawa 1998 SF36 from visible and near-infrared reflectance spectroscopy: Evidence for partial melting. Lunar Planet Sci XXXVII:1513

Adams JB (1974) Visible and near-infrared diffuse reflectance: Spectra of pyroxenes as applied to remote sensing of solid objects in the solar system. J Geophys Res 79:4829-4836

Adams JB (1975) Interpretation of visible and near-infrared diffuse reflectance spectra of pyroxenes and other rock-forming minerals. *In:* Infrared and Raman Spectroscopy of Lunar and Terrestrial Minerals. Karr C. III (ed) Academic Press, Inc., New York, p 91-116

A'Hearn MF, Feldman PD (1992) Water vaporization on Ceres. Icarus 98:54-60

Allen CC, Morris RV, McKay DS (1996) An experimental analog to maturing lunar soil. Lunar Planet Sci 27:13-14.

Baker J, Bizzarro M, Wittig N, Connelly J, Haack H (2005) Early planetesimal melting from an age of 4.5662 Gyr for differentiated meteorites. Nature 436:1127-1131

Barucci MA, Cruikshank DP, Mottola S, Lazzarin M (2002) Physical properties of Trojan and Centaur asteroids. *In*: Asteroids III. Bottke WF, Cellino A, Paolicchi P, Binzel RP (eds) University of Arizona Press, Tucson, p 273–287

Barucci MA, Fulchignoni M, Fornasier S, Dotto E, Vernazza P, Birlan M, Binzel RP, Carvano J, Merlin F, Barbieri C, Belskaya I (2005) Asteroid target selection for the new Rosetta mission baseline. 21 Lutetia and 2867 Steins. Astron Astrophys 430:313-317

Bell JF (1988) A probable asteroidal parent body for the CV or CO chondrites. Meteoritics 23:256-257.

Bell JF, Davis DR, Hartmann WK, Gaffey MJ (1989) Asteroids: The big picture. *In*: Asteroids II. Binzel RP, Gehrels T, Matthews MS (eds) Univ Arizona Press, Tucson, p 921-945

Bell JF, Owensby PD, Hawke BR, Gaffey MJ (1988) The 52-color asteroid survey: Final results and interpretation. Lunar Planet Sci XIX:57-58

Bender D, Bowell E, Chapman C, Gaffey M, Gehrels T, Zellner B, Morrison D, Tedesco E (1978) The Tucson revised index of asteroid data. Icarus 33:630-631

Bendjoya Ph, Zappalà V (2002) Asteroid family identification. *In*: Asteroids III. Bottke WF, Cellino A, Paolicchi P, Binzel RP (eds) University of Arizona Press, Tucson, p 613-618

Bendjoya PA, Cellino A, di Martino M, Saba L (2004) Spectroscopic observations of Jupiter Trojans. Icarus 168:374–384

Binzel RP, Bus SJ, Burbine TH (1999) The orbital distribution of Vesta-like asteroids. Lunar Planet Sci XXX:1216

Binzel RP, Bus SJ, Burbine TH, Sunshine JM (1996) Spectral properties of near-Earth asteroids: Evidence for sources of ordinary chondrite meteorites. Science 273:946-948

Binzel RP, Bus SJ, Xu S, Sunshine J, Burbine TH, Neely AW, Brown RW (1995) Rotationally resolved spectra of asteroid 16 Psyche. Icarus 117:443-445

Binzel RP, Lupishko DF (2005) Properties of the near-Earth object population: The ACM 2005 review. *In*: Asteroids, Comets, Meteors, Proceedings IAU Symposium No. 229. Lazzaro D, Ferraz-Mello S, Fernández JA (eds) Cambridge University Press, Cambridge, p 207-214

Binzel RP, Rivkin AS, Bus SJ, Sunshine JM, Burbine TH (2001) MUSES-C target asteroid (25143) 1998 SF36: A reddened ordinary chondrite. Meteoritics Planet Sci 36:1167-1172

Binzel RP, Rivkin AS, Stuart JS, Harris AW, Bus SJ, Burbine TH (2004) Observed spectral properties of near-Earth objects: results for population distribution, source regions, and space weathering processes. Icarus 170:259-294

Binzel RP, Thomas CA, Demeo FE, Tokunaga A, Rivkin AS, Bus SJ (2006) The MIT-Hawaii-IRTF joint campaign for NEO spectral reconnaissance. Lunar Planet Sci XXX:1491

Binzel RP, Xu S (1993) Chips off of asteroid 4 Vesta: Evidence for the parent body of basaltic achondrite meteorites. Science 260:186-191

Binzel RP, Xu S, Bus SJ, Skrutskie MF, Meyer MR, Knezek P, Barker ES (1993) Discovery of a main- belt asteroid resembling ordinary chondrite meteorites. Science 262:1541-1543

Birlan M, Vernazza P, Fulchignoni M, Barucci MA, Descamps P, Binzel RP, Bus SJ (2006) Near infra- red spectroscopy of the asteroid 21 Lutetia. I. New results of long-term campaign. Astron Astrophys 454:677-681

Bizzarro M, Baker JA, Haack H, Lundgaard KL (2005) Rapid timescales for accretion and melting of differentiated planetesimals inferred from ^{26}Al-^{26}Mg chronometry. Astrophys J 632:L41-L44

Bottke WF, Durda DD, Nesvorný D, Jedicke R, Morbidelli A, Vokrouhlický D, Levison HF (2005a) Linking the collisional history of the main asteroid belt to its dynamical excitation and depletion. Icarus 179:63-94

Bottke WF, Durda DD, Nesvorný D, Jedicke R, Morbidelli A, Vokrouhlický D, Levison HF (2005b) The fossilized size distribution of the main asteroid belt. Icarus 175:111-140

Bottke WF, Durda DD, Nesvorný D, Jedicke R, Morbidelli A, Vokrouhlický D, Levison HF (2005c) The origin and evolution of stony meteorites. *In:* Dynamics of populations of Planetary Systems. Bottke WF, Cellino A, Paolicchi P, Binzel RP (eds), Cambridge University Press, Cambridge, p 357-374

Bottke WF, Nesvorný D, Grimm RE, Morbidelli A, O'Brien DP (2006a) Iron meteorites as remnants of planetesimals formed in the terrestrial planet region. Nature 439:821-824

Bottke WF, Vokrouhlický D, Rubincam D, Brož M (2002) Dynamical evolution of asteroids and meteoroids using the Yarkovsky effect. *In*: Asteroids III. Knežević Z, Milani A (eds), University of Arizona Press, Tucson, p 395-408

Bottke WF Jr, Vokrouhlický D, Rubincam DP, Nesvorný D (2006b) The Yarkovsky and YORP effects: Implications for asteroid dynamics. Ann Rev Earth Planet Sci 34:157-191

Bowell E, Chapman CR, Gradie JC, Morrison D, Zellner B (1978) Taxonomy of asteroids. Icarus 35:313–335

Brearley AJ, Jones RH (1998) Chondritic meteorites. Rev Mineral 36:3-1–3-398

Britt DT, Bell JF, Haack H, Scott ERD (1992) The reflectance spectrum of troilite and the T-type asteroids. Meteoritics 27:207

Britt DT, Consolmagno GJ (2003) Stony meteorite porosities and densities: A review of the data through 2001. Meteor Planet Sci 38:1161-1180

Britt DT, Yeomans D, Housen K, Consolmagno G (2002) Asteroid density, porosity, and structure. *In:* Asteroids III. Bottke WF, Cellino A, Paolicchi P, Binzel RP (eds), University of Arizona Press, Tucson, p 485-500

Brunetto R, Romano F, Blanco A, Fonti S, Martino M, Orofino V, Verriento C (2006a) Space weathering of silicates simulated by nanosecond pulse UV excimer laser. Icarus 180:546-554

Brunetto R, Strazzulla G (2005) Elastic collisions on ion irradiation experiments: A mechanism for space weathering of silicates. Icarus 179:265-273.

Brunetto R, Vernazza P, Marchi S, Birlan M, Fulchignoni M, Orofino V, Strazzulla G (2006b) Modeling asteroid surfaces from observations and irradiation experiments: The case of 832 Karin. Icarus 184:327-337

Buratti BJ, Britt DT, Soderblom LA, Hicks MD, Boice DC, Brown RH, Meier R, Nelson RM, Oberst J, Owen TC, Rivkin AS, Sandel BR, Stern SA, Thomas N, Yelle RV (2004) 9969 Braille: Deep Space 1 infrared spectroscopy, geometric albedo, and classification. Icarus 167:129-135

Burbine TH (1998) Could G-class asteroids be the parent bodies of the CM chondrites? Meteor Planet Sci 33:253-258

Burbine TH (2000) Forging asteroid-meteorite relationships through reflectance spectroscopy. PhD Dissertation, Massachusetts Institute of Technology, Cambridge, Massachusetts

Burbine TH, Binzel RP (2002) Small main-belt asteroid spectroscopic survey in the near-infrared. Icarus 158:468-499

Burbine TH, Binzel RP, Bus SJ, Clark BE (2001a) K asteroids and CO3/CV3 chondrites. Meteoritics Planet Sci 36:245-253

Burbine TH, Buchanan PC, Binzel RP, Bus SJ, Hiroi T, Hinrichs JL, Meibom A, McCoy TJ (2001b) Vesta, Vestoids, and the HEDs: Relationships and the origin of spectral differences. Meteor Planet Sci 36:761-781

Burbine TH, Gaffey MJ, Bell JF (1992) S-asteroids 387 Aquitania and 980 Anacostia: Possible fragments of the breakup of a spinel-bearing parent body with CO3/CV3 affinities. Meteoritics 27:424-434

Burbine TH, McCoy TJ, Hinrichs JL, Lucey PG (2006) Spectral properties of angrites. Meteor Planet Sci 41:1139-1145

Burbine TH, McCoy TJ, Jarosewich E, Sunshine JM (2002a) Spectral measurements of meteorite powders: Implications for 433 Eros. Lunar Planet Sci XXXIII:1359

Burbine TH, McCoy TJ, Jarosewich E, Sunshine JM (2003) Deriving asteroid mineralogies from reflectance spectra: Implications for the Muses-C target asteroid. Antarct Met Res 16:185-195

Burbine TH, McCoy TJ, Meibom A, Gladman B, Keil K (2002b) Meteoritic parent bodies: Their number and identification. *In*: Asteroids III. Bottke WF, Cellino A, Paolicchi P, Binzel RP (eds), University of Arizona Press, Tucson, p 653–667

Burbine TH, McCoy TJ, Nittler LR, Benedix GK, Cloutis EA, Dickinson TL (2002c) Spectra of extremely reduced assemblages: Implications for Mercury. Meteor Planet Sci 37:1233-1244

Burbine TH, Meibom A, Binzel RP (1996) Mantle material in the main belt: Battered to bits? Meteoritics 31:607-620

Burns RG (1985) Thermodynamic data from crystal field spectra. Rev Mineral 14:277-316

Burns RG (1993) Mineralogical Applications of Crystal Field Theory. 2nd edition. Cambridge University Press, Cambridge

Burns RG, Huggins FE (1973) Visible-region absorption spectra of a Ti^{3+} fassaite from the Allende meteorite: A discussion. Am Min 58:955-961

Bus SJ (1999) Compositional structure in the asteroid belt. PhD Dissertation, Massachusetts Institute of Technology, Cambridge, Massachusetts

Bus SJ, Binzel RP (2002a) Phase II of the Small Main-belt Asteroid Spectroscopic Survey: The observations. Icarus 158:106-145

Bus SJ, Binzel RP (2002b) Phase II of the Small Main-belt Asteroid Spectroscopic Survey: A feature- based taxonomy. Icarus 158:146-177

Bus SJ, Vilas F, Barucci MA (2002) Visible-wavelength spectroscopy of asteroids. *In*: Asteroids III. Bottke WF, Cellino A, Paolicchi P, Binzel RP (eds), University of Arizona Press, Tucson, p 169- 182

Calvin WM, King TVV (1997) Spectral characteristics of Fe-bearing phyllosilicates: Comparison to Orgueil (CI1), Murchison and Murray (CM2). Meteoritics 32:693-701

Campins H, Swindle TD (1998) Expected characteristics of cometary meteorites. Meteor Planet Sci 33:1201-1211

Carruba V, Michtchenko TA, Roig F, Ferraz-Mello S, Nesvorný D. (2005) On the V-type asteroids outside the Vesta family. I. Interplay of nonlinear secular resonances and the Yarkovsky effect: The cases of 956 Elisa and 809 Lundia. Astron Astrophys 441:819-829

Carvano JM, Lazzaro D, Mothé-Diniz T, Angeli CA, Florczak M (2001) Spectroscopic survey of the Hungaria and Phocaea dynamical groups. Icarus 149:173-189

Cellino A, Bus SJ, Doressoundiram A, Lazzaro D (2002) Spectroscopic properties of asteroid families. *In*: Asteroids III. Bottke WF, Cellino A, Paolicchi P, Binzel RP (eds), University of Arizona Press, Tucson, p 633-643

Chamberlain MA, Brown RH (2004) Near-infrared spectroscopy of Himalia. Icarus 172:163–169

Chambers JE, Wetherill GW (1998) Making the terrestrial planets: N-Body integrations of planetary embryos in three dimensions. Icarus 136:304-327

Chapman CR (1996) S-type asteroids, ordinary chondrites, and space weathering: The evidence from Galileo's fly-bys of Gaspra and Ida. Meteor Planet Sci 31:699-725

Chapman CR (2004) Space weathering of asteroid surfaces. Ann Rev Earth Planet Sci 32:539-567

Chapman CR, Gaffey MJ (1979) Reflectance spectra for 277 asteroids. *In*: Asteroids. Gehrels T (eds), University of Arizona Press, Tucson, p 655-687

Chapman CR, Johnson TV, McCord TB (1971) A review of spectrophotometric studies of asteroids. *In*: Physical Studies of Minor Planets. Gehrels T (ed) NASA, Washington, p 51-65

Chapman CR, Morrison D, Zellner B (1975) Surface properties of asteroids using a synthesis of polarimetry, radiometry and spectrophotometry. Icarus 25:104–130

Chapman CR, Paolicchi P, Zappalà V, Binzel RP, Bell JF (1989) Asteroid families: Physical properties and evolution. *In*: Asteroids II. Binzel RP, Gehrels T, Matthews MS (eds) Univ Arizona Press, Tucson, p 386-415

Clark BE (1995) Spectral mixing models of S-type asteroids. J Geophys Res 100:14443-14456

Clark BE, Bus SJ, Rivkin AS, McConnochie T, Sanders J, Shah S, Hiroi T, Shepard M (2004a) E-type asteroid spectroscopy and compositional modeling. J Geophys Res 109:10.1029/2003JE002200

Clark BE, Bus SJ, Rivkin AS, Shepard MK, Shah S (2004b) Spectroscopy of X-type asteroids. Astron J 128:3070-3081

Clark RN (1981) The spectral reflectance of water-mineral mixtures at low temperatures. J Geophys Res 86:3074–3086

Clark RN (1999) Chapter 1: Spectroscopy of rocks and minerals, and principles of spectroscopy. *In:* Manual of Remote Sensing, Volume 3, Remote Sensing for the Earth Sciences. Rencz AN (ed) John Wiley and Sons, New York, p 3-58

Cloutis EA (2001) Spectral reflectance properties of calcium-aluminum inclusion minerals: 2. Melilites. Lunar Planet Sci XXXII:1128

Cloutis EA, Gaffey MJ (1991) Pyroxene spectroscopy revisited: Spectral-compositional correlations and relationship to geothermometry. J Geophys Res 96:22809-22826

Cloutis EA, Gaffey MJ (1993) The constituent minerals in calcium-aluminum inclusions: Spectral reflectance properties and implications for CO carbonaceous chondrites and asteroids. Icarus 105:568-579

Cloutis EA, Gaffey MJ, Jackowski TL, Reed KL (1986) Calibrations of phase abundance, composition, and particle size distribution of olivine-orthopyroxene mixtures from reflectance spectra. J Geophys Res 91:11641-11653

Cloutis EA, Gaffey MJ, Smith DGW, Lambert RStJ (1990) Reflectance spectra of "featureless" materials and the surface mineralogies of M- and E-class asteroids. J Geophys Res 95:281-293

Cloutis EA, Hawthorne FC, Mertzman SA, Krenn K, Craig MA, Marcino D, Methot M, Strong J, Mustard JF, Blaney DL, Bell JF III, Vilas F (2006) Detection and discrimination of sulfate minerals using reflectance spectroscopy. Icarus 184:121-157

Cloutis EA, Hudon P (2004) Reflectance spectra of ureilites: Nature of the mafic silicate absorption features. Lunar Planet Sci XXXV:1257

Cloutis EA, Sunshine JM, Morris RV (2004) Spectral reflectance-compositional properties of spinels and chromites: Implications for planetary remote sensing and geothermometry. Meteor Planet Sci 39:545-565

Cochran AL, Vilas F (1997) The McDonald Observatory serendipitous UV/blue spectral survey of asteroids. Icarus 127:121-129

Cochran AL, Vilas F (1998) The changing spectrum of Vesta: Rotationally resolved spectroscopy of pyroxene on the surface. Icarus 134:207-212

Cochran AL, Vilas F, Jarvis KS, Kelley MS (2004) Investigating the Vesta-vestoid-HED connection. Icarus 167:360-368

Criss RE, Farquhar J (200X) Abundance, notation, and fractionation of light stable isotopes. Rev Mineral Geochem 68:xxx-yyy.

Crown DA, Pieters CM (1989) Spectral properties of plagioclase and pyroxene mixtures and the interpretation of lunar soil spectra. Icarus 72:492-506

Cruikshank DP (2005) Solar system observations with Spitzer Space Telescope: Preliminary results. Adv Space Res 36:1070-1073

Cruikshank DP, Brown RH (1987) Organic matter on asteroid 130 Elektra. Science 238:183-184

Cruikshank DP, Tholen DJ, Bell JF, Hartmann WK, Brown RH (1991) Three basaltic earth-approaching asteroids and the source of the basaltic meteorites. Icarus 89:1-13

Cruikshank DP, Ore CMD, Roush TL, Geballe TR, Owen TC, de Bergh C, Cash MD, Hartmann WK (2001) Constraints on the composition of Trojan asteroid 624 Hektor. Icarus 153:348–360

Dahlgren M, Lagerkvist C–I, Fitzsimmons A, Williams IP, Gordon M (1997) A study of Hilda asteroids II. Compositional implications from optical spectroscopy. Astron Astrophys 323:606- 619

Davies JK, Harris AW, Rivkin AS, Wolters SD, Green SF, McBride N, Mann RK, Kerr TH (2007) Near-infrared spectra of 12 near-Earth objects. Icarus 186:111-125

Deer WA, Howie RA, Zussman J (1997) Single-Chain Silicates (2nd Edition). The Geological Society, Bath

Delbo M, Gai M, Lattanzi MG, Ligori S, Loreggia D, Saba L, Cellino A, Gandolfi D, Licchelli D, Blanco C, Cigna M, Wittkowski M (2006) MIDI observations of 1459 Magnya: First attempt of interferometric observations of asteroids with the VLTI. Icarus 181:618-622

de León J, Duffard R, Licandro J, Lazzaro D (2004) Mineralogical characterization of A-type asteroid (1951) Lick. Astron Astrophys 422:L59-L62

de León J, Licandro J, Duffard R, Serra-Ricarta M (2006) Spectral analysis and mineralogical characterization of 11 olivine-pyroxene rich NEAs. Adv Space Res 37:178-183

Di Martino M, Manara A, Migliorini F (1995) 1993 VW: An ordinary chondrite-like near-Earth asteroid. Astron Astrophys 302:609-612

Dotto E, Barucci MA, Brucato JR, Müller TG, Carvano J (2006a) 308 Polyxo: ISO-SWS spectrum up to 26 micron. Astron Astrophys 427:1081-1084

Dotto E, Fornasier S, Barucci MA, Licandro J, Boehnhardt H, Hainaut O, Marzari F, de Bergh C, De Luise F (2006b) The surface composition of Jupiter Trojans: Visible and near-infrared survey of dynamical families. Icarus 183:420-434

Duffard R, de León J, Licandro J, Lazzaro D, Serra-Ricart M (2006) Basaltic asteroids in the NEO population: A mineralogical analysis. Astron Astrophys 456:775-781

Duffard R, Lazzaro D, Licandro J, de Sanctis MC, Capria MT, Carvano JM (2004) Mineralogical characterization of some basaltic asteroids in the neighborhood of (4) Vesta: First results. Icarus 171:120-132

Dyar MD, Gunter ME (2007) Minerals and Optical Mineralogy: A Three-Dimensional Approach. Mineralogical Society of America, Washington

Ebel DS (2006) Condensation of rocky material in astrophysical environments. *In*: Meteorites and the Early Solar System II. Lauretta DS, McSween HY Jr (eds), University of Arizona Press, Tucson, p 253-277

Emery JP, Brown RH (2003) Constraints on the surface composition of Trojan asteroids from near- infrared (0.8-4.0 μm) spectroscopy. Icarus 164:104–121

Emery JP, Cruikshank DP, van Cleve J, Stansberry JA (2005) Mineralogy of asteroids from observations with the Spitzer Space Telescope. Lunar Planet Sci XXXVI:2072

Evans LG, Starr RD, Brückner J, Reedy RC, Boynton WV, Trombka JI, Goldsten JO, Masarik J, Nittler LR, McCoy TJ (2001) Elemental composition from gamma-ray spectroscopy of the NEAR- Shoemaker landing site on 433 Eros. Meteor Planet Sci 36:1639-1660.

Feierberg MA, Larson HP, Fink U, Smith HA (1980) Spectroscopic evidence for two achondrite parent bodies: Asteroids 349 Dembowska and 4 Vesta. Geochim Cosmochim Acta 44:513-524

Feierberg MA, Lebofsky LA, Tholen D (1985) The nature of C-class asteroids from 3-μm spectrophotometry. Icarus 63:183–191

Florczak M, Lazzaro D, Duffard R (2002) Discovering new V-type asteroids in the vicinity of 4 Vesta. Icarus 159:178-182

Florczak M, Lazzaro D, Mothé-Diniz T, Angeli CA, Betzler AS (1999) A spectroscopic study of the Themis family. Astron Astrophys Suppl Ser 134:463-471

Folco L, Burbine TH, D'Orazio M (2005) Surface mineralogy changes induced by impact melting on ordinary chondritic parent asteroids: Clues from the DaG 896 meteorite. Memorie della Societa Astronomica Italiana Suppl 6:116-121

Foley CN, Nittler LR, McCoy TJ, Lim L, Brown MRM, Starr RD, Trombka JI (2006) Minor element evidence that asteroid 433 Eros is a space-weathered ordinary chondrite parent body. Icarus 184:338-343

Fornasier S, Barucci MA, Binzel RP, Birlan M, Fulchignoni M Barbieri C, Bus SJ, Harris AW, Rivkin AS, Lazzarin M, Dotto E, Michalowski T, Doressoundiram A, Bertini I, Peixinho N (2003) A portrait of 4979 Otawara, target of the Rosetta space mission. Astron Astrophys 398:327-333

Fornasier S, Dotto E, Marzari F, Barucci MA, Boehnhardt H, Hainaut O, de Bergh C (2004) Visible spectroscopic and photometric survey of L5 Trojans: Investigation of dynamical families. Icarus 172:221-232

Fornasier S, Lazzarin M, Barbieri C, Barucci MA (1999) Spectroscopic comparison of aqueous altered asteroids with CM2 carbonaceous chondrite meteorites. Astron Astrophys Suppl Ser 135:65-73

Fukugita M, Ichikawa T, Gunn JE, Doi M, Shimasaku K, Schneider DP (1996) The Sloan Digital Sky Survey photometric system. Astron J 111:1748–1756

Gaffey MJ (1976) Spectral reflectance characteristics of the meteorite classes. J Geophys Res 81:905- 920

Gaffey MJ (1986) The spectral and physical properties of metal in meteorite assemblages: Implications of asteroid surface materials. Icarus 66:468-486

Gaffey MJ (1997) Surface lithologic heterogeneity of asteroid 4 Vesta. Icarus 127:130-157

Gaffey MJ (1998) Using nickel features in the spectra of olivine-dominated A- and S(I)-type asteroids to determine the oxidation state of the solar nebula. Lunar Planet Sci XXIX:2072

Gaffey MJ (2006) A plethora of partially melted asteroids? Lunar Planet Sci XXXVII:1223

Gaffey MJ, Bell JF, Brown RH, Burbine TH, Piatek J, Reed KL, Chaky DA (1993a) Mineralogic variations within the S-type asteroid class. Icarus 106:573-602

Gaffey MJ, Bell JF, Cruikshank DP (1989) Reflectance spectroscopy and asteroid surface mineralogy. *In*: Asteroids II. Binzel RP, Gehrels T, Matthews MS (eds) Univ Arizona Press, Tucson, p 98- 127

Gaffey M, Burbine TH, Binzel RP (1993b) Asteroid spectroscopy: progress and perspectives. Meteoritics 28:161–187

Gaffey MJ, Cloutis EA, Kelley MS, Reed KL (2002) Mineralogy of asteroids. *In*: Asteroids III. Bottke WF, Cellino A, Paolicchi P, Binzel RP (eds), University of Arizona Press, Tucson, p 183-204

Gaffey MJ, Gilbert SL (1998) Asteroid 6 Hebe: The probable parent body of the H-type ordinary chondrites and the IIE iron meteorites. Meteor Planet Sci 33:1281-1295

Gaffey MJ, Reed KL, Kelley MS (1992) Relationship of E-type asteroid 3103 (1982 BB) to the enstatite chondrite meteorites and the Hungaria asteroids. Icarus 100:95-109

Gastineau-Lyons HK, McSween HY Jr, Gaffey MJ (2002) A critical evaluation of oxidation versus reduction during metamorphism of L and LL group chondrites, and implications for asteroid spectroscopy. Meteor Planet Sci 37:75-89

Gladman BJ, Migliorini F, Morbidelli A, Zappalà V, Michel P, Cellino A, Froeschlé C, Levison HF, Bailey M, Duncan M (1997) Dynamical lifetimes of objects injected into asteroid belt resonances. Science 277:197-201

Gomes R, Levison HF, Tsiganis K, Morbidelli A (2005) Origin of the cataclysmic Late heavy bombardment period of the terrestrial planets. Nature 435:466-469

Gradie J, Chapman CR, Tedesco EF (1989) Distribution of taxonomic classes and the compositional structure of the asteroid belt. *In*: Asteroids II. Binzel RP, Gehrels T, Matthews MS (eds), University of Arizona Press, Tucson, p 316–335

Gradie J, Tedesco E (1982) Compositional structure of the asteroid belt. Science 216:1405-1407

Gradie JC, Tedesco EF (1988) Albedos and diameters for 350 asteroids from the IRTF 10 μm and 20 μm radiometry survey. Bull Am Astron Soc 20:866

Gradie JC, Zellner B (1977) Asteroid families: Observational evidence for common origins. Science 197:254-255

Granahan JC (1993) Investigations of asteroid family geology. PhD Dissertation, University of Hawaii, Honolulu

Granahan JC, Bell JF (1991) On the geologic reality of asteroid families. Lunar Planet Sci XXII:477-478

Greenberg R., Hartmann WK, Chapman CR, Wacker JF (1978) Planetesimals to planets - Numerical simulation of collisional evolution. Icarus 35:1-26

Grimm RE, McSween HY Jr (1992) Heliocentric zoning of the asteroid belt by aluminum-26 heating. Science 259:653-655

Grossman L (1972) Condensation in the primitive solar nebula. Geochim Cosmochim Acta 36:597-619

Hanner MS, Giese RH, Weiss K, Zerulli R (1981) On the definition of albedo and application to irregular particles. Astron Astrophys 104:42-46

Hapke B (1981) Bidirectional reflectance spectroscopy. 1. Theory. J Geophys Res 86:4571-4586

Hapke B (2001) Space weathering from Mercury to the asteroid belt. J Geophys Res 106:10039-10073

Hardersen PS, Gaffey MJ, Abell PA (2004) Mineralogy of Asteroid 1459 Magnya and implications for its origin. Icarus 167:170-177

Hardersen PS, Gaffey MJ, Abell PA (2005) Near-IR spectral evidence for the presence of iron-poor orthopyroxenes on the surfaces of six M-type asteroids. Icarus 175:141-158

Hardersen PS, Gaffey MJ, Cloutis EA, Abell PA, Reddy V (2006) Near-infrared spectral observations and interpretations for S-asteroids 138 Tolosa, 306 Unitas, 346 Hermentaria, and 480 Hansa. Icarus 181:94-106

Harris AW, Harris AW (1997) On the revision of radiometric albedos and diameters of asteroids. Icarus 126:450-454

Harris AW, Lagerros JSV (2002) Asteroids in the thermal infrared. *In*: Asteroids III. Bottke WF, Cellino A, Paolicchi P, Binzel RP (eds), University of Arizona Press, Tucson, p 205–218

Hasegawa S, Murakawa K, Ishiguro M, Nonaka H, Takato N, Davis CJ, Ueno M, Hiroi T (2003) Evidence of hydrated minerals on the surface of asteroid 4 Vesta. Geophys Res Lett 30:10.1029/2003GL018627

Hendrix AR, Vilas F (2006) The effects of space weathering at UV wavelengths: S-class asteroids. Astron J 132:1396–1404

Hilton JL (1999) US Naval Observatory ephemerides of the largest asteroids. Astron J 117:1077-1086

Hinrichs JL, Lucey PG, Robinson MS, Meibom A, Krot AN (1999) Implications of temperature- dependent near-IR spectral properties of common minerals and meteorites for the remote sensing of asteroids. Geophys Res Lett 26:1661-1664

Hiroi T, Abe M, Kitazato K, Abe S, Clark BE, Sasaki S, Ishiguro M, Barnouin-Jha OS (2006) Developing space weathering on the asteroid 25143 Itokawa. Nature 443:56-58

Hiroi T, Hasegawa S (2003) Revisiting the search for the parent body of the Tagish Lake meteorite: Case of a T/D asteroid 308 Polyxo. Antarct Meteorite Res 16:176-184

Hiroi T, Pieters CM, Rutherford MJ, Zolensky ME, Sasaki S, Ueda Y, Miyamoto M (2004) What are the P-type asteroids made of? Lunar Planet Sci XXXV:1616

Hiroi T, Pieters CM, Takeda H (1994) Grain size of the surface regolith of asteroid 4 Vesta estimated from its reflectance spectrum in comparison with HED meteorites. Meteoritics 29:394-396

Hiroi T, Pieters CM, Vilas F, Sasaki S, Hamabe Y, Kurahashi E (2001a) The mystery of 506.5 nm feature of reflectance spectra of Vesta and Vestoids: evidence for space weathering? Earth Planets Space 53:1071-1075

Hiroi T, Pieters CM, Zolensky ME, Lipschutz ME (1993) Evidence of thermal metamorphism on the C, G, B, and F asteroids. Science 261:1016-1018

Hiroi T, Takeda H (1991) Reflectance spectroscopy and mineralogy of primitive achondrites-lodranites. Proc NIPR Symp Antarct Met 4:163-177

Hiroi T, Tonui E, Pieters CM, Zolensky ME, Ueda Y, Miyamoto M, Sasaki S (2005) Meteorite WIS91600: A new sample related to a D-or T-type asteroid. Lunar Planet Sci XXXVI:1564

Hiroi T, Vilas F, Sunshine JM (1996a) Discovery and analysis of minor absorption bands in S-asteroid visible reflectance spectra. Icarus 119:202-208

Hiroi T, Zolensky ME, Pieters CM (2001b) The Tagish Lake meteorite: A possible sample from a D- type asteroid. Science 293:2234-2236

Hiroi T, Zolensky ME, Pieters CM, Lipschutz ME (1996b) Thermal metamorphism of the C, G, B, and F asteroids seen from the 0.7 μm, 3 μm and UV absorption strengths in comparison with carbonaceous chondrites. Meteor Planet Sci 31:321–327

Hörz F, Cintala MJ, See TH, Le L (2005) Shock melting of ordinary chondrite powders and implications for asteroidal regoliths. Meteor Planet Sci 40:1329-1346

Howell ES (1995) Probing asteroid composition using visible and near-infrared spectroscopy. PhD Dissertation, University of Arizona, Tucson, Arizona

Howell ES, Merenyi E, Lebofsky LA (1994) Classification of asteroid spectra using a neural network. J Geophys Res 99:10847-10865

Howell ES, Rivkin AS, Vilas F (2001a) Uneven distribution of aqueously altered minerals on asteroids. *In: Asteroids 2001: From Piazzi to the Third Millennium: 62 (is this a PAGE OR ABSTRACT #)*

Howell ES, Rivkin AS, Vilas F, Soderberg AM (2001b) Aqueous alteration in low albedo asteroids. Lunar Planet Sci XXXII:2058

Hutchison R (2004) Meteorites: A Petrologic, Chemical and Isotopic Synthesis. Cambridge University Press, Cambridge

Hutchison R, Alexander CMO, Barber DJ (1987) The Semarkona meteorite: First recorded occurrence of smectite in an ordinary chondrite, and its implications. Geochim Cosmochim Acta 51:1875-1882

Ivezić Ž, Lupton RH, Jurić M, Tabachnik S, Quinn T, Gunn JE, Knapp GR, Rockosi C M, Brinkmann J (2002) Color confirmation of asteroid families. Astron J 124:2943-2948

Ivezić Ž, Tabachnik S, Rafikov R, Lupton RH, Quinn T, Hammergren M, Eyer L, Chu J, Armstrong JC, Fan X, Finlator K, Geballe TR, Gunn JE, Hennessy GS, Knapp GR, Leggett SK, Munn JA, Pier JR, Rockosi CM, Schneider DP, Strauss MA, Yanny B, Brinkmann J, Csabai I, Hindsley RB, Kent S, Lamb DQ, Margon B, McKay TA, Smith JA, Waddel P, York DG, The SDSS Collaboration (2001) Solar system objects observed in the Sloan Digital Sky Survey commissioning data. Astron J 122:2749–2784

Jarvis KS, Vilas F, Larson SM, Gaffey MJ (2000) JVI Himalia: New compositional evidence and interpretations for the origin of Jupiter's small satellites. Icarus 145:445–453

Jedicke R, Metcalfe TS (1998) The orbital and absolute magnitude distributions of main belt asteroids. Icarus 131:245–260

Jewitt DC, Luu JX (1990) CCD spectra of asteroids. II – The Trojans as spectral analogs of cometary nuclei. Astron J 100:933–944

Jones TD, Lebofsky LA, Lewis JS, Marley MS (1990) The composition and origin of the C, P, and D asteroids: Water as a tracer of thermal evolution in the outer belt. Icarus 88:172–192

Kanno A, Hiroi T, Nakamura R, Abe M, Ishiguro M, Hasegawa S, Miyasaka S, Sekiguchi T, Terada H, Igarashi G (2003) The first detection of water absorption on a D type asteroid. Geophys Res Lett 30:10.1029/2003GL017907

Keller LP, McKay DS (1993) Discovery of vapor deposits in the lunar regolith. Science 261:1305-1307

Keller LP, McKay DS (1997) The nature and origin of rims on lunar soil grains. Geochim Cosmochim Acta 61:2331-2341

Keller LP, Wentworth SJ, McKay DS, Taylor LA, Pieters CM, Morris RV (2000) Space weathering in the fine size fractions of lunar soil: Mare/highland differences. Lunar Planet Sci XXXI:1655

Kelley MS, Gaffey MJ (1997) 9 Metis and 113 Amalthea: A genetic asteroid pair. Icarus 144:27-38

Kelley MS, Gaffey MJ (2002) High-albedo asteroid 434 Hungaria: Spectrum, composition and genetic connections. Meteor Planet Sci 37:1815-1827

Kelley MS, Vilas F, Gaffey MJ, Abell PA (2003) Quantified mineralogical evidence for a common origin of 1929 Kollaa with 4 Vesta and the HED meteorites. Icarus 165:215-218

Kiang T (1971) The distribution of asteroids in the direction perpendicular to the ecliptic plane. *In*: Physical Studies of Minor Planets. Gehrels T (ed) NASA, Washington, p 187-195

King TVV, Clark RN (1989) Spectral characteristics of chlorites and Mg-serpentines using high- resolution reflectance spectroscopy. J Geophys Res 94:13997-14008

King TVV, Clark RN (1997) The presence of a single absorption feature: What it does and doesn't imply. Lunar Planet Sci XXVIII:727-728

King TVV, Clark RN, Calvin WM, Sherman DM, Brown RH (1992) Evidence for ammonium-bearing minerals on Ceres. Science 255:1551-1553

King TVV, Ridley WI (1987) Relation of the spectroscopic reflectance of olivine to mineral chemistry and some remote sensing implications. J Geophys Res 92:11457-11469

Kitts K, Lodders K (1998) Survey and evaluation of eucrite bulk compositions. Meteor Planet Sci 33:A197-A213

Kleine T, Mezger K, Palme H., Scherer E., Munker C (2005) Early core formation in asteroids and late accretion of chondrite parent bodies: Evidence from ^{182}Hf-^{182}W in CAIs, metal-rich chondrites, and iron meteorites. Geochim Cosmochim Acta 69:5805-5818

Klima RL, Pieters CM, Dyar MD (2007) Spectroscopy of synthetic Mg-Fe pyroxenes I: Spin-allowed and spin-forbidden crystal field bands in the visible and near-infrared. Meteor Planet Sci 42:235-253

Krot AN, Meibom A, Weisberg MK, Keil K (2002) Invited review: The CR chondrite clan: Implications for early solar system processes. Meteor Planet Sci 37:1451–1490

Kuzmanoski M, Kovacevic A (2002) Motion of the asteroid (13206) 1997GC22 and the mass of (16) Psyche. Astron Astrophys 395:L17-L19

Lagerkvist C–I, Moroz L, Nathues A, Erikson A, Lahulla F, Karlsson O, Dahlgren M (2005) A study of Cybele asteroids II. Spectral properties of Cybele asteroids. Astron Astrophys 432:349-354

Larson HP, Feierberg MA, Fink U, Smith HA (1979) Remote spectroscopic identification of carbonaceous chondrite mineralogies: Applications to Ceres and Pallas. Icarus 39:257-271

Larson HP, Feierberg MA, Lebofsky LA (1983) The composition of asteroid 2 Pallas and its relation to primitive meteorites. Icarus 56:398-408

Larson HP, Fink U (1975) Infrared spectral observations of asteroid 4 Vesta. Icarus 26:420-427

Lazzarin M, Marchi S, Barucci MA, Di Martino M, Barbieri C (2004) Visible and near-infrared spectroscopic investigation of near-earth objects at ESO: First results. Icarus 169:373-384

Lazzarin M, Marchi S, Moroz LV, Brunetto R, Magrin S, Paolicchi P, Strazzulla G (2006) Space weathering in the main asteroid belt: The big picture. Astrophys J 647:L179-L182

Lazzaro D, Angeli CA, Carvano JM, Mothé-Diniz T, Duffard R, Florczak M (2004) S3OS2: The visible spectroscopic survey of 820 asteroids. Icarus 172:179-220

Lazzaro D, Michtchenko T, Carvano JM, Binzel RP, Bus SJ, Burbine TH, Mothé-Diniz T, Florczak M, Angeli CA, Harris AW (2000) Discovery of a basaltic asteroid in the outer main belt. Science 288:2033-2035

Lebofsky LA, Feierberg MA, Tokunaga AT, Larson HP, Johnson JR (1981a) The 1.7- to 4.2-micron spectrum of asteroid 1 Ceres: Evidence for structural water in clay minerals. Icarus 48:453-459

Lebofsky LA, Howell ES, Britt DT (1991) Characterization of low albedo asteroids. Bull Am Astron Soc 23:1140

Lebofsky LA, Spencer JR (1989) Radiometry and thermal modeling of asteroids. *In:* Asteroids II. Binzel RP, Gehrels T, Matthews MS (eds) University of Arizona Press, Tucson, p 128-147

Lebofsky LA, Sykes MV, Tedesco EF, Veeder GJ, Matson DL, Brown RH, Gradie JC, Feierberg MA, Rudy RJ (1986) A refined "standard" thermal model for asteroids based on observations of 1 Ceres and 2 Pallas. Icarus 68:239-251

Lebofsky LA, Veeder GJ, Rieke GH, Lebofsky MT, Matson DL, Kowal C, Wynn-Williams CG, Becklin EE (1981b) The albedo and diameter of 1862 Apollo. Icarus 48:335-338

Lecar M, Franklin FA, Holman MA (2001) Chaos in the solar system. Ann Rev Astron Astrophys 39:581-631

Levison HF, Agnor C (2003) The role of giant planets in terrestrial planet formation. Astron J 125:2692- 2713

Lewis JS (1997) Physics and Chemistry of the Solar System. Academic Press, London. 591 pp

Lewis JS, Prinn RG (1984) Planets and their atmospheres: Origin and evolution. Academic Press, Orlando. 480 pp

Li J-Y, McFadden LA, Parker JWm, Young EF, Stern SA, Thomas PC, Russell CT, Sykes MV (2006) Photometric analysis of 1 Ceres and surface mapping from HST observations . Icarus 182:143- 160

Licandro J, Campins H, Mothé-Diniz T, Pinilla-Alonso N, de León J (2007) The nature of comet- asteroid transition object (3200) Phaethon. Astron Astrophys 461:751-757

Lim LF, McConnochie TH, Bell JF, Hayward TL (2005) Thermal infrared (8-13 μm) spectra of 29 asteroids: The Cornell Mid-Infrared Asteroid Spectroscopy (MIDAS) survey. Icarus 173:385- 408

Longhi J, Bertka CM (1996) Graphical analysis of pigeonite-augite liquidus equilibria. Am Mineral 81:685-695

Lupishko DF, Belskaya IN (1989) On the surface composition of the M-type asteroids. Icarus 78:395- 401

Luu JX, Jewitt DC (1989) On the relative numbers of C types and S types among near-Earth asteroids. Astron J 98:1905-1911

Luu JX, Jewitt DC (1990) Charge-coupled device spectra of asteroids. I. Near-Earth and 3:1 resonance asteroids. Astron J 99:1985-2011

Magri C, Nolan MC, Ostro SJ, Giorgini JD (2007) A radar survey of main-belt asteroids: Arecibo observations of 55 objects during 1999–2003. Icarus 186:126-151

Magri C, Ostro SJ, Rosema KD, Thomas ML, Mitchell DL, Campbell DB, Chandler JF, Shapiro II, Giorgini JD, Yeomans DK (1999) Mainbelt asteroids: Results of Arecibo and Goldstone radar observations of 37 objects during 1980-1985. Icarus 140:379-407

Mao HK, Bell PM (1975) Crystal field effects in spinel: Oxidation states of iron and chromium. Geochim Cosmochim Acta 39:865-874

Marchi S, Brunetto R, Magrin S, Lazzarin M, Gandolfi D (2005a) Space weathering of near-Earth and main belt silicate-rich asteroids: Observations and iron irradiation experiments. Astron Astrophys 443:769-775

Marchi S, Lazzarin M, Paolicchi P, Magrin S (2005b) New V-type asteroids in near-Earth space. Icarus 175:170-174

Marchi S, Magrin S, Nesvorný D, Paolicchi P, Lazzarin M (2006a) A spectral slope versus perihelion distance correlation for planet-crossing asteroids. Mon Not R Astron Soc Lett 368:L39–L42

Marchi S, Paolicchi P, Lazzarin M, Magrin S (2006b) A general spectral slope-exposure relation for S- type main belt and near-Earth asteroids. Astron J 131:1138-1141

Margot JL, Brown ME (2003) A low-density M-type asteroid in the main belt. Science 300:1939-1942

Matson DL, Veeder GJ, Tedesco EF, Lebofsky LA (1989) The IRAS asteroid and comet survey. *In*: Asteroids III. Bottke WF, Cellino A, Paolicchi P, Binzel RP (eds), University of Arizona Press, Tucson, p 269-281

Matson DL, Veeder GJ, Tedesco EF, Lebofsky LA, Walker RG (1986) IRAS survey of asteroids. Adv Space Res 6:47-56

Mayne RG, Sunshine JM, McCoy TJ, McSween HY Jr (2006) Substantial lithologic diversity on 4 Vesta: Evidence from the petrology and spectra of Antarctic eucrites. Lunar Planet Sci XXXVII:1796

McCammon C (2005) The paradox of mantle redox. Science 308:807-808

McCord TB, Adams JB, Johnson TV (1970) Asteroid Vesta: Spectral reflectivity and compositional implications. Science 178:745-747

McCord TB, Carlson RW, Smythe WD, Hansen GB, Clark RN, Hibbitts CA, Fanale FP, Granahan JC, Segura M, Matson DL, Johnson TV, Martin PD (1997) Organics and other molecules in the surfaces of Callisto and Ganymede. Science 278:271-275

McCord TB, Hansen GB, Matson DL, Johnson TV, Crowley JK, Fanale FP, Carlson RW, Smythe WD, Martin PD, Hibbitts CA, Granahan JC, Ocampo A (1999) Hydrated salt minerals on Europa's surface from the Galileo near-infrared mapping spectrometer (NIMS) investigation. J Geophys Res 104:11827-11852

McCord TB, Sotin C (2005) Ceres: Evolution and current state. J Geophys Res 110:10.1029/2004JE002244

McCoy TJ, Burbine TH, McFadden LA, Starr RD, Gaffey MJ, Nittler LR, Evans LG, Izenberg N, Lucey P, Trombka JI, Bell JF III, Clark BE, Clark PE, Squyres SW, Chapman CR, Boynton WV, Veverka J (2001) The composition of 433 Eros: A mineralogical-chemical synthesis. Meteor Planet Sci 36:1661-1672

McCoy TJ, Nittler LR, Burbine TH, Trombka JI, Clark PE, Murphy ME (2000) Anatomy of a partially differentiated asteroid: A "NEAR"-sighted view of acapulcoites and lodranites. Icarus 148:29-36

McCoy TJ, Robinson MS, Nittler LR, Burbine TH (2002) The Near Earth Asteroid Rendezvous Mission to asteroid 433 Eros: A milestone in the study of asteroids and their relationship to meteorites. Chem Erde 62:89-121

McEwen AS, Moore JM, Shoemaker EM (1997) The Phanerozoic impact cratering rate: Evidence from the farside of the Moon. J Geophys Res 102:9231-9242

McFadden LA, Gaffey MJ, McCord TB (1985) Near-Earth asteroids: Possible sources from reflectance spectroscopy. Science 229:160-163

McFadden LA, Goldman NJ, Gaffey MJ, Izenberg NR (2005) Evidence for partial melting in reflectance spectra of 433 Eros. Lunar Planet Sci XXXVI:1561

McFadden LA, Wellnitz DD, Schnaubelt MW, Gaffey MJ, Bell JF III, Izenberg N, Chapman CR (2001) Mineralogical interpretation of reflectance spectra of Eros from NEAR NIS low phase flyby. Meteor Planet Sci 36:1711-1726

McKay DS, Heiken GH, Basu A, Blanford G, Simon S, Reedy R, French BM, Papike J (1991) The lunar regolith. *In:* The Lunar Sourcebook. Heiken GH, Vaniman DT, French BM (eds), Cambridge University Press, New York, p 284-356

Michel P, Benz W, Richardson DC (2003) Disruption of fragmented parent bodies as the origin of asteroid families. Nature 421:608-611

Michel P, Benz W, Richardson DC (2004) Catastrophic disruption of pre-shattered parent bodies. Icarus 168:420-432

Michelsen R, Nathues A, Lagerkvist C-I (2006) Spectroscopy of near-Earth asteroids. Astron Astrophys 451:331-337

Michtchenko TA, Lazzaro D, Ferraz-Mello S, Roig F (2002) Origin of the basaltic asteroid 1459 Magnya: A dynamical and mineralogical study of the outer main belt. Icarus 158:343-359

Migliorini F, Zappalà V, Vio R, Cellino A (1995) Interlopers within asteroid families. Icarus 118:271- 291

Milliken RE, Mustard JF (2005) Quantifying absolute water content of minerals using near-infrared reflectance spectroscopy. J Geophys Res 110:doi:10.1029/2005JE002534

Mitchell DL, Ostro SJ, Rosema KD, Hudson RS, Campbell DB, Chandler JF, Shapiro II (1995) Radar observations of asteroids 7 Iris, 9 Metis, 12 Victoria, 216 Kleopatra, and 654 Zelinda. Icarus 118:105-131

Mittlefehldt DW, Bogard DD, Berkley JL, Garrison DH (2003) Brachinites: Igneous rocks from a differentiated asteroid. Meteor Planet Sci 38:1601-1625

Mittlefehldt DW, Killgore M, Lee MT (2002) Petrology and geochemistry of D'Orbigny, geochemistry of Sahara 99555, and the origin of angrites. Meteor Planet Sci 37:345-369

Mittlefehldt DW, McCoy TJ, Goodrich CA, Kracher A (1998) Non-chondritic meteorites from asteroidal bodies. Rev Mineral 36:4-1–4-195

Miyamoto M, Zolensky ME (1994) Infrared diffuse reflectance spectra of carbonaceous chondrites: Amount of hydrous minerals. Meteoritics 29:849–853

Morbidelli A, Levison HF, Tsiganis K, Gomes R (2005) Chaotic capture of Jupiter's Trojan asteroids in the early solar system. Nature 435:462–465

Moretti PF, Maras A, Somma F, Aloe P (2006) Simulation of low-velocity bombardment of asteroid surfaces: Regolith formation and reddening of the spectra. Astron Astrophys 459:245-248

Moroz L, Baratta G, Strazzulla G, Starukhina L, Dotto E, Barucci MA, Arnold G, Distefano E (2004a) Optical alteration of complex organics induced by ion irradiation: 1. Laboratory experiments suggest unusual space weathering trend. Icarus 170:214-228

Moroz LV, Fisenko AV, Semjonova LF, Pieters CM, Korotaeva NN (1996) Optical effects of regolith processes on S-asteroids as simulated by laser shots on ordinary chondrite and other mafic minerals. Icarus 122:366-382

Moroz LV, Hiroi T, Shingareva TV, Basilevsky AT, Fisenko AV, Semjonova LF, Pieters CM (2004b) Reflectance spectra of CM2 chondrite Mighei irradiated with pulsed laser and implications for low-albedo asteroids and Martian moons. Lunar Planet Sci XXXV:1279

Moroz L, Schade U, Wäsch R (2000) Reflectance spectra of olivine–orthopyroxene-bearing assemblages at decreased temperatures: Implications for remote sensing of asteroids. Icarus 147:79-93

Mothé-Diniz T, Carvano JM (2005) 221 Eos: A remnant of a partially differentiated parent body? Astron Astrophys 442:727-729

Mothé-Diniz T, Carvano JM, Lazzaro D (2003) Distribution of taxonomic classes in the main belt of asteroids. Icarus 162:10-21

Mothé-Diniz T, Roig F, Carvano JM (2005) Reanalysis of asteroid families structure through visible spectroscopy. Icarus 174:54-80

Murchie SL, Pieters CM (1996) Spectral properties and rotational spectral heterogeneity of 433 Eros. J Geophys Res 101:2201-2214

Mustard JF, Pieters CM (1989) Photometric phase functions of common geologic minerals and applications to quantitative analysis of mineral mixture reflectance spectra. J Geophys Res 94:13619-13634

Nakamura T (2006) Yamato 793321 CM chondrite: Dehydrated regolith material of a hydrous asteroid. Earth Plan Sci Lett 242:26-38

Nesvorný D, Bottke WF (2004) Detection of the Yarkovsky effect for main-belt asteroids. Icarus 170:324-342

Nesvorný D, Jedicke R, Whiteley RJ, Ivezić Ž (2005) Evidence for asteroid space weathering from the Sloan Digital Sky Survey. Icarus 173:132-152

Nittler LR, Starr RD, Lim L, McCoy TJ, Burbine TH, Reedy RC, Trombka JI, Gorenstein P, Squyres SW, Boynton WV, McClanahan TP, Bhangoo JS, Clark PE, Murphy ME, Killen R (2001) X-ray fluorescence measurements of the surface elemental composition of asteroid 433 Eros. Meteor Planet Sci 36:1673-1695

Noble SK, Pieters CM, Keller LP (2003) The optical properties of nanophase iron: Investigation of a space weathering analog. Lunar Planet Sci XXXIV:1172

Noble SK, Pieters CM, Taylor LA, Morris RV, Allen CC, McKay DS, Keller LP (2001) The optical properties of the finest fraction of lunar soil: Implications for space weathering. Meteor Planet Sci 36:31-42

Okada T, Shirai K, Yamamoto Y, Arai T, Ogawa K, Hosono K, Kato M (2006) X-ray fluorescence spectrometry of asteroid Itokawa by Hayabusa. Science 312:1338-1341

Olsen E, Davis A, Clarke RS, Schultz L, Weber HW, Clayton R, Mayeda T, Jarosewich E, Sylvester P, Grossman L, Wang M-S, Lipschutz ME, Steele IM, Schwade J (1994) Watson: A new link in the IIE iron chain. Meteoritics 29:200-213

Ostro SJ, Campbell DB, Shapiro II (1985) Mainbelt asteroids: Dual-polarization radar observations. Science 229:442-446

Ostro SJ, Hudson RS, Nolan MC, Margot J-L, Scheeres DJ, Campbell DB, Magri C, Giorgini JD, Yeomans DK (2000) Radar observations of asteroid 216 Kleopatra. Science 288:836-839

Ostro SJ, Rosema KD, Campbell DB, Chandler JF, Hine AA, Hudson RS (1991) Asteroid 1986 DA – Radar evidence for a metallic composition. Science 252:1399-1404

Petaev MI, Barsukova LD, Lipschutz ME, Wang M-S, Ariskin AA, Clayton RN, Mayeda TK (1994) The Divnoe meteorite: Petrology, chemistry, oxygen isotopes and origin. Meteoritics 29:182-199

Petit J-M, Chambers J, Franklin F, Nagazaw M (2002) Primordial excitation and depletion of the main belt. *In*: Asteroids III. Bottke WF, Cellino A, Paolicchi P, Binzel RP (eds), University of Arizona Press, Tucson, p 711-723

Petit J-M, Morbidelli A, Chambers J (2001) The primordial excitation and clearing of the asteroid belt. Icarus 153:338-347

Pieters CM (1996) Plagioclase and maskelynite diagnostic features. Lunar Planet Sci XXVII:1031-1032

Pieters CM, Binzel RP, Bogard D, Hiroi T, Mittlefehldt DW, Nyquist L, Rivkin A, Takeda H (2005) Asteroid-meteorite links: The Vesta conundrum(s). *In*: Asteroids, Comets, Meteors, Proceedings IAU Symposium No. 229. Lazzaro D, Ferraz-Mello S, Fernández JA (eds), Cambridge University Press, Cambridge, p 273-288

Pieters CM, Fischer EM, Rode O, Basu A (1993) Optical effects of space weathering: the role of the finest fraction. J Geophys Res 98:20817-20824

Pieters CM, Taylor LA, Noble SK, Keller LP, Hapke B, Morris RV, Allen CC, McKay DS, Wentworth S (2000) Space weathering on airless bodies: Resolving a mystery with lunar samples. Meteor Planet Sci 35:1101-1107

Price SD (2004) The surface properties of asteroids. Adv Space Res 33:1548-1557

Prinz M, Keil K, Hlava PF, Berkley JL, Gomes CB, Curvello WS (1977) Studies of Brazilian meteorites, III. Origin and history of the Angra dos Reis achondrite. Earth Planet Sci Lett 35:317-330

Rajan S, Gaffey MJ (1984) Spectral reflectance characteristics of Allende white inclusions. Lunar Planet Sci 15:659-660

Rayner JT, Toomey DW, Onaka PM, Denault AJ, Stahlberger WE, Vacca WD, Cushing MC, Wang S (2003) SpeX: A medium-resolution 0.8-5.5 micron spectrograph and imager for the NASA Infrared Telescope Facility. Publ Astron Soc Pac 115:362-382

Reed KL, Gaffey MJ, Lebofsky LA (1997) Shape and albedo variations of asteroid 15 Eunomia. Icarus 125:446-454

Rivkin AS (1997) Observations of main-belt asteroids in the 3-μm Region. PhD Dissertation, University of Arizona, Tucson, Arizona

Rivkin AS Binzel RP, Bus SJ (2005) Constraining near-Earth object albedos using near-infrared spectroscopy. Icarus 175:175-180

Rivkin AS, Binzel RP, Sunshine J, Bus SJ, Burbine TH, Saxena A (2004a) Infrared spectroscopic observations of 69230 Hermes (1937 UB): Possible unweathered endmember among ordinary chondrite analogs. Icarus 172:408-414

Rivkin AS, Davies JK, Clark BE, Trilling DE, Brown RH (2001) Aqueous alteration on S asteroid 6 Hebe? Lunar Planet Sci XXXII:1723

Rivkin AS, Davies JK, Johnson JR, Ellison SL, Trilling DE, Brown RH, Lebofsky LA (2003a) Hydrogen concentrations on C-class asteroids derived from remote sensing. Meteor Planet Sci 38:1383–1398

Rivkin AS, Howell ES, Britt DT, Lebofsky LA, Nolan MC, Branston DD (1995) 3-μm spectrophotometric survey of M and E-class asteroids. Icarus 117:90–100

Rivkin AS, Howell ES, Bus SJ (2004b) Diversity of types of hydrated minerals on C-class asteroids. Lunar Planet Sci XXXV:1646

Rivkin AS, Howell ES, Bus SJ, Hicks M, Reach WT, Jarrett TH, Binzel RP (2003b) Spectroscopy and photometry of the Earth grazer 2002 NY40. Lunar Planet Sci XXXIV:1722

Rivkin AS, Howell ES, Vilas F, Lebofsky LA (2002) Hydrated minerals on asteroids: The astronomical record. *In*: Asteroids III. Bottke WF, Cellino A, Paolicchi P, Binzel RP (eds), University of Arizona Press, Tucson, p 235–253

Rivkin AS, Lebofsky LA, Clark BE, Howell ES, Britt DT (2000) The nature of M-class asteroids in the 3-μm region. Icarus 145:351–368

Rivkin AS, McFadden LA, Binzel RP, Sykes M (2006a) Rotationally-resolved spectroscopy of Vesta I: 2-4 μm region. Icarus 180:464-472

Rivkin AS, Volquardsen EL, Clark BE (2006b) The surface composition of Ceres: Discovery of carbonates and iron-rich clays. Icarus 185:563-567

Roig F, Gil-Hutton R (2006) Selecting candidate V-type asteroids from the analysis of the Sloan Digital Sky Survey colors. Icarus 183:411-419

Roush TL, Singer RB (1987) Possible temperature variations effects on the interpretation of spatially resolved reflectance observations of asteroid surfaces. Icarus 69:571-574

Rubin AE (1997a) Mineralogy of meteorite groups. Meteor Planet Sci 32:231-247

Rubin AE (1997b) Mineralogy of meteorite groups: An update. Meteor Planet Sci 32:733-734

Rubin AE, Wasson JT (1995) Variations of chondrite properties with heliocentric distance. Meteoritics 30:569

Ruzicka A, Killgore M, Mittlefehldt DW, Fries MD (2005) Portales Valley: Petrology of a metallic-melt meteorite breccia. Meteor Planet Sci 40:261-295

Salisbury JW, D'Aria DM, Jarosewich E (1991) Midinfrared (2.5–13.5 μm) reflectance spectra of powdered stony meteorites. Icarus 92:280–297

Sasaki S, Nakamura K, Hamabe Y, Kurahashi E, Hiroi T (2001) Production of iron nano particles by laser irradiation in a simulation of lunar-like space weathering. Nature 410:555-557

Sato K, Miyamoto M, Zolensky ME (1997) Absorption bands near three micrometers in diffuse reflectance spectra of carbonaceous chondrites: Comparison with asteroids. Meteor Planet Sci 32:503–507

Scerri ER (2000) Have orbitals really been observed? J Chem Ed 77:1492-1494

Schade U, Wäsch R (1999) Near-infrared reflectance spectra from bulk samples of the two SNC meteorites Zagami and Nakhla. Meteor Planet Sci 34:417-424

Schade U, Wäsch R, Moroz L (2004) Near-infrared reflectance spectroscopy of Ca-rich clinopyroxenes and prospects for remote spectral characterization of planetary surfaces. Icarus 168:80-92

Schulze H, Bischoff A, Palme H, Spettel B, Dreibus G, Otto J (1994) Mineralogy and chemistry of Rumuruti: The first meteorite fall of the new R chondrite group. Meteoritics 29:275-286

Sears DWG (1998) The case for the rarity of chondrules and CAI in the early solar system and some implications for astrophysical models. Astrophys J 498:773-778

Shingareva TV, Basilevsky AT, Fisenko AV, Semjonova LF, Korotaeva NN (2004) Mineralogy and petrology of laser irradiated carbonaceous chondrite Mighei. Lunar Planet Sci XXXV:1137

Singer RB, Roush TL (1985) Effects of temperature on remotely sensed mineral absorption features. J Geophys Res 90:12434-12444

Smith JV, Brown WL (1988) Feldspar Minerals: Volume 1, Crystal Structures, Physical, Chemical, and Microtextural Properties. Springer-Verlag, Berlin. 828 pp

Straub DW, Burns RG, Pratt SF (1991) Spectral signature of oxidized pyroxenes: Implications to remote sensing of terrestrial planets. J Geophys Res 96:18819-18830

Strazzulla G, Dotto E, Binzel R, Brunetto R, Barucci MA, Blanco A, Orofino V (2004) Spectral alteration of the meteorite Epinal (H5) induced by heavy ion irradiation: A simulation of space weathering effects on near-Earth asteroids. Icarus 174:31-35

Strom RG, Malhotra R, Ito T, Fumi R, Kring DA (2005) The origin of planetary impactors in the inner solar system. Science 309:1847-1850

Sunshine JM (1997) Continuing towards more sophisticated compositional interpretations of silicate- rich lithologies on the surfaces of asteroids. Lunar Planet Sci XXVIII:1181

Sunshine JM, Binzel RP, Burbine TH, Bus SJ (1998) Is asteroid 289 Nenetta compositionally analogous to the Brachinite meteorites? Lunar Planet Sci XXIX:1430

Sunshine JM, Bus SJ, Corrigan CM, McCoy TJ, Burbine TH (2007) Olivine dominated asteroids and meteorites: Distinguishing nebular and igneous histories. Meteor Planet Sci 42:155-170

Sunshine JM, Bus SJ, McCoy TJ, Burbine TH, Corrigan CM, Binzel RP (2004) High-calcium pyroxene as an indicator of igneous differentiation in asteroids and meteorites. Meteor Planet Sci 39:1343-1357

Sunshine JM, Hinrichs JL, Lucey PG (2000) Temperature dependence of individual absorptions bands in olivine: Implications for inferring compositions of asteroid surfaces from spectra. Lunar Planet Sci 31:1605

Sunshine JM, Pieters CM (1993) Estimating modal abundances from the spectra on natural and laboratory pyroxene mixtures using the modified Gaussian model. J Geophys Res 98:9075-9087

Sunshine JM, Pieters CM (1998) Determining the composition of olivine from reflectance spectroscopy. J Geophys Res 103:13675-13688

Sunshine JM, Pieters CM, Pratt S F (1990) Deconvolution of mineral absorption bands: An improved approach. J Geophys Res 95:6955-6966

Sykes MV, Vilas F (2001) Closing in on HED meteorite sources. Earth Planets Space 53:1077-1083

Takato N, Bus SJ, Terada H, Pyo T-S, Kobayashi N (2004) Detection of a deep 3-μm absorption feature in the spectrum of Amalthea (JV). Science 306:2224-2227

Taylor LA, Morris RV, Keller LP, Pieters CM, Pachen A, Taylor D, Wentworth SJ McKay DS (2000) Major contributions to spectral reflectance opacity by non-agglutinitic, surface-correlated nanophase iron. Lunar Planet Sci XXXI:1842

Tedesco EF (1986) The infrared astronomical satellite asteroid database. Asteroids, Comets, Meteors II:13-17

Tedesco EF, Cellino A, Zappalá V (2005) The statistical asteroid model. I. The main-belt population for diameters greater than 1 kilometer. Astron J 129:2869-2886

Tedesco EF, Noah PV, Noah M, Price SD (2002) The supplemental IRAS minor planet survey. Astron J 123:1056–1085

Tholen DJ (1984) Asteroid taxonomy from cluster analysis of photometry. PhD Dissertation, University of Arizona, Tucson, Arizona

Tholen DJ (1989) Asteroid taxonomic classifications. *In*: Asteroids II. Binzel RP, Gehrels T, Matthews MS (eds) Univ Arizona Press, Tucson, p 1139-1150

Thomas PC, Binzel RP, Gaffey MJ, Storrs AD, Wells EN, Zellner BH (1997a) Impact excavation on asteroid 4 Vesta: Hubble Space Telescope results. Science 277:1492-1495

Thomas PC, Binzel RP, Gaffey MJ, Zellner BH, Storrs AD, Wells E (1997b) Vesta: Spin pole, size, and shape from HST images. Icarus 128:88-94

Thomas PC, Parker JWm, McFadden LA, Russell CT, Stern SA, Sykes MV, Young EF (2005) Differentiation of the asteroid Ceres as revealed by its shape. Nature 437:224-226

Tomeoka K, Kiriyama K, Nakamura K, Yamahana Y, Sekina T (2003) Interplanetary dust from the explosive dispersal of hydrated asteroids by impacts. Nature 423:60–62

Trombka JI, Squyres SW, Brückner J, Boynton WV, Reedy RC, McCoy TJ, Gorenstein P, Evans LG, Arnold JR, Starr RD, Nittler LR, Murphy ME, Mikheeva I, McNutt RL Jr, McClanahan TP, McCartney E, Goldsten JO, Gold RE, Floyd SR, Clark PE, Burbine TH, Bhangoo JS, Bailey SH, Petaev M (2000) The elemental composition of asteroid 433 Eros: Results of the NEAR- Shoemaker X-Ray spectrometer. Science 289:2101-2105

Ueda Y, Hiroi T, Pieters CM, Miyamoto M (2002a) Changes of Band I Center and Band II/Band I Area Ratio in reflectance spectra of olivine-pyroxene mixtures due to the space weathering and grain size effects. Lunar Planet Sci XXXIII:2023

Ueda Y, Miyamoto M, Hiroi T (2002b) Expanding the modified Gaussian model: Estimating the composition of olivine-rich asteroid. Meteor Planet Sci 37:A141

Vernazza P, Birlan M, Rossi A, Dotto E, Nesvorny D, Brunetto R, Fornasier S, Fulchignoni M, Renner S (2006a) Physical characterization of the Karin family. Astron Astrophys 460:945-951

Vernazza P, Brunetto R, Strazzulla G, Fulchignoni M, Rochette P, Meyer-Vernet N, Zouganelis I (2006b) Asteroid colors: a novel tool for magnetic field detection? The case of Vesta. Astron Astrophys 451:L43-L46

Vernazza P, Mothé-Diniz T, Barucci MA, Birlan M, Carvano JM, Strazulla G, Fulchignoni M, Miglorini A (2005) Analysis of near-IR spectra of 1 Ceres and 4 Vesta, targets of the Dawn mission. Astron Astrophys 436:1113-1121

Viateau B (2000) Mass and density of asteroids (16) Psyche and (121) Hermione. Astron Astrophys 354:725-731

Vilas F (1994) A cheaper, faster, better way to detect water of hydration on solar system bodies. Icarus 111:456–467

Vilas F, Cochran AL, Jarvis KS (2000) Vesta and the Vestoids: A new rock group? Icarus 147:119-128

Vilas F, McFadden LA (1992) CCD reflectance spectra of selected asteroids: I. Presentation and data analysis considerations. Icarus 100:85–94

Weisberg MK, McCoy TJ, Krot AN (2006) Systematics and evaluation of meteorite classification. Lauretta DS, McSween HY Jr (eds), University of Arizona Press, Tucson, p 19-52

Weissman PR, A'Hearn MF, McFadden LA, Rickman H (1989) Evolution of comets into asteroids. *In*: Asteroids II. Binzel RP, Gehrels T, Matthews MS (eds) Univ Arizona Press, Tucson, p 880-920

Wentworth SJ, Keller LP, McKay DS, Morris RV (1999) Space weathering on the Moon: Patina on Apollo 17 samples 75075 and 76015. Meteor Planet Sci 34:593-603

Wetherill GW (1992) An alternative model for the formation of asteroids. Icarus 100:307–325

Wood BJ (1974) Crystal field spectrum of Ni^{2+} in olivine. Am Mineral 59:244-248

Xu S, Binzel RP, Burbine TH, Bus SJ (1995) Small main-belt asteroid spectroscopic survey: Initial results. Icarus 115:1-35

Yamada M, Sasaki S, Nagahara H, Fujiwara A, Hasegawa S, Yano H, Hiroi T, Otake H (1999) Simulation of space weathering of planet-forming materials: Nanosecond pulse laser irradiation and proton implantation on olivine and pyroxene samples. Earth Planets Space 51:1255-1265

Zappalà V, Cellino A, Dell'Oro A, Paolicchi P (2002) Physical and dynamical properties of asteroid families. *In*: Asteroids III. Bottke WF, Cellino A, Paolicchi P, Binzel RP (eds), University of Arizona Press, Tucson, p 619-631

Zappalà V, Cellino A, Farinella P, Milani A (1994) Asteroid families: II. Extension to unnumbered multiopposition asteroids. Astronom J 107:772-801

Zellner B (1979) Asteroid taxonomy and the distribution of compositional types. *In*: Asteroids. Gehrels T (eds), University of Arizona Press, Tucson, p 783–806

Zellner B, Leake M, Morrison D, Williams JG (1977) The E asteroids and the origin of the enstatite achondrites. Geochim Cosmochim Acta 41:1759-1767

Zellner B, Thirunagari A, Bender D (1985a) The large-scale structure of the asteroid belt. Icarus 62:505- 511

Zellner B, Tholen DJ, Tedesco EF (1985b) The eight-color asteroid survey: Results for 589 minor planets. Icarus 61:355-416

Zellner B, Wisniewski WZ, Anderson L, Bowell E (1975) Minor planets and related objects. XVIII. UBV photometry and surface composition. Astron J 80:986-995

Ziffer J, Campins H, Licandro J, Pinilla-Alonso N, Fernandez Y, Bus SJ (2005) Near infrared spectra of two asteroids with low Tisserand invariant. Earth Moon Planets 97:203-212

Zolensky ME, Bodnar RJ, Gibson EK, Nyquist LE, Reese Y, Shih C-Y, Wiesmann H (1999) Asteroidal water within fluid inclusion-bearing halite in an H5 chondrite, Monahans (1998). Science 285:1377–1379

Zolensky M, Ivanov A (2003) The Kaidun microbreccia meteorite: A harvest from the inner and outer asteroid belt. Chem Erde 63:185-246